NTNU
Norwegian University of
Science and Technology

Internal Combustion Engine Friction Testing and Virtual Modeling

Jøran Melby

THE NORWEGIAN UNIVERSITY
OF SCIENCE AND TECHNOLOGY
DEPARTMENT OF ENGINEERING DESIGN
AND MATERIALS

MASTER THESIS SPRING 2016
FOR
STUD.TECHN. JØRAN MELBY

INTERNAL COMBUSTION ENGINE FRICTION TESTING AND VIRTUAL MODELING

Internal Combustion Engine Friction Testing and Virtual Modeling

The supervisor has together with MXRR and Fedem Tech. AS developed a virtual testing tool for internal combustion 2 and 4 stroke engines. This tool is based on the Fedem software that enables accurate integrity analysis of engines including both flexible bodies and control systems.

In order to virtually predict the engine performance (max speed, output torque and effect) the efficiency loss caused by various damping and friction effects must be identified. The objective is to predict the performance of engines when the mass and inertia properties for the most critical components are altered.

One research question is how do these properties influence the inertia and hence friction forces and net output torque/effect. Another question is how does the design of connecting rods (O,I and H beams) influence the drag effects at high speeds. To identify these effects, physical tests on a customized "motor dyno" must be performed

Tasks to be completed are:

1. Identify engine friction and damping effects that must be taken into account

2. Establish a test plan to identify the effects identified in task 1

3. Design a simple engine test rig for HONDA CRF 250 R engines (with different connecting rods)

4. Perform physical tests to identify the various friction and damping effects

5. Identify modeling features and properties that can be used to capture the physical damping and friction effects from task 4

6. Model a virtual test rig matching the physical test rig and HONDA engines

7. Tune the virtual engine model to match the physical test results

8. Prepare a paper together with MXRR and the supervisor
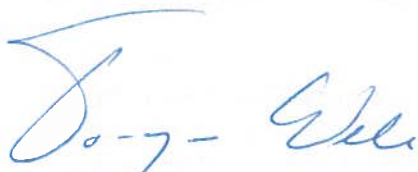
Formal requirements:

Three weeks after start of the thesis work, an A3 sheet illustrating the work is to be handed in. A template for this presentation is available on the IPM's web site under the menu "Masteroppgave" (http://www.ntnu.no/ipm/masteroppgave). This sheet should be updated one week before the master's thesis is submitted.

Risk assessment of experimental activities shall always be performed. Experimental work defined in the problem description shall be planed and risk assessed up-front and within 3 weeks after receiving the problem text. Any specific experimental activities which are not properly covered by the general risk assessment shall be particularly assessed before performing the experimental work. Risk assessments should be signed by the supervisor and copies shall be included in the appendix of the thesis.

The thesis should include the signed problem text, and be written as a research report with summary both in English and Norwegian, conclusion, literature references, table of contents, etc. During preparation of the text, the candidate should make efforts to create a well arranged and well written report. To ease the evaluation of the thesis, it is important to cross-reference text, tables and figures. For evaluation of the work a thorough discussion of results is appreciated.

The thesis shall be submitted electronically via DAIM, NTNU's system for Digital Archiving and Submission of Master's theses.

The contact person is Matteo Bella from MXRR.
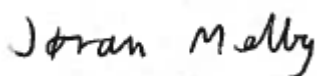
Torgeir Welo
Head of Division

Terje Rølvåg
Professor/Supervisor

NTNU
Norges teknisk-
naturvitenskapelige universitet
Institutt for produktutvikling
og materialer

Preface

The work presented herein is the final requirement concluding a five year education at the Norwegian University of Science and Technology, resulting in the degree "Master of Science" in Mechanical Engineering. The issues raised by the problem definition, and the understanding of combustion engines in general, are important topics relevant to the automotive industry. It is also something I personally find fascinating to work with and gain a deeper understanding of.

Some changes to the original problem definition were necessary, due to practical considerations during the course of this work. These changes were all discussed with the supervisor and approved. The biggest changes were that the influence of the connecting rod shank design (O-, I- or H-beam) on the drag effects was not investigated, and that all testing and simulation was performed on a single engine configuration: Honda OEM piston assembly, connecting rod and crankshaft. The first draft for a paper based on the findings in this thesis can be found in the appendix.

A number of people have assisted me in overcoming various challenges and contributed to my increased knowledge in the field of mechanical engineering. Without the help of these individuals, the quality of this work would most certainly have suffered, and they deserve to be acknowledged for their contributions. I want to thank my supervisor, Professor Terje Rølvåg, and the CEO of MX Real Racing, Matteo Celeste Bella, for providing invaluable advice and support throughout the design of the test rig, the experimental work, and the writing of this thesis. My gratitude also goes to Halvard Støwer for assisting in the planning and acquisition of the necessary equipment for the test rig, and to Bjørn Haugen for advice on the numerical behavior of the dynamic solver in FEDEM. I also want to thank Børge Holen and Carl-Magnus Midtbø for their support and help in the workshop during the test rig build.

Jøran Melby

Abstract

A virtual test bench capable of performing integrity analysis of internal engine components has previously been developed in FEDEM. It does however not include any damping and friction effects. As a result, engine performance is overestimated and shows little dependency on the inertia and mass of engine components. In this thesis, the friction and damping effects related to the piston assembly, connecting rod, and crankshaft of an engine were identified. A customized engine test rig was designed, and motored testing performed from 3000 rpm to 9000 rpm to measure the friction torque of a partial assembly of a Honda CRF 250 R engine. A virtual test bench representing the physical testing was developed and tuned in FEDEM.

Problems were encountered with a damaged torque transducer, possibly affecting the accuracy of the measurements, and resulting in less experimental data than desired. Engine oil was found to squeeze past the piston rings as a consequence of testing without cylinder pressure, possibly affecting lubrication conditions. Test results showed that the dominating piston assembly lubrication regime changes from boundary, via mixed, to hydrodynamic with increasing engine speed. This caused the measured friction torque to go from 1 Nm (3000 rpm), via a peak of 1.6 Nm (5000 rpm), to 1.5 Nm (9000 rpm). The engine friction's sensitivity to oil temperature was noted. Engine friction and oil shearing produced enough heat to keep the oil temperature at 87 °C at 4000 rpm, exemplifying the need for cooling systems, even in motored testing. Measurements taken before and after engine break-in clearly showed the importance of break-in on the engine's friction losses.

The virtual test bench was successfully able to recreate the measurements from physical engine testing. Simulation with reduced connecting rod mass did not produce the expected friction reduction, and it was suspected that a weakness in the modeling approach was responsible. The friction modeling formulation in FEDEM did not have the capability to capture the changes in lubrication regime for the piston assembly. It did not support a variable coefficient of friction, but required the Coulomb coefficient to have a constant value. Compensating for this weakness by adding additional viscous damping resulted in a less realistic model behavior.

It is concluded that more test data and improved friction modeling in FEDEM is required to obtain a virtual test bench accurate enough to predict real engine behavior, when inertia and mass properties of critical engine components are changed.

Sammendrag

En virtuell testbenk i stand til å utføre integritetsanalyse av motorkomponenter har tidligere blitt utviklet i FEDEM. Den inkluderer imidlertid ikke dempings- og friksjonseffekter. Dette resulterer i at motorytelsen blir overestimert og viser liten avhengighet av motordelers treghet og masse. I denne avhandlingen ble dempings- og friksjonseffekter relatert til stempel, råde, og veivaksel i en motor identifisert. En testrigg ble konstruert, og motorisert testing ble utført fra 3000 rpm til 9000 rpm for å måle friksjonsmomentet til en delvis komplett Honda CRF 250 R motor. En virtuell testbenk som representerer den fysiske testingen ble utviklet og kalibrert i FEDEM.

En skadet momentføler førte til utfordringer med testingen. Nøyaktigheten av målingene ble muligens påvirket, i tillegg til at antallet tester ble mindre enn ønsket. Noe motorolje presset seg forbi stempelringene som følge av at testene ble utført uten sylindertrykk, og dette påvirket muligens smøringsforholdene. Testresultatene viste at det dominerende smøringsregimet for stempelet skifter fra metallkontakt, via blandet, til hydrodynamisk med økende motorhastighet. Dette gjorde at det målte friksjonsmomentet gikk fra 1 Nm (3000 rpm), via en maksimalverdi på 1.6 Nm (5000 rpm), til 1.5 Nm (9000 rpm). Motorfriksjonens følsomhet for oljetemperatur ble observert. Motorfriksjon og oljefriksjon produserte nok varme til å holde oljetemperaturen på 87 °C ved 4000 rpm, noe som eksemplifiserer behovet for kjøling, også under motorisert testing. Målinger tatt før og etter innkjøring viste tydelig viktigheten av innkjøring for motorens friksjonsegenskaper.

Den virtuelle testbenken var i stand til å gjenskape målingene fra den fysiske testingen. Simulering med redusert vekt på råden resulterte ikke i den forventede reduksjonen av friksjonsmoment, og det ble mistenkt at en svakhet i modelleringen var ansvarlig. Friksjonsmodelleringen i FEDEM hadde ikke mulighet til å fange opp endringene i smøringsregimet for stempelet. Den støttet ikke variabel friksjonskoeffisient, men krevde at Coulomb-koeffisienten skulle ha en konstant verdi. Å kompensere for denne svakheten ved å legge til ekstra viskøs demping resulterte i at modellen oppførte seg mindre realistisk.

Det konkluderes med at flere tester og forbedret friksjonsmodellering i FEDEM er nødvendig for å oppnå en virtuell testbenk nøyaktig nok til å forutse reell motoroppførsel når treghets- og masseegenskapene til kritiske motorkomponenter endres.

Contents

Contents

Contents

List of Figures

List of Figures

List of Tables

Nomenclature

BDC   Bottom Dead Center

BMEP   Brake Mean Effective Pressure

CAD   Computer-Aided Design

CMS   Component Mode Synthesis

DOF   Degrees Of Freedom

FE   Finite Element

FEDEM Finite Element Dynamics in Elastic Mechanisms

FLAME Friction and Lubrication Analysis Model for Engines

FMBS   Flexible Multi-Body Simulation

FMEP   Friction Mean Effective Pressure

FVTB   FEDEM Virtual Test Bench

HHT   Hilbert Hughes Taylor

IMEP   Indicated Mean Effective Pressure

MBS   Multi-Body Simulation

MOFT   Minimum Oil Film Thickness

MXRR   MX Real Racing

OEM   Original Equipment Manufacturer

PI   Proportional-Integral

TDC   Top Dead Center

Chapter 1

Introduction

Internal combustion engines are in widespread use for a large number of applications. They are relatively complex machines subjected to a range of phenomena such as inertia forces, temperature fluctuations, pressure cycling, varying load, friction, wear, and fluid mechanic related losses. In motor vehicle applications, the engine's main purpose is to convert the chemical energy in the fuel into mechanical energy used to propel the vehicle. Some of the fuel energy is lost in the engine through various effects such as as incomplete combustion, heat transfer, pumping losses, viscous drag, and friction. These effects do not contribute to propulsion. In other words, some fuel is being used for other purposes than what is desired.

It is estimated that 1/3 of the fuel energy in passenger cars is used to overcome friction in the engine, transmission, tires, and brakes. In 2009 this corresponded to a worldwide consumption of 208 000 million liters of fuel to overcome friction [13]. This means that reducing the losses is beneficial in terms of both fuel consumption and performance. Since an engine contains a lot of moving parts, friction and drag effects (between parts and air or oil) are present throughout the whole system and contribute to the total losses. Friction losses also contribute to increased operating temperatures and component wear. As a consequence of this, less friction loss means less heat generation and thereby requires less cooling. Reducing friction can also be beneficial for component life and durability.

As a step towards improving existing engine designs, or designing new highly efficient engines, computer modeling and simulation is used to predict engine behavior prior to the production and assembly of the engine itself. This reduces both time and cost compared to successive prototyping, testing and modification. In order to successfully apply the modeling and simulation approach, knowledge of an engine's losses and friction effects is required. Engines contain a lot of moving parts, which are all subjected to friction of varying significance. Due to the vast number of moving parts, combined with their varying speed, load, thermal expansion, dynamic modes and inertia effects, calculation of friction and prediction of losses are complicated. Performing measurements directly on the parts is also difficult. Both from a practical point of view, and due to the fact that many parts are interconnected and affected by other parts in addition to the aforementioned effects.

Professor Terje Rølvåg, in cooperation with MX Real Racing (MXRR) and Fedem Technology AS, has developed a virtual test bench for internal combustion engines. The virtual test bench is built in the FEDEM computer software environment and is capable of performing integrity analysis of the internal engine components, while providing extensive control over the virtual engine test cycle. This enables dynamic simulation of the engine (including flexible body models), providing information about stress, strain, displacement, fatigue, etc. In addition to this, the virtual test bench allows for engine characteristics such as speed, torque, and power to be virtually measured. These characteristics are highly dependent on the numerous damping and friction losses occurring in the engine, and the virtual test bench does not include these effects in the simulation. As a result, the engine performance is overestimated and shows little dependency on changes in the inertia and mass of critical engine components.

In this thesis, the overall objective is to identify the friction and damping effects related to the piston assembly, connecting rod, and crankshaft, and model a virtual testing tool that accounts for these. This allows for more accurate predictions of engine performance, while enabling comparative studies of different connecting rod designs and their effect on engine behavior. To identify the effects in question, a customized engine test rig is designed and a

test scheme developed and executed. A virtual model representing the engine test is made and tuned in FEDEM. The basis for the work performed in this thesis is a single-cylinder four-stroke Honda CRF 250 R motocross engine.

The main steps towards successfully developing an accurate virtual testing tool is to:

1. Identify engine friction and damping effects that must be taken into account

2. Establish a test plan to identify the effects from step 1.

3. Design a simple engine test rig for the Honda CRF 250 R engine

4. Perform physical tests to identify the various friction and damping effects

5. Identify modeling features and properties that can be used to capture the effects from step 4.

6. Model a virtual test representing the physical testing of the Honda engine

7. Tune the virtual model to match the physical test results

These steps are also used as a guide for the content and composition of this thesis. Chapter 3 presenting FEDEM and the previously developed virtual test bench, and subsection 9.1.2 presenting the modeling and meshing of the OEM connecting rod, are sourced from my recent project work on the matter.

Chapter 2

Literature Review of Previous Work

2.1   Literature Search

Various papers were obtained using the NTNU Oria search engine available at
http://ntnu.oria.no/. The search engine searches NTNU's library resources, both printed and
digital. It has access to a number of online engineering databases and contains books, articles,
papers, theses, etc. The literature reviewed in this thesis was found using the following keywords
when searching with Oria: engine + friction, piston + friction, engine + viscous, "connecting
rod" + oil, "connecting rod" + lub*, and "connecting rod" + drag.

In addition to the literature obtained through Oria, a number of relevant papers were provided
by Professor Terje Rølvåg. This includes unpublished work by Rølvåg and Bella [19]. The
FEDEM Virtual Test Bench is developed and presented in their paper, and its potential is
demonstrated by benchmarking a Honda OEM steel connecting rod and a MXRR titanium
design. This was done using a single test run to capture the most critical load cases. The
results show the advantages of reducing the connecting rod mass in terms of ten different
key performance indicators related to both structural integrity and performance. The paper
demonstrates the benefits of using the FEDEM approach for the design of a connecting rod,
with ease of use in addition to short development and simulation time. The approach enables
race teams to benchmark existing engine components against new concepts before prototyping
and physical testing, saving development time and significantly reducing the costs involved.
The FEDEM Virtual Test Bench was proven to be a robust, accurate, and efficient tool for
connecting rod design and testing. Information on the inner workings of the FEDEM Virtual
Test Bench is reviewed and presented in chapter 3.

2.2   Daniels and Braun:
Friction Contributions During Warm-up

A paper by Daniels and Braun [5] presents the friction behavior of individual components of a 2
L four-cylinder gasoline engine during warm-up from 25 °C to 85 °C. The engine was installed in
the test apparatus in brand new condition, without a wear-in period. The engine temperature
was controlled by heating both engine oil and coolant in custom plumbing systems, with the
water temperature being raised approximately 40 °C an hour. An electric motor together with
a belt drive transmission made the test rig capable of driving the engine at speeds up to 6000
rpm, but the tested speeds were 1100 and 1700 rpm (due to idle speed proximity). An in-line
shaft torque meter was used to measure the torque necessary to drive the engine. The torque
meter was placed between the engine and the belt drive transmission and connected by two
torsionally rigid single-flex couplings to remove damping of instantaneous torque. This allowed
for accurate torque measurements as a function of crank angle with good angular resolution.
A signal conditioner with a low-pass filter was use to remove any signals over 500 Hz. Overall,
the data acquisition system had a repeatable error of ±1.19 Nm. Two thermocouples (one in
the oil pan and one in a spark plug port) together with a pressure transducer in a spark plug
port were non-intrusively installed in the engine. Cold junction compensation was used for the
thermocouples, and the pressure transducer had internal temperature compensation.

The first motoring test was performed on a complete engine without the internal water pump. Using the strip method, parts were removed and the test re-run to investigate the contribution of the parts in question. The difference in the measured torque before and after the removal of a part was taken as the part's contribution. The first parts to be removed were the intake and exhaust manifolds, and the spark plugs. Then the valve train train was removed. Next, the piston and connecting rods. The final test removed the oil pump as well, leaving only the crankshaft to be tested. This test scheme revealed the friction effects of pumping losses, valve train assembly, pistons and connecting rod assembly, oil pump, and crankshaft.

Test results at 1100 rpm revealed that the cylinder pressure at TDC did not show any trends with increasing engine temperature. The recorded torque measurements clearly showed peaks and troughs as the engine crank was rotated, and the cycle-averaged values were used for the strip test comparisons. Torque peaks occurred at 17 and 204 degrees after TDC, where all four pistons were accelerating. The peak in motoring torque just after TDC was attributed to the piston rings encountering a thicker oil film on the down-stroke. The thicker film tries to push the piston rings inwards, but radial movement is opposed by the friction between the piston and the rings under high cylinder pressure. Minimum torque was recorded at 139 and 324 degrees after TDC, where all four pistons were at their maximum velocity.

Test results at 1700 rpm revealed that measured torque still showed peaks and troughs, but the peaks occurred at 22 and 208 degrees after TDC, still being attributed to piston ring–oil film interaction. Minimum torque was recorded at 78 and 246 degrees after TDC, with all four pistons at peak velocity. Increasing the test speed from 1100 to 1700 rpm caused an increase in measured torque by an average of 4.9% in the tested temperature range (complete engine assembly).

Piston and connecting rod assembly contributed the most to engine losses. The valve train assembly's contribution to Friction Mean Effective Pressure (FMEP) was 19% at 1100 rpm and 13% at 1700 rpm. The crankshaft's contribution was 11% and the oil pump's 9% at both speeds. When spark plugs and manifolds were removed from the engine, the cycle-averaged motoring torque was observed to increase. The reason for this being that without spark plugs, no cylinder pressure was helping the power stroke, and extensive pumping of air through the spark plug holes resulted in increased losses. Engine temperature was found to have a significant impact on engine losses. In the case of the complete engine, at both engine speeds, FMEP was reduced by approximately 26% as engine coolant temperature was raised from 25 °C to 85 °C. The piston and connecting rod assembly was responsible for a large portion of this reduction, 76% at 1100 rpm and 46% at 1700 rpm. The FMEP contributions of the oil pump and crankshaft were also reduced at 85 °C. The oil pump reduction was 35% at 1100 rpm and 69% at 1700 rpm. The crankshaft reduction was 84% at 1100 rpm and 57% at 1700 rpm. The valve train assembly did not show a significant reduction in FMEP contribution as the temperature increased, but the authors noted that this was an expected result from a roller-follower type valve train.

2.3   Fadel et al:
Direct Measurement of Piston Friction

Fadel et al. [8] investigated the piston assembly friction force in a single-cylinder engine using motoring and direct measurement. The engine's cylinder head was removed and the cylinder machined to accommodate a steel sleeve. The cylinder liner was mounted inside the sleeve by means of a protruding edge and a slight slope in the steel sleeve's inner surface. The sleeve did not contact the engine block, but was carried by two 3D load cells mounted diametrically opposite each other (at the thrust and anti-thrust sides) near the TDC. Near the BDC, three 1D load cells were equally spaced around the steel sleeve to prevent any rotational motion. These load cells did not carry any of the sleeve's weight. The shell and liner mounting system allowed for direct measurement of the occurring friction forces in all three directions. As a consequence of the modification done to the engine bore, the bore size was reduced to 59.96 mm. This required the use of a different piston than the one used in the unmodified engine. A piston with 59.76 mm diameter was chosen and installed in the modified engine. A brushless servo motor, capable of producing 111 Nm of torque at a maximum speed of 3000 rpm, was used to motor the modified engine. A torque transducer was used between the engine's crankshaft and the electric motor to measure the torque during engine testing. The use of an optical encoder on the crankshaft enabled data collected from the load cells to be matched with crankshaft position, with 2048 pulses per crank revolution. The measurement software (LabView) used the time between the optical encoder's pulses to calculate the crankshaft velocity.

As a consequence of using a freshly machined parts for the test rig, the engine had to go through a break-in period to smoothen rubbing surfaces. After 60 hours at room temperature (21 °C) with SAE 40 grade oil and the motor running at 320 rpm, the friction profile from the measurements became repeatable, indicating that the break-in was complete. Measurements collected 2 hours into the break-in procedure revealed that large spikes in the friction force appeared at TDC and BDC (87 N and 109 N respectively). Friction between the dead centers settled at a lower value, independent of piston velocity. These results indicated a mixed lubrication regime, with a boundary regime (metal contact carrying the contact pressure) occurring at the dead centers. Towards the end of the break-in period, the piston assembly displayed boundary, mixed and hydrodynamic lubrication regimes during a complete engine cycle. Hydrodynamic lubrication was observed around the mid-strokes, where a decrease in piston velocity resulted in reduced friction force.

After completion of break-in, tests were conducted at room temperature to examine the coefficient of friction. Each test run lasted under a minute, and they were separated by sufficient time to keep the test rig at room temperature at all times. The coefficient of friction was determined at 77 degrees before, 2.5, and 77 degrees after TDC. The 77 degree points was the location of maximum piston velocity during the up- and down-strokes. The coefficient values, plotted in a Stribeck diagram, revealed that both boundary and mixed lubrication were dominant at TDC when SAE 10 and 20 oils were used. Using SAE 30 and 40 showed boundary, mixed and hydrodynamic lubrication regimes, and SAE 50 and 60 showed only mixed and hydrodynamic lubrication regimes. The piston assembly operated in a hydrodynamic lubrication regime during the down-stroke (where the liner is generously covered with oil) and mixed and hydrodynamic lubrication regimes during the up-stroke, resulting in different coefficients of friction for the up- and down-strokes. The coefficient was observed to decrease with increasing

oil grade under both boundary and mixed lubrication regimes, but increase with increasing oil viscosity during hydrodynamic lubrication. The maximum friction force and its location was found to be governed by the lubrication regime. During dominant hydrodynamic lubrication, maximum friction was found at maximum piston velocity. In the case of boundary and mixed lubrication, maximum friction was found at the dead centers. Engine teardown tests were performed to investigate the effect of different piston ring configurations on the friction force and lubrication regime. The tests revealed that under motored conditions, the oil control ring was the main contributor to the friction force. The piston skirt was found to contribute the least to the total friction of the piston assembly.

2.4   Gore et al: Floating Liner Piston Friction Measurement

Direct measurement of piston friction using the floating liner principle was performed by Gore et al. [12]. A Honda CRF 450 R four-stroke single-cylinder motocross engine was modified with a floating liner and connected to a dynamometer through the transmission, engaged in second gear (4:1). Chamber pressure, air to fuel ratio, test cell humidity, test cell temperature, input temperatures of the fuel and the coolant, as well as friction force, were logged during testing. The cylinder liner was suspended so that three piezoelectric load cells (120 degree spacing) could measure the forces occurring between the liner and rigidly mounted components. The pre-load seen by the load cells when the engine is stationary was measured so that during testing, the difference between the load cell measurements and the pre-load was taken as the net friction force produced. Finite element analysis was performed to ensure that the resonance frequencies of the test apparatus were not reached during engine testing speeds. A labyrinth seal was utilized at the top of the floating liner, to ensure that the cylinder pressure did not act on the floating liner, and to ensure smooth frictionless operation at the liner top rim. As the labyrinth seal did allow for some cylinder pressure leak, a pressure transducer was used to measure the leakage pressure and use this to correct the actual liner pressure load. A testing procedure was performed to ensure the operational integrity of the floating liner system.

The cylinder pressure generated at 2500 rpm was around 19 bar for the Honda CRF 450 R engine. The maximum pressure occurred at TDC. Friction values measured at BDC for the transition between power and exhaust strokes differ from the values at the BDC during the intake to compression stroke transition. The higher friction in the power stroke to exhaust stroke transition was attributed to a higher pressure gradient change.

A strip-test was performed to investigate the effect of the piston rings (compression and oil control rings). Removing both rings resulted in the piston skirt being the only source of piston-liner friction. Stipulated Poiseuille shear friction occurred precisely at BDC, and not slightly delayed as in the case with piston rings. This indicated that the compression ring maintains a pressure gradient during normal operation, affecting Poiseuille shear of the oil film. Without piston rings, it was observed that the friction at the mid-strokes and piston reversal was reduced due to oil flooding. With the compression ring installed, the peak transition friction occurred closer to piston reversal. The results indicated that piston-liner friction is dominated by compression ring sealing at piston reversals, particularly the transition between

the compression and power strokes. At the transition between the exhaust and intake strokes, and the BDC reversals, Poiseuille shear was determined to be the governing source of friction. For most of the engine cycle, lubrication shear (Couette flow or Poiseuille flow) was determined to be the main contribution to the friction force. The exception was the TDC transition from the compression stroke to the power stroke.

Fired tests revealed that the oil film thickness and the friction due to viscous shear was reduced as a consequence of lower effective viscosity (associated with increased temperature). Friction at dead centers and during the power stroke increased as the thinner oil film enabled boundary lubrication regimes. The viscous shear friction near TDC under compression was significantly reduced due to the higher side load seen by the piston. This caused better sealing for the compression ring and thereby a lower pressure gradient. The Poiseuille shear influence was significantly reduced compared to motored tests. It was noted that the unbalanced nature of a single-cylinder engine introduced some vibration and noise in the measured data.

2.5   Johnson et al: Reducing Rotating and Reciprocating Mass

In a paper by Johnson et al. [15] the impact of reduced rotating and reciprocating mass on throttle response in a four cylinder, four-stroke motorcycle engine was investigated. Two Honda CBR600F4i engines were built and tested, the only differences between them were that one engine contained lighter connecting rods and crankshaft, and had gears five and six (including cogs and shift forks) removed from the gearbox. The total weight reduction was 4.17 kg, with 4.04 kg defined as rotating and reciprocating mass. The engines were tested in a Formula SAE race car, where dynamometer readings were used to plot power and torque as a function of rpm, and speed as a function of time.

A linear interpolation of the speed-time curves revealed that the throttle response (defined as the rate of increase in vehicle speed) was 17.74% higher in the engine with a lower amount of rotating and reciprocating mass. The maximum speed was also higher for the lighter engine, and the power and torque increased by 8.4% and 7.0% respectively. The overall conclusion was that reducing reciprocating and rotating mass will increase throttle response, maximum speed, torque, and power. All beneficial effects in a high performance race engine. An anomaly in the results was that between 0 and 0.6 seconds, the heavier engine appeared to accelerate faster than the lighter one. The authors suggested that slight variation in engine output and (manually actuated) throttle position combined with low resolution of the data acquisition device might be the explanation. (Note: Figure 1 and 2, and possibly figures derived from them seems to be mixed up, and a typo referring to which engine is stock and which is modified exists in the text).

2.6   Meng et al: Effects of the Connecting Rod Design

Effects of the connecting rod-related design parameters on the piston dynamics and the skirt-liner lubrication were investigated by Meng et al. [17]. Based on a new analytical model, side force, oil film thickness, frictional force and piston dynamics were investigated for engine speeds of 6000 rpm and 2000 rpm.

Reducing the connecting rod's mass and rotational inertia resulted in a decrease in the secondary motion amplitude and total side force amplitude generated as the engine runs, the exception being at the combustion top dead center. In that case, the total side force was increased, as less inertia force was available to to counteract the transverse force from the piston during combustion. The minimum oil film thickness (MOFT) decreased as a result of having more side force to support, causing a larger friction force at that position.

Varying the location of the center of mass of the connecting rod also had a significant impact on the transverse force. Moving the center of mass closer to the small end resulted in an increase in transverse force amplitude during the upper half-stroke and a decrease during the lower half-stroke. The opposite was observed for moving the center of mass closer to the big end. For the piston position immediately after combustion, moving the center of mass towards the big end caused an increase in peak side force and friction, and a reduction in MOFT. Increasing the length of the connecting rod was observed to have a similar effect to moving the center of mass towards the small end. The amplitude of the transverse force increased during the upper half-stroke and a decrease during the lower half-stroke. The MOFT right after combustion was found to increase with connecting rod length, lowering the friction at that position.

Changing the piston offset had a significant impact on piston secondary motion, and it was observed that as the offset changes from the thrust to the anti-thrust side, the piston secondary motion changes from swinging clockwise to anti-clockwise. Moving the piston offset closer to the thrust side of the cylinder tends to increase the transverse force in the intake and power strokes, but decrease it in the compression and exhaust strokes. Piston offset closer to the anti-thrust side tends to have the opposite effect. It is also noted that the peak side force declines as an effect of this, but the minimum friction loss occurs with a slight offset towards the thrust side.

In summary, the connecting rod's mass, rotational inertia, position of the center of mass, and length, had great influence on the extra transverse force from the connecting rod and the total side force. The influence on the friction force, oil film thickness and the piston's secondary motion was however not too significant. Parameters such as piston pin offset and vertical connection point position (between connecting rod and piston) had a much greater influence on these aspects. It was noted that the vertical connection point position had a negligible effect on the extra transverse force and the side force, but the piston pin offset had some influence. Results from 6000 rpm and 2000 rpm were similar, but the influence of the center of mass position on the side force at 2000 rpm was small.

2.7 Mufti:
Total and Component Friction in an Engine

The PhD thesis by Mufti [18] involves extensive tests and analyses regarding engine friction, both theoretical and experimental. The main focus of the research was to validate an engine friction model called Friction and Lubrication Analysis Model for Engines (FLAME), developed in a separate study. The three major systems contributing to engine friction were examined: Valve train, piston assembly, and bearing friction. The work related to valve train friction is not described in detail in this review, as it is not directly applicable to the modeling performed in this thesis.

A single-cylinder Ricardo Hydra test engine was used in the experimental work. The engine was instrumented with pressure transducers to measure cylinder pressure, temperature sensors, valve train pulley torque transducers, a rotation encoder, and a strain gage on the connecting rod shank. Indicated Mean Effective Pressure (IMEP) was used to measure piston assembly friction. Engine crankshaft bearing friction during fired engine operation was found using a PV-diagram to measure total engine friction, and subtracting piston assembly friction (using IMEP) and valve train friction (using pulley torque transducers). Engine friction was analyzed during both motored and fired tests, at 800, 1500 and 2000 rpm. Two different engine oils were used, SAE 5W-30 with friction modifier and SAE 0W-20 without friction modifier. Tested oil temperatures were 24 °C, 40 °C, 60 °C, and 80 °C, and the oil used for FLAME validation was the SAE 0W-20 without friction modifier.

The motored tests were run right after the fired tests, resulting in close to normal operating temperatures. A drop in surface liner temperature of 3 - 5 °C was still noted, and the piston assembly friction during motored conditions was lower than during fired conditions. This was attributed to the effect of combustion pressure and temperature during the power stroke, as a higher liner contact pressure along with increased temperature (reduced viscosity) promotes boundary lubrication, increasing friction. During the exhaust, intake, and compression strokes under motored conditions, the decreased temperature resulted in decreased friction at low viscosity as the lubrication changed towards pure hydrodynamic.

It was concluded that low oil temperatures promote hydrodynamic lubrication in the piston assembly. Friction decreased with increasing oil temperature up to a certain point, where transition from hydrodynamic to mixed/boundary lubrication became a factor and the friction started to increase. At low temperatures, the piston assembly friction for SAE 5W-30 with friction modifier was higher than for SAE 0W-20 without friction modifier due to higher shear losses. The effect of the friction modifier was found to be beneficial as the lubrication regime transitions towards mixed lubrication. Increasing the engine speed was seen to improve the piston ring lubrication around dead centers, but increase the power loss from the piston skirt. Both oil grades tested showed a decrease in engine bearing friction with increasing oil temperature, and the oil grade with the highest viscosity resulted in the highest friction loss, characteristic for hydrodynamic lubrication. The engine bearings were found to be the largest contributor to engine friction at low oil temperatures, but at high temperatures, the piston assembly was the largest contributor.

Using the FLAME model was seen to overpredict the piston skirt friction (due to excessive

shear loss), as it did not account for piston secondary motion. The piston and the cylinder was assumed to be concentric at all times. Using a different approach, Leeds Piston Skirt Lubrication and Dynamics Analysis (accounting for secondary motion), showed a better correlation with measured data. The oil control ring was assumed to operate under boundary lubrication regardless of oil temperature and engine speed. This might not be an accurate assumption, as FLAME was seen to overpredict the piston assembly power loss. Three different FLAME engine bearing fiction models (short bearing theory, finite width method, and Petroff zero eccentricity method) were compared to measured results. Short bearing theory provided the best fit. Power loss from the bearings was underpredicted at 80 °C oil temperature. It was mentioned that the true oil temperature in the bearings might differ from the bulk temperature (due to cooling as it travels through the engine), and that this might be responsible for reduced viscosity and increased loss during physical testing. Crankcase bearing seals were also mentioned as a possible source of inaccuracy. FLAME did not include these in the predictions.

2.8 Rohr et al: Observing FMEP Differences Between Oils

Rohr et al. [20] investigated the feasibility of observing small differences in Friction Mean Effective Pressure (FMEP) between different lubricating oil formulations. A Hatz 517 cm^3 single-cylinder air-cooled diesel engine was motored at 1800 rpm by an electric motor, and the required torque was measured by a torque meter installed between the engine and motor shafts. Thermocouples were used to measure engine temperatures at the oil sump, crankcase, valve cover, top dead center of the liner, and mid-stroke of the liner. A pressure transducer was used to measure oil pressure, and a hollow shaft incremental encoder enabled measurement of the crank angle. The engine temperature was controlled with an enclosure and a cartridge heater installed in the oil sump. The cartridge heater was limited to 150 °C to avoid damage to the oil. Testing started at 20 - 25 °C room temperature and liner temperature could be increased to 75 °C. The average torque over 300 revolutions was used to calculate FMEP. Motoring torque was seen to vary with crank angle from approximately -5 Nm to 15 Nm, resulting in a average torque of ~5 Nm.

FMEP was plotted as a function of dynamic viscosity for SAE 10W-30 and SAE 5W-20 engine oils in three stages of production: Base oil, improved commercial oil without friction and wear reducing additives, and fully formulated commercial oil. Vogel's equation was used to calculate the dynamic viscosity at mid-stroke cylinder liner temperature. Linear regression and average FMEP (over all tests for an oil) was also used to easier compare different oils, and a SAE 5W-30 commercial engine oil was used to examine repeatability of the test. Engine oil was flushed between tests to minimize mixing of different oils.

The engine was broken-in prior to testing, and two different configurations were used. Pushrods, tappets, and intake valve were removed so that the engine could be motored without compression, only breathing through the intake and air filter. This configuration tested the piston assembly, main journal bearings, timing gears, piston pin, connecting rod bearings, and the internal oil pump. For the second configuration, the internal oil pump was replaced with an external electric one, and the timing gears were removed. The SAE 10W-30 oil was tested in

the first engine configuration, with the internal oil pump. Lack of repeatability due to internal oil pressure relief valve malfunction was observed, so the second configuration with external oil pump was used for testing the SAE 5W-20 oil. The change in test configuration caused a change in expected FMEP (due to fewer parts) so the results for the two different oil grades were not directly comparable. The same trends were however evident.

The base oils were seen to have the highest friction at a given viscosity, but the lowest average FMEP, and the commercial oils with additives had the lowest friction at a given viscosity, but the highest average FMEP. The fully formulated oils had higher friction at a given viscosity and a higher average FMEP than the oils without additives. It was noted that equal viscosities for the oils did not occur at the same time or temperature in the tests. The reason for the base oils low average FMEP was attributed to their generally lower average viscosity reached during testing. The viscosity difference between improved and fully commercial oils was not significant, highlighting the additives effects on the FMEP. The commercial oils without additives had slightly lower friction than the fully formulated versions, indicating that the additives were more optimized towards wear reduction than friction, or that the engine operated outside the optimal regime of the tested oils. The authors concluded that observing small differences in FMEP due to engine oil is feasible using a small motored single-cylinder engine.

Chapter 3

FEDEM Overview

3.1 FEDEM Software Package

Conventional Finite Element (FE) programs usually have difficulties estimating and modeling combustion and inertia forces. This results in the need for Multi-Body Simulation (MBS) software to perform this task. As a result, data needs to be transferred between different programs, with added complexity and chance of errors. This also neglects stress stiffening effects occurring at high rpm during the simulation. Using Flexible Multi-Body Simulation (FMBS) software allows the use of flexible modes in the simulation, but requires the analyst to know and incorporate the correct modes. The dynamic behavior and flexible mode amplitudes can then be used in a FE program to calculate stresses [19]. Using an integrated nonlinear FE program (such as FEDEM) eliminates any errors from data transfer, and stress stiffening, gyro, and Coriolis effects are taken into consideration. Usually, these considerations result in a high computational cost, but FEDEM uses model reduction techniques to help reduce simulation times [9, 19].
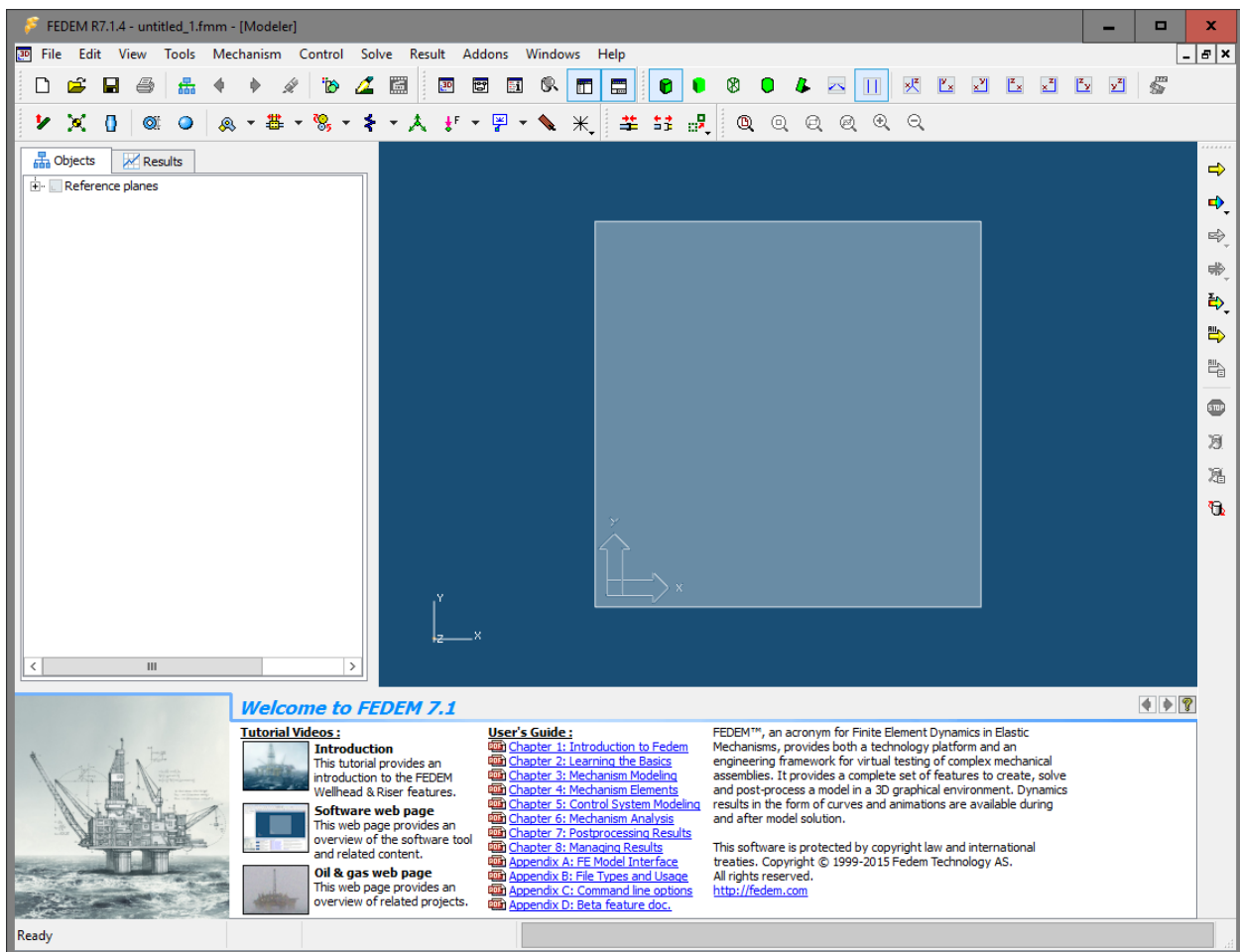

Figure 3.1: FEDEM environment

FEDEM (Finite Element Dynamics in Elastic Mechanisms) is a software package capable of virtual testing of complex mechanical assemblies. FEDEM includes tools for model creation, simulation solving, and post processing of results. Plots and animations are generated and can

be viewed both during and after solution. The post processor enables full stress analysis, eigenmode calculations, strain gage solutions, and fatigue analysis for selected time steps. FEDEM solutions assume elements with linear material parameters (no yielding effects are considered), but the problem is solved as a nonlinear case due to the dynamic effects and the large geometric variations. The parts used in a FEDEM simulation can be made in the integrated modeler or imported as FE models. Each part is reduced (by FEDEM) to a superelement with a co-rotated frame, for separation of elastic and rigid body movement. The mass matrix is Component Mode Synthesis (CMS) reduced, and therefore remains fully populated. This allows gyro effects to be correctly represented. FEDEM uses the Newmark-β and HHT-α (Hilbert Hughes Taylor) time integration algorithm to solve the dynamic equation with respect to displacement increments. Iteration with the Newton-Raphson method is used to correct nodal displacements and modal amplitudes towards equilibrium before the next increment is solved [9, 19]. Control parameter equations are solved with Runge-Kutta methods. An overview of the FEDEM program environment can be seen in figure 3.1.

3.2   FEDEM Virtual Test Bench

The FEDEM Virtual Test Bench (FVTB) consists of a model containing the setup for two sets of connecting rods, crankshafts, flywheels, pistons, piston pins, and balance shafts for single-cylinder four-stroke Honda CRF 250 R motocross engines (figure 3.2). This enables a comparative study of two different connecting rods (ex: OEM vs. optimized) in one simulation run. FVTB has a full control system for the simulation cycle, allowing customized case studies, data extraction and manipulation. The control system includes electric starters, power control, sensors, and actuators, enabling closed loop control [19]. In addition to this, a .dll file controls ignition timing and cylinder pressure cycles, effectively powering the engine. The user inputs for this .dll file is seen in figure 3.3, and the resulting pressure cycle is seen in figure 3.4. Input variables and outputs from FVTB are listed in table 3.1 and table 3.2 respectively.

Discipline	Variable
Mechanism	Part, joint, gear, spring, damper, friction, sensor, and actuator properties
Structural	Mesh density, element types, material and damping properties, and fatigue properties
Control	Filter and transfer functions properties, logical switches, PD, PI and PID engine controller properties (electric starter)
Loads	Torque vs. rpm curves, combustion pressure distribution vs. stroke, rpm limiter properties, and crank reference speed

Table 3.1: FVTB input variables [19]

Discipline	Output
Mechanism	Piston and crank translational and rotational position, velocity and acceleration, bearing loads, and output torque
Structural	Stress and displacement distributions for selected or all parts, vibration modes (parts or assembly level), and fatigue life
Control	Electric current, voltage, applied energy or power, sensor inputs, and actuator outputs

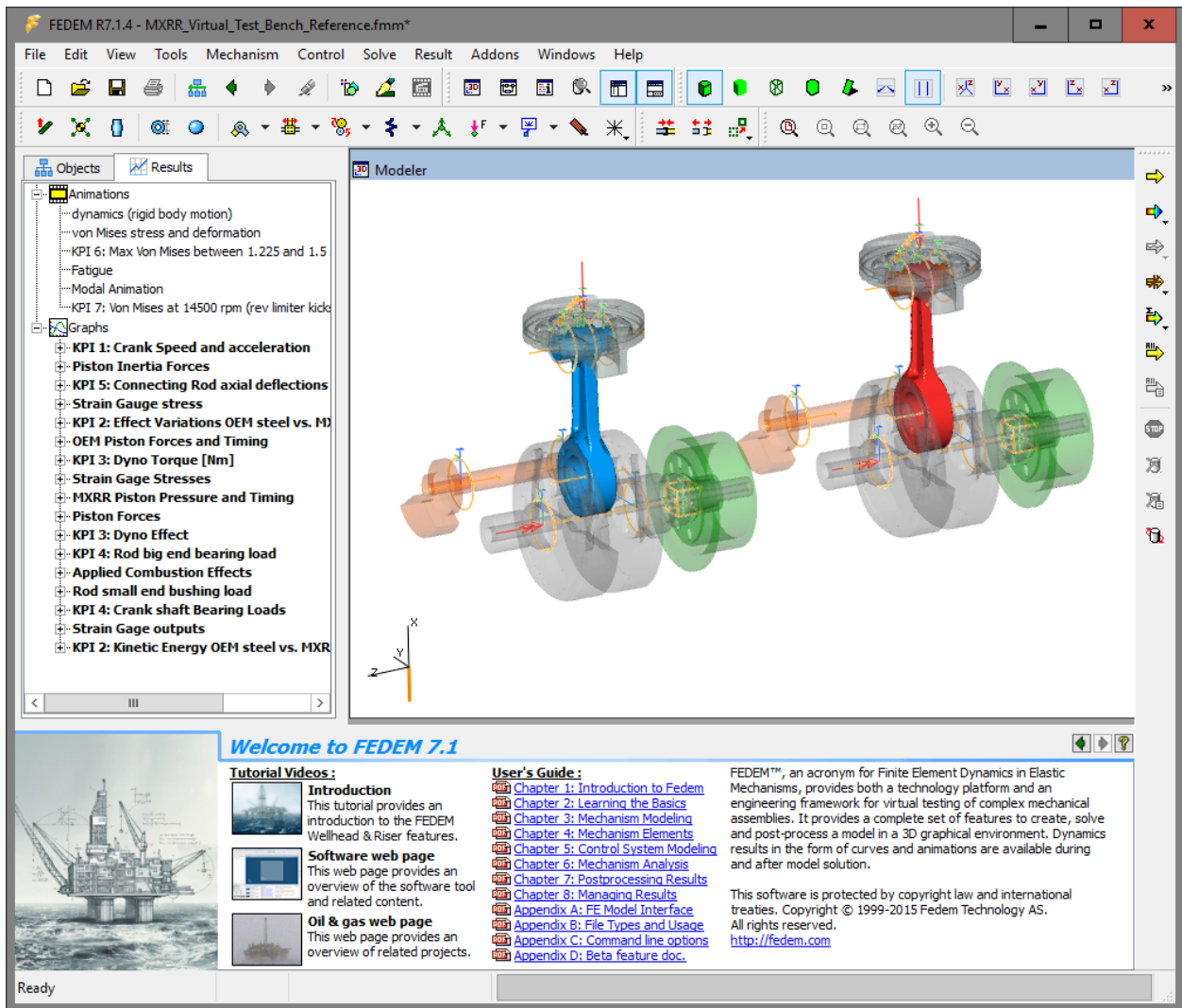Table 3.2: FVTB outputs [19]

Figure 3.2: FEDEM Virtual Test Bench

Using the post processor, it is possible to retrieve stresses at chosen time steps or crankshaft angles. Animating deflections and stress distributions is also possible. Modal analysis can be performed at different engine speeds, and includes the effects from stress stiffening. In terms of fatigue, virtual brittle lacquer and S-N curves can be incorporated to evaluate the life expectancy of components. Damage plots can be shown and hot spots identified. Strain gages can be applied to hot spots to monitor their conditions, without having to perform a strain analysis of the complete model. A wide number of output plots are available, including, but not limited to: bearing loads, crankshaft speed, engine brake torque, engine brake power, axial displacements, energy loss due to connecting rod vibrations, and strain time histories [19].

Using FVTB for optimization of an engine part is quite straight forward, as all of the assembly considerations and component interactions are already established in the model. A design proposal is modeled and meshed in a suitable Computer-Aided Design (CAD) program, and imported into FEDEM as a Nastran finite element file. In the FVTB model, the reference for the part file is updated to the new one. Crankshaft balancing can be performed by changing values for two balancing masses (per crankshaft) using bob weight calculations. The simulation is ready for solving, and the same result output is available for the new design, including the plots and animations generated (adding new ones is also possible). The result might lead the designer to do some design changes, and then start the simulation again. In this way, design iterations are quick and easy. As mentioned earlier, FEDEM uses model reduction techniques before solving the dynamic simulation. The reduction only occurs once for each FE model, and this means that when a new design proposal for a part is imported, this is the only file that needs to be reduced before solving. The other model parts have already been reduced and stored in the previous simulation run, facilitating shorter simulation times.

Crank angle at max combustion pressure [360 degrees is TDC]	373.0
Standard deviation for combustion pressure [15-30 degrees]	17.0
Maximum gas pressure during combustion stroke [MPa]	11.5
Minimum pressure during suction stroke [MPa]	0.1
Maximum pressure during exhaust stroke [MPa]	0.6
Piston Area (set to 1 to get piston pressure) [mm^2]	1.0
Rev. limiter (no ignition above given rpm) [rpm]	14 500.0
Compression pressure (when no ignition) [MPa]	1.2

Figure 3.3: Cylinder pressure cycle parameters
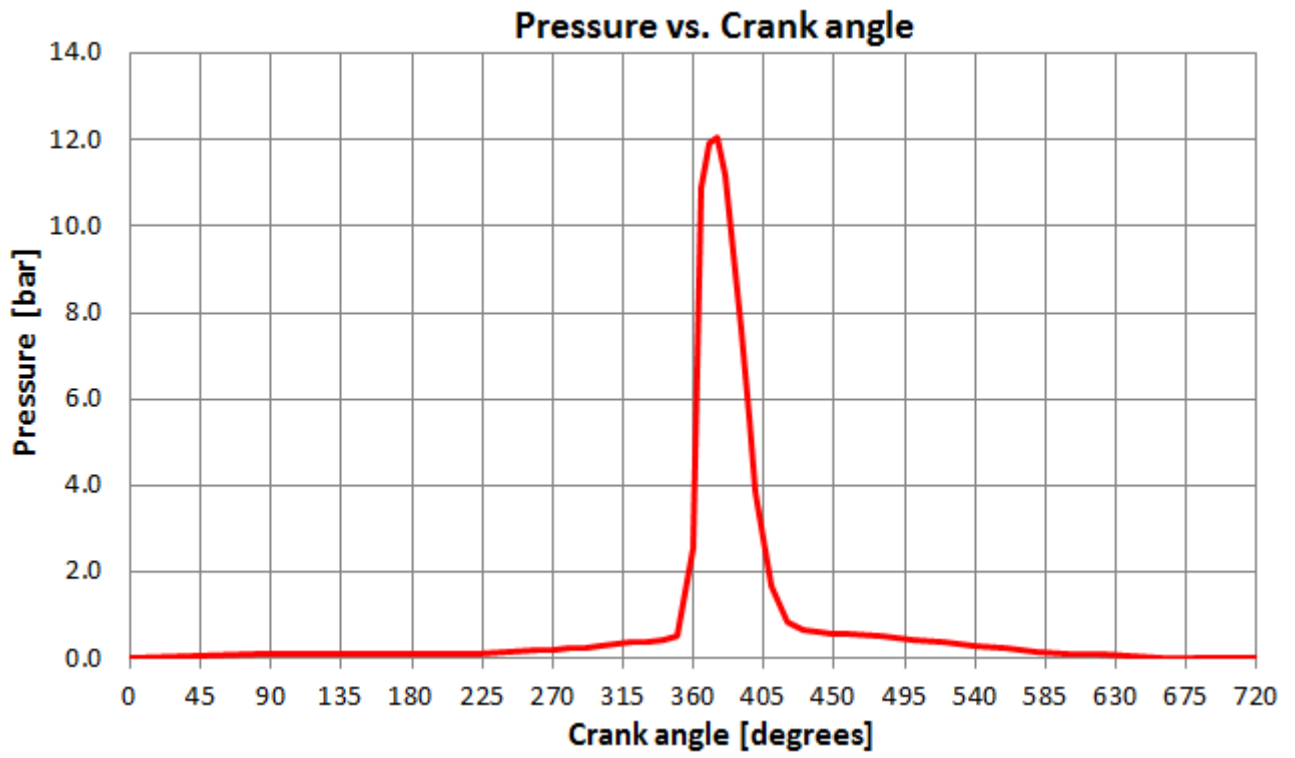
Figure 3.4: Cylinder pressure cycle

Chapter 4

Engine Component Motion and Forces

4.1 Four-Stroke Engine Overview
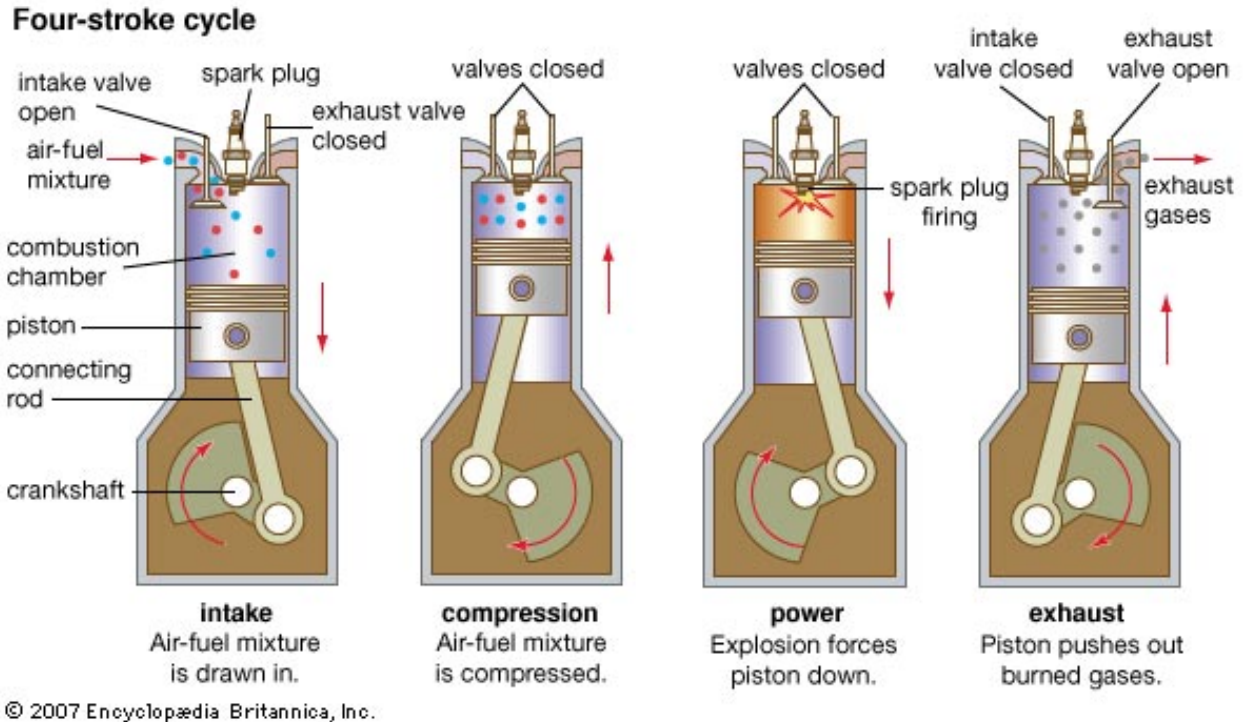
Figure 4.1: Four-stroke engine operation [7]

Figure 4.1 shows the basic operation of a spark-ignited four-stroke engine:

1. Intake stroke: Air-fuel mixture is drawn into the cylinder through the intake valve

2. Compression stroke: The mixture is compressed with both valves closed

3. Power stroke: The mixture is ignited by a spark plug, causing it to expand and force the piston down

4. Exhaust stroke: Combustion gases are evacuated through the exhaust valve.
   After the exhaust stroke is complete, the cycle starts again from the intake stroke.

The piston operates in a reciprocating manner, stopping and reversing its motion at the Top Dead Center (TDC) and Bottom Dead Center (BDC). The connecting rod is responsible for transferring the reciprocation of the piston to the rotation of the crankshaft. This gives the connecting rod a combined motion. The connecting rod is connected to the piston pin in its small end and to the crankshaft in its big end. The connecting rod usually has bearings in both ends, and the crankshaft is connected to the engine block by bearings as well. Figure 4.2 shows an overview of the piston and connecting rod assembly. The movement of the piston assembly is mainly reciprocating along the cylinder axis, but secondary motion (such as tilting and transverse motion) also occurs. This is related to the radial clearance between the piston and cylinder liner and the inertial forces in the piston and connecting rod during

operation. While the piston rings do help center the piston inside the liner, their stiffness are no match for the dynamic forces and pressures encountered in a running engine. Piston rotation about the cylinder axis can also occur, particularly in cases of connecting rod resonance. The thrust side of the cylinder is where it experiences the transverse reaction force as a response to the connecting rod's instantaneous angle when the piston is forced down by the combustion pressure. The anti-thrust side is the opposite one.
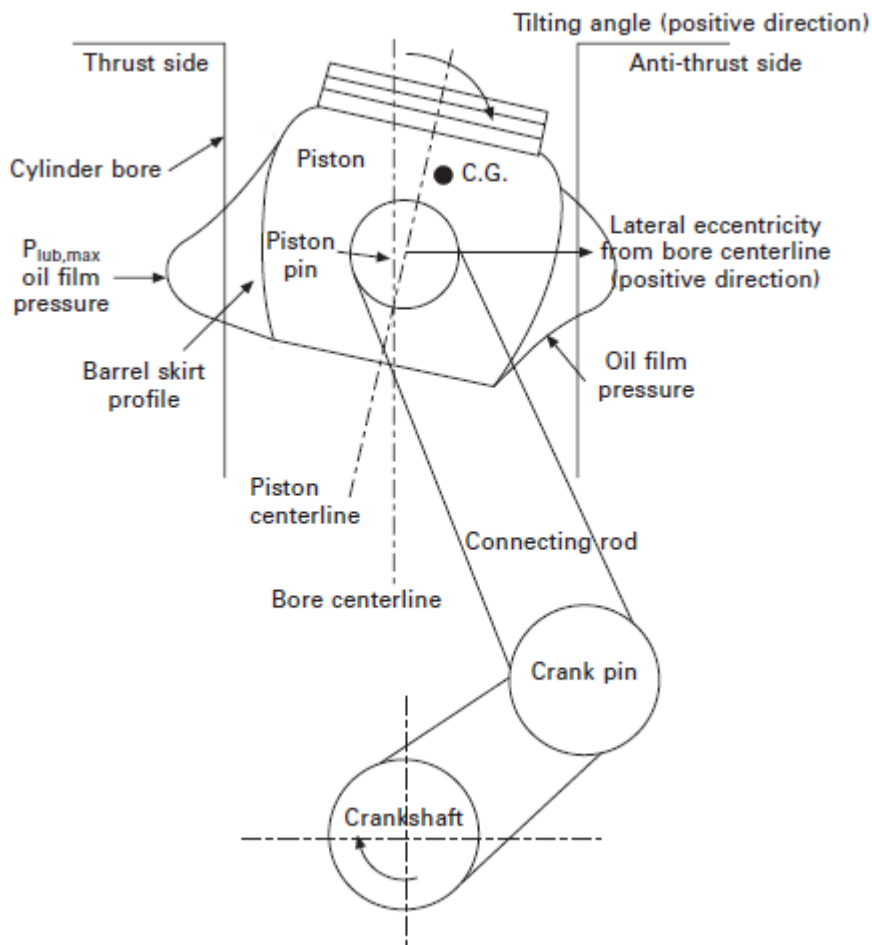
Figure 4.2: Piston and connecting rod overview [21]

4.2 Piston Assembly and Connecting Rod Motion and Forces
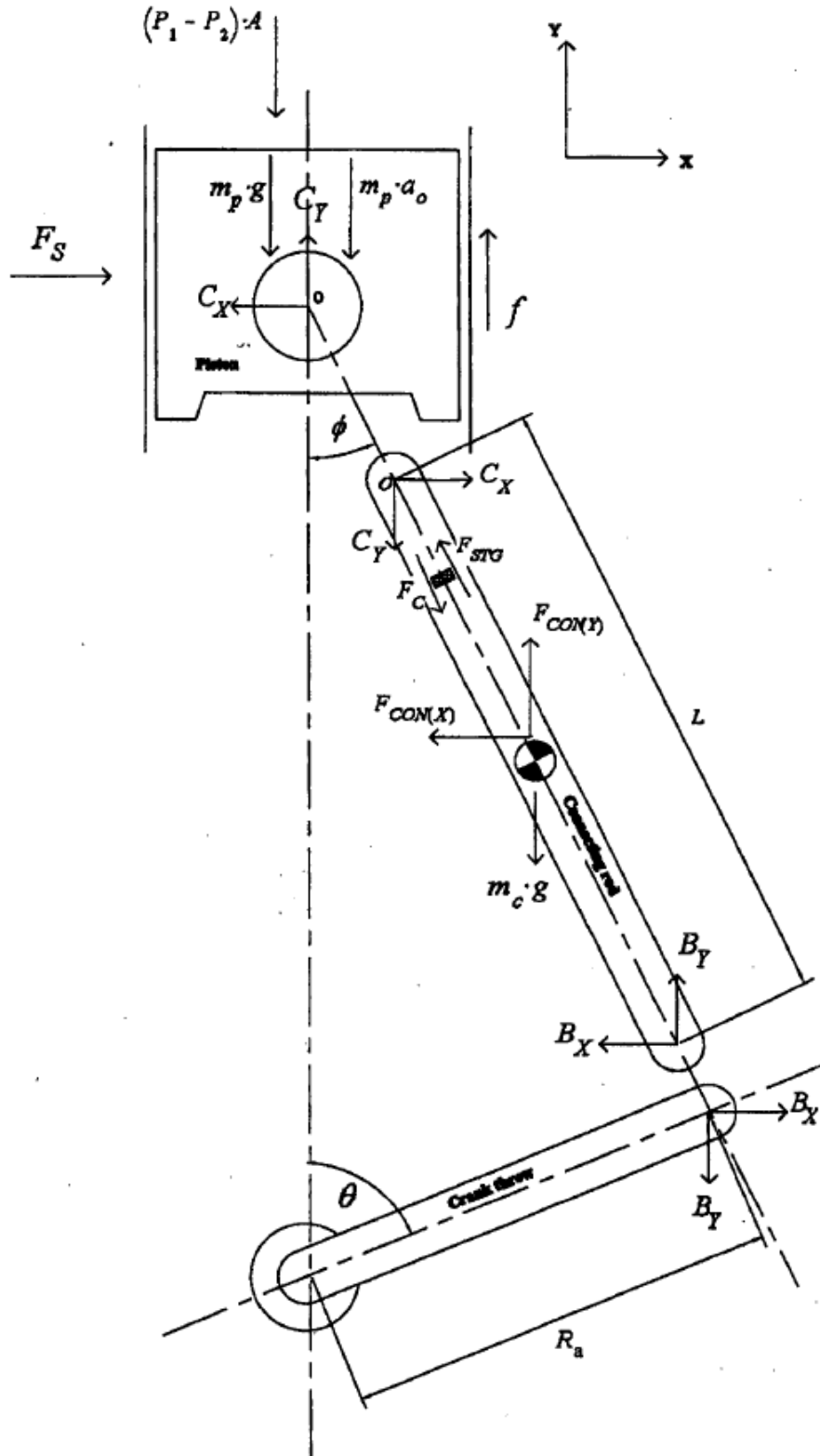
Figure 4.3: Assembly forces [18]

An overview of the forces seen by the piston assembly during its reciprocating motion can be seen in figure 4.3. The piston is subjected to side-force from the cylinder liner, axial and transverse reaction forces from the connecting rod, gravity load, and inertia force arising from the piston's acceleration during a stroke. The cylinder pressure that acts on top of the piston, and the friction from contact between the piston, rings and cylinder liner, both result in axial forces.

The force C_Y, pushing the connecting rod down, is found through equilibrium of the mentioned forces acting on the piston in the Y-direction [18]:

$$C_Y = (P_1 - P_2)\, A + m_p g - f + m_p a_o \tag{4.1}$$

$P_1 - P_2$ is the gas pressure acting on the piston, where P_1 is the cylinder pressure and P_2 is the pressure in the crankcase (on the underside of the piston). A is the cylinder bore area, a_o is the piston's acceleration, m_p is the mass of the piston assembly (piston, piston rings, piston pin and the small end of the connecting rod), f is the piston assembly friction, and g is gravity acceleration.

Solving equation 4.1 for the piston assembly friction yields:

$$f = (P_1 - P_2)\, A + m_p g + m_p a_o - C_Y \tag{4.2}$$

In order to find the friction of the piston assembly using equation 4.2, the pressures in the engine, the piston's acceleration, and the force in the connecting rod (in global Y-direction) need to be known. Values for pressures and connecting rod force can be obtained using pressure transducers and fitting the connecting rod with a strain gage or a load cell. The acceleration of the piston can be found using kinematic relations [18]:

Piston displacement from TDC:

$$S = -R_a \left(1 - \cos(\theta) + \frac{1 - \sqrt{1 - \lambda^2 \sin^2(\theta)}}{\lambda} \right) \tag{4.3}$$

Piston velocity:

$$\frac{d}{dt}S = -R_a \omega \left(\sin(\theta) + \frac{\lambda}{2} \frac{\sin(2\theta)}{\sqrt{1 - \lambda^2 \sin^2(\theta)}} \right) \tag{4.4}$$

Piston acceleration:

$$\frac{d^2}{dt^2}S = -R_a \omega^2 \left(\cos(\theta) + \frac{\lambda \cos(2\theta) + \lambda^3 \sin^4(\theta)}{\sqrt{(1 - \lambda^2 \sin^2(\theta))^3}} \right) \tag{4.5}$$

Where $\lambda = \frac{R_a}{L}$, L being the length of the connecting rod, R_a is the radius of the crankshaft, θ is the crank angle, and ω is the engine's angular velocity. As a result of changes in the

connecting rod angle during the stroke, the piston will move more per crank angle near the TDC (±90°) than near the BDC (±90°). This means that more than half of the piston stroke is done during the first 90° after TDC (this can be seen from equation 4.3). The explanation of this behavior lies in the shortening and lengthening of the connecting rod's projected length along the cylinder axis. As the big end of the connecting rod moves away from the cylinder vertical axis it effectively pulls the piston down, in addition to the downwards movement already imposed by crankshaft rotation. The opposite effect is observed near BDC, where the connecting rod's projected vertical length is increased, moving the piston up (counteracting some of the downwards movement from the crankshaft rotation).

Since velocity and acceleration are derivatives of displacement, they are also influenced by the nature of piston motion. The largest piston acceleration occurs at TDC, where the piston changes direction the fastest. Acceleration at BDC is smaller due to the fact that the piston reversal is spread out over a larger portion of the total crankshaft rotation. This can be observed in figure 4.4, where percent-wise piston acceleration is plotted as a function of crankshaft angle (for chosen values of L and R_a). 0 and 360 degrees correspond to TDC, and 180 degrees is BDC.
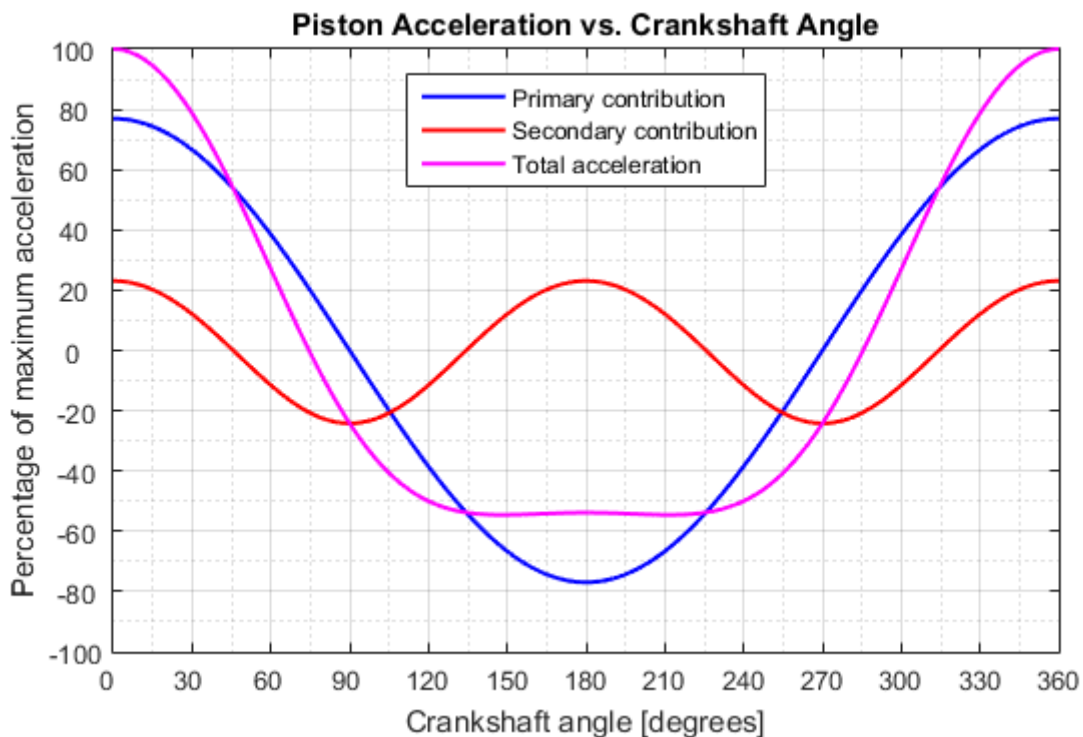
Figure 4.4: Piston acceleration

The primary contribution (first term of equation 4.5) is the acceleration resulting from the rotation of the crankshaft. It has a sinusoidal shape, and occurs once for each crankshaft revolution. The secondary contribution (second term of equation 4.5) is the acceleration resulting from the shortening and lengthening of the connecting rod's projected length along the cylinder axis. This contribution also has a sinusoidal shape, but occurs twice for each crankshaft revolution. The combination of these contributions gives the total acceleration a rather special shape near BDC. Depending on stroke and connecting rod length, different behavior of displacement,

velocity, and acceleration can be expected. If the secondary contribution is large enough, the total piston acceleration can exhibit additional reversals on both sides of BDC, affecting the forces and vibration characteristics of the engine.

Piston (and connecting rod) acceleration is the source of reciprocating forces and vibrations in the engine assembly, and therefore needs to be balanced out as much as possible. Depending on overall engine configuration (type of engine, number of cylinders, bank angle, etc.), the forces can inherently cancel each other out, or need additional balancing weights. For a single-cylinder engine, counterweights on the crankshaft are used to balance the primary forces, and one or two balance shafts (spinning at twice the speed of the crankshaft) are used to balance the secondary forces. This solution is not perfect, as balancing of forces in the stroke-direction by the use of rotating weights, also introduces transverse forces and vibrations.

In a running four-stroke engine, there will be a slight variation in instantaneous engine speed, because power is only supplied during the power stroke. During the exhaust, intake, and compression strokes, the instantaneous engine speed drops slightly. This effect is reduced in engines with several cylinders, as the cycle of one or more cylinders overlaps others. In the case of a single-cylinder engine, the effect is significant and the crankshaft acceleration needs to be taken into consideration. This results in the following equation for the piston acceleration [18]:

$$\frac{d^2}{dt^2}S = -R_a \left[\alpha \left\{ \sin(\theta) + \frac{\lambda}{2} \frac{\sin(2\theta)}{\sqrt{1 - \lambda^2 \sin^2(\theta)}} \right\} \right.$$
$$\left. + \omega^2 \left\{ \cos(\theta) + \frac{\lambda \cos(2\theta) + \lambda^3 \sin^4(\theta)}{\sqrt{(1 - \lambda^2 \sin^2(\theta))^3}} \right\} \right] \tag{4.6}$$

From the kinematics in figure 4.3, the angular position of the connecting rod ϕ and its angular velocity $\dot{\phi}$ is [18]:

$$\phi = \sin^{-1} \left(\frac{R_a \sin(\theta)}{L} \right) \tag{4.7}$$

$$\dot{\phi} = \omega \frac{R_a}{\sqrt{1 - \frac{R_a^2}{L^2} \sin^2(\theta)}} \frac{\cos(\theta)}{L} \tag{4.8}$$

4.3 Big End Bearing Motion and Forces
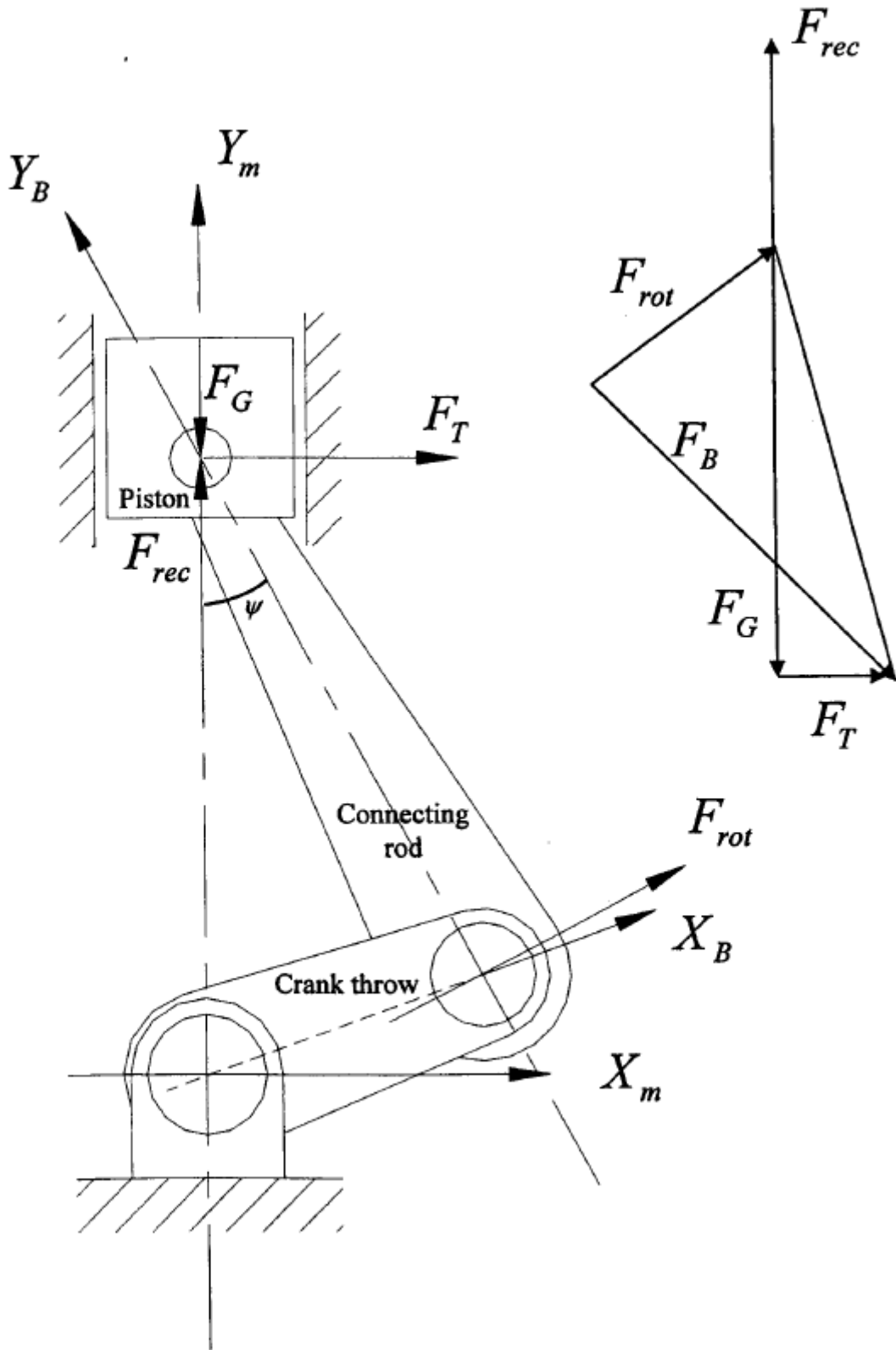
Figure 4.5: Bearing forces [18]

The friction loss from the small end bearing is negligible compared to the losses in the big end and the crankshaft bearings [18]. The big end bearing is subjected to loads from several mechanisms. Mainly the combustion force F_G, the inertia force from the reciprocating part of the connecting rod and piston assembly F_{rec}, and the rotating inertia force from the lower part of the connecting rod F_{rot}. The acceleration of the reciprocating mass is the same as the piston acceleration described earlier, with the crankshaft acceleration term omitted [18]:

$$a_a = \frac{d^2}{dt^2} S = -R_a \omega^2 \left(\cos(\theta) + \frac{\lambda \cos(2\theta) + \lambda^3 \sin^4(\theta)}{\sqrt{(1 - \lambda^2 \sin^2(\theta))^3}} \right) \tag{4.9}$$

If the connecting rod is considered as a two-point mass system (big end and small end), and it is assumed that the small and big ends are responsible for $\frac{1}{3}$ and $\frac{2}{3}$ of the connecting rod's mass m_c, the reciprocating mass (located at the piston pin) can be considered as the mass of the piston assembly plus $\frac{1}{3}$ of the connecting rod's mass. The rotating mass is located at the big end, and is considered to be the remaining $\frac{2}{3}$ of the connecting rod's mass. This means that the reciprocating and rotating inertia force can be calculated as [18]:

$$F_{rec} = \left(m_p + \frac{1}{3} m_c \right) a_a \tag{4.10}$$

$$F_{rot} = \frac{2}{3} m_c R_a \omega^2 \tag{4.11}$$

An overview of the bearing forces can be seen in figure 4.5. The combustion force F_G can be calculated as a function of chamber pressure p and bore diameter D [18]:

$$F_G = \frac{\pi}{4} p D^2 \tag{4.12}$$

Due to the instantaneous angle of the connecting rod, a transverse side-thrust force F_T on the piston arises from the axial forces. Using equilibrium in the transverse direction, the piston side-thrust force can be calculated as [18]:

$$F_T = (F_G + F_{rec}) \tan(\psi) = \left[\frac{\pi}{4} p D^2 + \left(m_p + \frac{1}{3} m_c \right) a_a \right] \tan(\psi) \tag{4.13}$$

ψ being the angle between the connecting rod and piston axes. The resultant force F_B acting on the big end bearing is the vector sum of the forces F_G, F_{rec}, F_{rot} and F_T.

Chapter 5

Engine Friction and Damping Effects

5.1   Sources of Engine Friction and Damping

As mentioned in the introduction, fuel energy is lost in mechanisms that do not contribute to vehicle propulsion. While a significant amount of energy is lost as thermal energy during and after the combustion process, about 12% is used to overcome friction losses in the engine [13]. Due to the complex nature of an internal combustion engine, a wide variety of sources of friction and damping exist:

- Mechanical friction losses

  - Piston assembly

    * Pistons
    * Piston rings

  - Connecting rod system

    * Big end bearings
    * Small end bearings

  - Crankshaft system

    * Crankshaft bearings
    * Oil seals

  - Balance shaft system

    * Driving gear/chain/belt and tensioner
    * Balance shaft bearings
    * Oil seals

  - Valve train system

    * Valve stems and guides
    * Valve stem seals
    * Valve rocker shafts
    * Cams and lifters
    * Camshaft bearings
    * Timing gear/chain/belt and tensioner

- Windage and oil drag losses

  - Connecting rod system
  - Crankshaft system
  - Balance shaft system
  - Valve system

- Pumping losses

  - Intake and exhaust

- – Crankcase pumping

- Auxiliary device losses

  - – Inner auxiliary devices

    * Oil pump
    * Oil supplying gear
    * Distributor
    * Fuel pump

  - – Outer auxiliary devices

    * Water pump
    * Alternator and electrical equipment
    * Cooling fan
    * Auxiliary belt

(This list is inspired by Hoshi [14], but additional items have been added).

The piston assembly is without a doubt the largest source of engine friction. Exact numbers depend on engine configuration, operating speed, load, and temperature, but the relative contributions of different mechanisms in a complete, representative, four-cylinder engine can be seen in table 5.1. Combined, crankshaft and connecting rod bearings and seals account for 30% - 40% of the losses [4, 13, 14].

Mechanism	Percentage of total engine friction	
Piston assembly	38% - 60%	[4, 13, 14]
Crankshaft system	16% - 19%	[5, 14]
Connecting rod system	14% - 18%	[14]
Valve train system	8% - 21%	[5, 13, 14]

Table 5.1: Friction loss contributions in four-cylinder engines

The percentages mentioned in table 5.1 summarize the findings from various papers. Contributions in the lower end of the percentage spans are expected for low engine speeds and loads, whereas higher contributions are expected when the engine is subjected to high speeds and loads (except for the valve train, which shows the opposite trend). Due to differences in engine configurations between these sources, and the fact that the percentages given here are only the largest contributors, the numbers might not add up to 100% for all available choices of values. The values presented are meant to give an indication of the various systems contributions as opposed to exact values. Roughly speaking, one can say that the piston assembly alone is responsible for the same amount of friction loss as the crankshaft, connecting rod, and valve train systems combined.

Windage and oil drag losses are related to parts moving thorough air/gas and engine oil. Depending on engine design, different components might be affected by these losses. Of particular

interest are the connecting rod and crankshaft, and how their designs might affect the drag during high speed operation. The literature search was unsuccessful in obtaining information regarding this matter.

As the piston reciprocates in the cylinder, combustion gases and air are being pumped around in the engine. This pumping action causes drag effects and is the source of the so called pumping losses. These drag effects depend on parameters such as engine speed, throttle position, and valve openings. The pumping losses not only include the intake of air-fuel mixture and expulsion of exhaust gases, but also crankcase pumping losses. Crankcase pumping happens when the air/gas trapped on the underside of the piston is compressed during piston reciprocation. In a multi-cylinder engine, some pistons move up while others move down and this effectively pumps the air/gas between them. Since cylinders are separated in the engine block, the pumping usually happens through the crankcase. Depending on engine design and operating parameters, these losses might have an impact on engine performance. Using a dry sump lubrication design might reduce losses by allowing more room for the pumping action.

The main focus of this thesis is the friction and damping effects related to the piston assembly, connecting rod, and crankshaft. These three aspects are therefore the only ones presented and investigated further in the following sections. It is worth mentioning that the percentage-wise contributions of different engine systems mentioned earlier in this section are largely based on medium sized four-cylinder car engines. The Honda CRF 250 R engine is a small displacement single-cylinder engine, which means that the distribution of friction losses might be different. Only one piston and cylinder means that less energy is lost compared to four, but it also means that the rest of the engine is downsized with smaller and lighter parts in addition to fewer bearings and seals.

5.2   Lubrication Regimes

The three lubrication regimes of greatest importance to engine friction are boundary, hydrodynamic, and mixed lubrication. The boundary regime is characterized by metal to metal contact. In this case, the contact force is carried by the material asperities. Hydrodynamic lubrication occurs when the oil film separating the moving parts is thicker than the combined height of their surface asperities. This means that no metal contact takes place, and that the oil film is entirely responsible for carrying the contact force. If the oil film thickness is equal to or slightly less than the combined asperity height, some metal to metal contact might occur. The mixed lubrication regime is therefore a combination of boundary and hydrodynamic lubrication (as the name suggests), where some contact force is carried by the oil film and some by asperity contact. Common for these regimes is that they relate to the thickness of the oil film, making this the key parameter to determine the lubrication regime under different operating conditions [8]. As the oil film thickness depends on a number of properties such as temperature, contact pressure, surface roughness, and engine speed, these are all important in determining the engine's instantaneous lubrication regime [3].

Newly machined parts can display a large degree of boundary and mixed lubrication due to surfaces with large asperities. During engine break-in, the friction decreases rapidly as as-

perities are worn down. Fully broken-in engines display boundary, mixed, and hydrodynamic lubrication regimes throughout the engine cycle. The piston rings experience boundary and mixed lubrication around the dead centers, where the piston velocity is low, and hydrodynamic lubrication around the mid-strokes, where the piston velocity is high [4, 8, 12, 14]. When the piston moves slowly, it experiences less viscous resistance from the engine oil, making it easier to penetrate the oil film and cause direct metal contact. The piston skirt operates mostly under hydrodynamic lubrication [18].

Under mixed lubrication, the coefficient of friction between the piston assembly and cylinder liner decreases with increasing engine speed, as higher piston velocity results in a thicker oil film and a larger hydrodynamic lubrication effect. When the engine speed is sufficient, this causes a transition to hydrodynamic lubrication. For the piston skirt, already operating in the hydrodynamic regime, an increase in engine speed will result in increased losses [18]. This can be observed in a Stribeck diagram (figure 5.1) where the friction coefficient is plotted as a function of the "duty parameter", $\frac{viscosity \times speed}{load}$. EHD is elastohydrodynamic lubrication, which means that elastic deformation results in separation of the metal surfaces, enabling hydrodynamic sliding. During dominant hydrodynamic lubrication, maximum friction is found at maximum piston velocity. In the case of boundary and mixed lubrication, maximum friction is found at the dead centers [8].
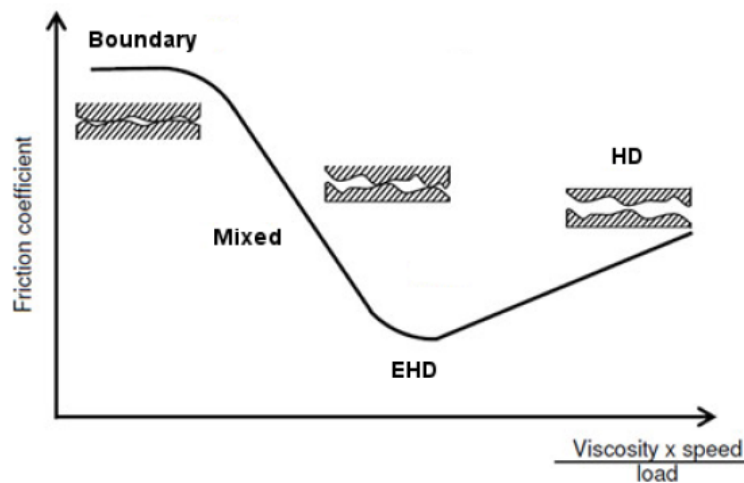
Figure 5.1: Stribeck diagram [4]

In hydrodynamic lubrication, the friction loss is mainly accredited shearing of the oil film and is therefore proportional to the engine speed [5]. In addition to shearing of the oil film through relative movement of the parts (Couette flow), pressure gradient driven shearing (Poiseuille flow) is also involved for the piston when the cylinder pressure increases due to compression or combustion. This increased pressure pushes against the oil film and piston rings, causing an oil shearing effect [12]. It is worth noting that the maximum friction force under hydrodynamic lubrication is significantly lower than the forces in boundary and mixed regimes [8]. Despite the large friction forces associated with boundary and mixed lubrication, these do not contribute to a significant energy loss compared to hydrodynamic lubrication. Hydrodynamic lubrication is responsible for a substantial part of the total engine losses, the reason being that boundary and mixed lubrication usually dominate near the dead centers, a relatively small portion of the

engine cycle compared to the hydrodynamic region. Reducing the friction force at the dead centers is therefore mainly of interest to reduce wear and improve durability [8, 12, 14].

Various modified forms of Reynolds equation are used to describe the hydrodynamic lubrication regime. Using appropriate boundary conditions, the equation can be solved in the three regions of full oil film, oil film cavitation, and oil film reformation. Boundary lubrication friction is usually described by Coulomb friction as [4]:

$$R = \mu \times p \times A \tag{5.1}$$

μ is the coefficient of friction, p is the contact pressure and A is the area of metal contact. The contact pressure can be described by several models, such as Greenwood-Tripp [4, 11].

5.3 Oil Viscosity and Temperature

The total friction force depends largely on oil viscosity and oil film thickness. Because the oil viscosity is temperature dependent, this means that the lubrication conditions and thereby friction force varies significantly as the engine experiences temperature fluctuations during cold start, normal operation and high load [1, 4]. During normal operating temperatures at low speed, the effect of using thicker or thinner oils is minimal. The difference is more pronounced as the engine speed is increased, and severe when the oil temperature is low (cold start). A 50 °C drop in engine oil temperature from normal operating conditions can increase oil viscosity by an order of magnitude [1].

During high speed operation at low oil temperature, the piston friction has a significant impact on the total engine loss, since the oil viscosity is relatively high. As the engine oil warms up, the effective dynamic viscosity is reduced, resulting in lower friction for hydrodynamic lubrication [3, 14, 16]. Friction losses can be reduced as much as 50% when the engine warms up from a cold start to high operating temperatures [4].

A consequence of the viscosity reduction is that the Minimum Oil Film Thickness (MOFT) and its load carrying capacity is significantly reduced. This might lead to a mixed lubrication regime throughout the stroke, increasing friction loss and component wear [3, 4, 6, 14]. The connection between temperature and MOFT only seems to hold where the lubrication is hydrodynamic. In regions of mixed and boundary lubrication (dead centers), the MOFT is very small at all times and seemingly unaffected by oil temperature [6]. The asperity contact losses in these areas are considerably higher at high temperatures than low, despite the MOFT remaining approximately the same. Reduced viscosity due to elevated temperature causes less squeeze film force around the dead centers, resulting in greater asperity contact [6].

The coefficient of friction (and the peak friction power losses) between the piston assembly and cylinder liner decreases with increasing oil viscosity under both boundary and mixed lubrication regimes (predominantly at dead centers). However, in the case of hydrodynamic lubrication, the total friction power loss during one complete crank revolution increases [6, 8]. This is due to the fact that when hydrodynamic lubrication dominates, the high oil viscosity causes higher losses over a large part of the cycle. Depending on the oil viscosity used, the engine might/might

not see all of the different lubrication conditions (boundary, mixed, and hydrodynamic), which results in significant variation of the engine friction [4]. As long as lubrication stays in the hydrodynamic regime, reduced viscosity is beneficial for reducing losses. However, as soon as the transition towards mixed lubrication starts, reduced viscosity will increase losses (refer to the Stribeck diagram in figure 5.1). In general, the higher the viscosity, the more the lubrication regime shifts from boundary/mixed towards mixed/hydrodynamic [8].

All of the effects mentioned above highlight the importance of using engine oil with correct specifications and temperature properties to ensure sufficient lubrication at both low and high temperatures, without causing unnecessary losses and wear. A challenge is the fact that different engine parts react differently to oil properties. As an example, low viscosity might reduce bearing and piston skirt friction (hydrodynamic), but increase piston ring losses (mixed/boundary). Care must be taken in the design and oil selection process to choose the solution yielding minimum friction loss and maximum engine output. A wide variety of engine oils are available, ranging from basic oils to advanced multi-grade formulations with friction reducing additives and shear thinning properties.

5.4 Piston Assembly

Piston assembly friction results from the reciprocating motion of the piston inside the cylinder liner. This includes piston rings as well as piston skirt contact. Transverse, tilting, and twisting motion of the piston assembly can also occur depending on piston geometry, wear, inertia effects from the connecting rod, and the transverse reaction force resulting from the connecting rod angle during piston reciprocation. This side loading affects the friction loss, and can be of significant magnitude, depending on engine design (ex: 5 kN for Honda CRF 450 R [12]).

In a properly designed and normally functioning engine, the cylinder liner is lubricated by the engine oil. As a consequence, the friction between the liner, piston, and rings is governed by lubrication conditions and properties such as oil film thickness, temperature and viscosity. The nature of piston motion (varying velocity during the stroke, secondary motion), force variations during a cycle, and engine oil system design, causes the oil film thickness to vary during a complete engine revolution. At TDC and BDC, the piston comes to a halt before reversing direction, which has an impact on lubrication conditions. The piston assembly experiences the most complex lubrication conditions, and it is estimated that 80% is hydrodynamic lubrication (including squeeze film effect at dead centers), 10% is mixed lubrication, and 10% is boundary lubrication [13]. The varying piston velocity and acceleration over the course of a stroke, combined with several changes in the lubrication regime during each revolution of the crankshaft, causes the engine's instantaneous friction to be a function of piston position (or crankshaft angle). Adding the fact that engine speed (or mean piston velocity) and effective oil viscosity also influence the friction behavior, further complicates the situation.

In a typical cylinder liner, a greater amount of wear can be observed near the dead centers. Hydrodynamic lubrication occurs for most parts of the stroke, but a significant increase in asperity contact load and friction near both TDC and BDC due to mixed lubrication can be observed [2, 3, 6]. The friction peaks occur closer to the dead centers when the contact load

is increased. One might expect that the maximum friction would occur exactly at the dead centers, but the the squeeze film effect between the liner surface and the piston ring causes the oil flow reversal to be slightly delayed. The peaks occur later in the piston stroke (further from the dead centers) and with lower amplitude, as the engine speed is increased [6].

The surface roughness of the piston skirt, piston rings, and liner also influences the total piston assembly friction. A rough surface has more friction in the case of mixed/boundary lubrication, but also holds the oil film better than a fine honed surface. This means that a rougher surface can in some cases reduce friction losses through promoting mixed/hydrodynamic lubrication. Different coatings and surface treatments can be used to control the asperity friction, and also to manipulate the oil film distribution and thickness. Laser-structured pockets in the liner around the piston TDC and BDC locations are sometimes used as oil reservoirs in smooth liners to avoid oil starvation issues as piston rings scrape away the oil film [16]. Scraping away too much of the oil film increases the chance of boundary lubrication and asperity contact between the piston, rings, and liner.

5.4.1   Piston Rings

The friction force between the piston rings and the cylinder liner has contributions from viscous shearing of the oil film, asperity contact, and the stroke-direction component of the asperity contact pressure [2]. During the engine's power stroke, the friction between piston rings and cylinder liner increases significantly. This is a direct consequence of the large compressive force experienced by the connecting rod and its instantaneous orientation. The connecting rod's angle during the power stroke and the piston's restricted movement (stroke-direction only) dictates that some of the force transferred from the piston to the connecting rod is directed towards the cylinder wall. The reaction force between the cylinder wall and the piston rings is a normal force acting in the radial direction, causing friction as the piston moves down. As the normal load on the piston rings is increased, the oil film thickness decreases [2, 3]. This is important to consider to avoid a breakdown of the oil film and a change in lubrication regime during the power stroke.

Many different piston ring configurations can be used in an engine. The rings maintain compression, piston centering and distributes/scrapes oil off the cylinder liner walls. In a two-ring configuration, the top (compression) ring is responsible for the sealing action, and the bottom (oil control) ring is responsible for oil distribution. If too much oil reaches the top ring, it could possibly enter the combustion chamber and result in excessive oil consumption and inefficient combustion. On the other hand, too little oil will cause starvation of the top ring, resulting in excessive friction loss and wear. In a three-ring configuration, a ring is placed between the top and bottom rings. It is partly responsible for sealing and reducing blow-by of combustion gases, and partly responsible for oil distribution. Depending on piston ring pack design, the friction and lubrication regimes might be different during up-strokes and down-strokes [1, 6, 8]. Piston ring profile should have a large radius of curvature for promoting the oil squeeze film effect near the dead centers, but a more moderate curvature to promote hydrodynamic wedge effect during mid-stroke [6]. The number of rings and ring thickness do also have an effect on piston assembly friction [1]. As does distortion of piston and liner, gas and oil flow through the ring pack, and ring movement in the piston ring slots.

Using torque measurements, one can clearly observe peaks and troughs in piston ring friction as the engine crank is rotated [5]. The peak friction value normally occurs a few degrees after TDC when the piston accelerates downwards. Because engine oil is normally supplied to the cylinder liner below the piston, this means that a more generous supply of oil is available when the piston performs its downward motion. The thicker film causes a radial compressive force on the piston rings, but ring movement is resisted by the friction between the piston ring slots and the rings under high cylinder pressure [5]. This causes increased normal force between the piston rings and liner, and thereby increased friction. Under fired engine operation, the combustion pressure increases the back-pressure of the compression ring, pushing it harder against the liner [8, 12]. This causes better sealing and thereby a lower pressure gradient across the ring, reducing Poiseuille shear of the oil film significantly compared to motored tests. The result is that the piston-liner friction is dominated by the compression ring at the dead center between the compression and power strokes. At the transition between the exhaust and intake strokes, and at the BDC, Poiseuille shear is the governing source of friction [12]. During motored engine testing, the oil control ring is the main contributor to the piston assembly friction [8].

5.4.2 Piston Skirt

The nature of piston skirt contact depends on the piston movement, the skirt design, clearance, the finish of the contacting surfaces, and the lubrication regime. Choosing the correct material and surface roughness for the piston and liner can significantly reduce the friction losses in the case of high engine speed and oil viscosity [16].

As excessive piston tilting/secondary motion can have a severe impact on the amount of piston skirt contact, piston design is of utmost importance. Changing the piston pin offset from the thrust side to the anti-thrust side, causes a change in secondary motion, as it transitions from swinging clockwise to anti-clockwise. Offsets closer to the thrust side increases the piston's transverse force in the intake and power strokes, but decreases it in the compression and exhaust strokes. Offsetting in the other direction has the opposite effect [17].

At normal operating temperatures, piston ring friction is relatively small compared to piston skirt friction [1], but the piston skirt is found to contribute the least to the total friction loss of the piston assembly [8]. Piston ring friction acts over a large portion of the engine cycle, encompassing all of the three lubrication regimes. Piston skirt contact primarily occurs near dead centers, which is a relatively small portion of the total engine cycle.

5.5   Connecting Rod

The direct connecting rod losses are mainly friction in the big end bearing, windage, and oil drag losses. The friction loss from the small end bearing is negligible compared to the losses in the big end and the crankshaft bearings [18]. The combination of rotating and reciprocating motion makes the connecting rod move through both oil and air, potentially resulting in drag losses at higher engine speeds. If the losses are significant, the drag force might also influence the transverse force transferred to the piston assembly. Intuitively, an oval-beam connecting rod shank would produce less drag than an H-beam, but literature on whether the difference is significant or not, is limited.

Different designs for big and small end bearings are used. Roller and needle bearings are possible candidates as well as advanced polymer and ceramic designs. The most commonly used engine bearings are journal bearings. They operate in the hydrodynamic lubrication regime as long as the engine is running, but mixed/boundary lubrication is experienced in the transient start-up and shut-down phases [4, 13]. This is because journal bearings utilize relative (rotating) motion of the bearing and the axle to maintain local oil pressure and oil film thickness. Because hydrodynamic lubrication is the dominating regime, the losses increase with engine speed and oil viscosity. The big end bearing of the connecting rod will see full journal bearing operating conditions, but the small end does not have the continuously rotating motion as the big end does. Instead, it pivots back and forth as a result of the connecting rod motion. This might result in a larger degree of mixed and boundary lubrication. The OEM connecting rod in the Honda CRF 250 R engine uses a needle bearing in its big end. As the engine speed increases, so does the pressure of the oil being forced through the crankshaft and into the bearing. The effect of this is that the bearing transitions from needle bearing operation towards hydrodynamic journal bearing operation as the engine speed is increased.

The connecting rod can indirectly have an impact on engine friction through the transverse inertia force transferred to the piston and piston rings. The connecting rod's motion is a combination of crankshaft rotation in the big end and piston reciprocation in the small end. This causes reaction forces on the piston's thrust and anti-thrust sides as the engine runs, due to the mass and inertia properties of the connecting rod. In general, as the connecting rod mass and inertia is reduced, the transverse force transferred to the piston assembly gets smaller [17]. This again means less friction force from the piston-liner interaction, the exception being right after top dead center during the power stroke. The friction loss at this point becomes larger, because less transverse inertia force is available to counteract the sideways reaction force due to the connecting rod angle during combustion [17]. The weight and inertia of the connecting rod can also influence the friction in the crankshaft bearings through transfer of dynamic forces.

Changing the connecting rod's center of mass can also cause changes to the transverse force transferred to the piston. As the distance between the center of mass and the small end is reduced, the transverse force increases in the upper half-stroke and decrease during the lower half-stroke. Moving the center of mass the other way causes the opposite effect [17]. The exception relating to the moments right after combustion also apply here. If the center of mass is near the big end, an increase in peak friction is observed. Increasing the length of the connecting rod has a similar effect to moving the center of mass towards the small end [17].

5.6 Crankshaft

The crankshaft is connected to the engine block through bearings, and usually rotates through the engine oil contained in the oil sump (except in dry sump systems). The dominating losses related to the crankshaft is therefore bearing friction and oil drag. Crankshaft journal bearings usually operate under hydrodynamic lubrication, the exception being during the transient start-up and shut-down phases [4, 13]. As with all journal bearings operating in the hydrodynamic lubrication regime, the losses increase with engine speed and oil viscosity. The OEM crankshaft in the Honda CRF 250 R engine uses two roller bearings, and this causes the friction behavior to be slightly different from pure journal bearing designs.

Oil seals on the ends of the crankshaft are usually responsible for keeping the engine oil within the sump, and some friction loss is attributed to this. Depending on engine oil sump design and vehicle operation (engine tilting, lateral acceleration in sharp turns), the crankshaft might come into contact with more or less of the oil in the sump during operation. This impacts the crankshaft oil drag force.

Chapter 6

Modeling Engine Friction and Damping Effects

6.1 Engine Modeling Overview

In detailed engine modeling, there are many aspects and complex interactions to consider. One approach includes using a database with information on a variety of engines and components. This is a quite fast approach which can give valuable information on the magnitude of losses and where they appear, but the accuracy of the results might vary when detailed design changes are made. The models resulting from this approach are usually specialized for one exact engine or engine type, so limited flexibility is available. Depending on how detailed the model is, it might also be time consuming to develop, due to the amount of test data required.

Semi-empirical friction models also exist. As the name suggests, these are based on experimental data, and they rely on some of the engine's design parameters. These can be very quick and easy to use, but depending on how the models are developed, they might not be an accurate fit. Detailed design changes of the components are not accounted for to the same extent as in detailed analyses.

More in-dept analyses can be performed by advanced engine modeling techniques. They usually involve a large number of complex interconnected formulations for lubrication and friction models, contact analysis, dynamics, fluid mechanics, thermodynamics, bearing models, oil models, and component wear. Typically, various modified forms of Reynolds equation are solved to find the state of the oil film, lubrication regime, and the friction forces. Different boundary conditions solve for regions of full oil film, oil film cavitation, and oil film reformation. Because of the complexity involved with these techniques, they are often time consuming to set up and run, but they provide superior flexibility in terms of testing detailed changes in part design and operating conditions. It is crucial that the formulations used are correct and able to predict the behavior observed in physical tests.

The FVTB approach is a combination of the techniques mentioned. It includes engine part dynamics, separation of elastic and rigid body movement, nonlinear geometry changes, stress stiffening and gyro effects. This means that the model behavior and forces largely depend on the properties and design of the parts. After determining the friction and damping contributions of engine components through testing, these need to be integrated in the FVTB. Modeling the contributions as related to individual components and their properties allows comparisons of different part designs. This approach does involve some detailed formulations (especially in terms of dynamic behavior), but bears a more striking resemblance to the "database approach" described in the beginning of this section. The resulting model is specialized for one particular engine configuration, and detailed behavior of sub-assemblies are not considered. As an example, the oil film interaction between the piston assembly and liner is not modeled in detail, but as a "piston loss" under normal operating conditions. The effects of variations in operating temperature, viscosity, oil film thickness, part wear, or detailed design (such as piston ring profile and surface roughness) are not considered in this approach.

6.2 FEDEM Modeling Features

6.2.1 Damping Modeling in FEDEM

FEDEM uses proportional (Rayleigh) damping for structural damping of parts. Considering a superelement after model reduction, assuming the damping force is proportional to the velocity of each mass point, we have $\mathbf{c} = \alpha_1 \mathbf{m}$. Assuming the damping force to be proportional to the strain velocity in each point, we have $\mathbf{c} = \alpha_2 \mathbf{k}$. Combining these two yields the Rayleigh/proportional damping matrix [9]:

$$\mathbf{c} = \alpha_1 \mathbf{m} + \alpha_2 \mathbf{k} \tag{6.1}$$

Here, α_1, α_2 are constants and $\mathbf{m}$, $\mathbf{k}$ are the point masses and stiffnesses respectively. Damping ratios λ_i for natural frequencies can be calculated by [9]:

$$\lambda_i = \frac{1}{2} \left(\frac{\alpha_1}{\omega_i} + \alpha_2 \omega_i \right) \tag{6.2}$$

ω_i is the natural frequency in question. As seen from the equation, α_1 is responsible for damping of low frequencies while α_2 dampens the higher ones. If a damping ratio is chosen for two frequencies, the alpha constants can be calculated [9]:

$$\alpha_1 = \frac{2\omega_1 \omega_2}{\omega_2^2 - \omega_1^2} \left(\lambda_1 \omega_2 - \lambda_2 \omega_1 \right) \tag{6.3}$$

$$\alpha_2 = \frac{2 \left(\omega_2 \lambda_2 - \omega_1 \lambda_1 \right)}{\omega_2^2 - \omega_1^2} \tag{6.4}$$

When CMS model reduction is used in FEDEM, the reduced superelement mass- and stiffness matrices are stored in sub-matrices for the supernodes with their degrees of freedom and component modes. This means that different damping factors can be chosen for each component mode [9]:

$$\begin{bmatrix} \mathbf{c}_{11} & \mathbf{c}_{12} \\ \mathbf{c}_{21} & \mathbf{c}_{22} \end{bmatrix} = \begin{bmatrix} \alpha_1 \mathbf{m}_{11} & (\alpha_m \mathbf{m}_{21})^T \\ \alpha_m \mathbf{m}_{21} & \alpha_m \mathbf{m}_{22} \end{bmatrix} + \begin{bmatrix} \alpha_2 \mathbf{k}_{11} & \mathbf{0} \\ \mathbf{0} & \alpha_k \mathbf{k}_{22} \end{bmatrix} \tag{6.5}$$

$\alpha_m = \lceil \alpha_{mi} \rfloor$ and $\alpha_k = \lceil \alpha_{ki} \rfloor$ are diagonal matrices with the component mode damping factors. Both $\mathbf{m}_{22}$ and $\mathbf{k}_{22}$ are also diagonal matrices.

6.2.2 Friction Modeling in FEDEM

Friction between parts connected by a joint is in FEDEM calculated from forces, moments, and relative joint velocity. Viscous friction is effectively modeled as a damper (see subsection 6.2.3), and the friction force (or torque) depends on a viscous coefficient c and the velocity of the damper V [9]:

$$F_{viscous} = cV \tag{6.6}$$

Coulomb friction is a widely used friction formulation for sliding motion, where the friction force only depends on the equivalent normal load F_e and the coefficient of friction $\mu_{Coulomb}$ [9]:

$$F_{Coulomb} = \mu_{Coulomb} F_e sgn(V) \tag{6.7}$$

Here, $sgn(V)$ is the sign of the velocity (± 1, direction of movement). As opposed to viscous friction, Coulomb friction does not depend on the relative velocity between parts, but takes on a constant value during sliding motion (as long as the normal load does not change). Any external forces smaller than $F_{Coulomb}$ are not sufficient to overcome the friction, so no movement will take place. In mechanisms where components are pre-stressed, the friction force resulting from this (F_0) is added to Coulomb friction as [9]:

$$F_{prestress} = F_0 sgn(V) \tag{6.8}$$

Modified Stribeck friction is defined as [9]:

$$F_{Stribeck} = F_{Coulomb} \left(1 + Se^{-\left(\frac{V}{V_{slip}}\right)^2} \right) sgn(V) \tag{6.9}$$

$$S = \frac{F_{static} - F_{Coulomb}}{F_{Coulomb}} \tag{6.10}$$

The Coulomb friction includes the force from pre-stress. S is the stick-slip factor, describing the magnitude of the Stribeck effect, and V_{slip} is the critical velocity for the Stribeck effect. The magnitude of the Stribeck friction force depends on velocity, and is in that regard a more complete friction model than Coulomb friction. Stribeck friction captures the transition from static (higher) to kinetic (lower) friction when the sliding velocity is increased. Combining the contributions from viscous friction, Coulomb friction, modified Stribeck friction, and pre-stress friction, the total friction model is obtained [9]:

$$F_{total} = F_{viscous} + \left[F_0 + \mu_{Coulomb} F_e \left(1 + Se^{-\left(\frac{V}{V_{slip}}\right)^2} \right) \right] sgn(V) \tag{6.11}$$

6.2.3   Joint Springs and Dampers in FEDEM

Parts in the FVTB are connected by joints with various Degrees Of Freedom (DOF). In addition to controlling the available DOF and their range, it is also possible to impose spring and damper behavior on each joint. This makes it possible to add damping directly to a joint connection without using the total friction definition from subsection 6.2.2.

Four basic types of characteristics are available for springs and dampers. For a spring they are: force-translation, torque-rotation, stiffness-translation, and stiffness-rotation. For a damper they are: force-velocity, torque-angular velocity, coefficient-velocity, and coefficient-angular velocity [10]. Spring and damper joints allow linear and nonlinear stiffness and damping characteristics. In the case of linear behavior, a constant coefficient is used. In the case of nonlinear behavior, the relationship between force/torque and displacement or velocity is defined by a function controlling the coefficient value [10]. Possible functions are poly line, poly line from file, constant, linear, ramp, and limited ramp.

Chapter 7

Engine Friction Test Methods

7.1   Engine Testing Overview

Testing engine friction and damping effects can be done using a variety of approaches. If the main goal is to investigate specific design parameter variations and their influence, specialized test rigs can be constructed and used. These types of tests are mainly used to investigate the interaction between a few chosen parts, and therefore do not consider the whole engine assembly and operating conditions. Examples of these types of tests are oil film thickness measurements, temperature and viscosity influence, coefficients of friction, piston design, piston ring profile influence, and asperity contact.

If the goal is to determine the influence of various parameters on engine behavior, it is common to perform testing on engine assemblies as opposed to a few chosen parts. Testing on engine assemblies can be difficult, because some effects might be masked and interconnected with others. Examples are separating piston ring and piston skirt losses, and separating valve train component contributions. Another problematic aspect is that test parameters such as part temperature, load, and speed might be difficult to control accurately.

In most engine testing, the engine temperature at different locations, and the load seen by individual parts are of great interest. These parameters provide valuable information on the inner workings of the engine, which is hard to deduct from the outside of the engine assembly. In some cases, strain gages are used to evaluate structural integrity at critical locations, and load cells can be incorporated in the engine construction to reveal forces during operation. Floating liner modification and strain gaged connecting rods are examples of this. In order for these measurements to be taken, modifications to the engine are necessary. Such modifications might affect engine performance and durability, and in some cases exclude the engine from being used normally after testing is done.

In the case of engine assembly testing, it is important to be aware that engine friction properties changes significantly during break-in of engine parts [8]. If the goal of the testing is to determine engine behavior during normal operating conditions, performing a break-in of the engine before testing commences is essential. Failing to do so will yield time dependent results for the rubbing surfaces (particularly piston-liner interaction), where friction can be seen to decrease as engine test time increases. This makes comparisons of multiple tests very difficult.

Friction Mean Effective Pressure is often used as a measure of engine friction losses. For a four-stroke engine it is defined as [5, 16, 20]:

$$FMEP = \frac{4\pi T}{V} \tag{7.1}$$

T is the torque required to overcome engine friction and V is the displacement volume. Because FMEP is scaled with displacement volume, it enables comparison between different engine designs. However, it does not take into account how the friction losses vary as a function of crankshaft angle. To investigate characteristics of the friction losses, FMEP can be plotted as a function of time, piston position, engine temperature, oil viscosity, oil pressure, etc.

7.2 Fired Tests

In fired tests, the engine is fully assembled and a variety of speed sweeps, loads, and throttle positions can be explored. Because the engine runs under its own power, very few parts can be removed without rendering the engine useless. Intake, exhaust, and some auxiliaries, are a few exceptions. This means that fired tests require additional instrumentation and modifications to the engine in order to separate friction contributions from different mechanisms and sub-assemblies. It is however possible to run the engine with different internal components to chart the effect of these. The major advantage of a fired test is the similarity to actual engine operating conditions. The engine runs under its own power with correct cylinder pressure, resulting in correct piston transverse force and oil film contact pressure. Oil, coolant, and parts are at normal operating temperatures, causing correct thermal expansion, clearances, and oil viscosity. Since the engine is firing normally, the temperature fluctuations resulting from combustion are also included.

The Indicated Mean Effective Pressure (IMEP) method uses the cylinder pressure and the output torque to calculate the engine friction. IMEP is calculated from the measured cylinder pressure, bore and stroke (work performed by the expanding gas), and Brake Mean Effective Pressure (BMEP). BMEP is calculated analogous to FMEP, except that the torque used is the measured output torque. The difference between IMEP and BMEP gives the FMEP, indicating total engine friction loss. A major disadvantage of this method is that the IMEP and BMEP values are relatively large compared to FMEP, making this method highly sensitive to measurement inaccuracies.

The run-out method is based on bringing the engine up to a constant speed, and stopping the fuel injection for a certain number of revolutions before starting it again. When the fuel is cut off, the engine speed will reduce, and this reduction in speed is used to calculate the friction torque responsible for slowing down the engine.

Willans Line test measures the engine's fuel consumption at different loads at constant engine speed. These test points are plotted (fuel consumption against BMEP) and extrapolated to zero fuel consumption to find the FMEP. These methods require very accurate control over the engine, and are prone to measurement inaccuracies and extrapolation error.

The Morse fired test is employed on multi-cylinder engines to find the friction and pumping losses at a chosen speed. The brake torque produced by the engine is measured, and one cylinder is then deactivated. This causes a reduction in speed and output torque, and the load is reduced to regain the initially chosen speed. The difference between the initial torque produced and the torque produced with one cylinder deactivated, is used as that cylinder's indicated torque. Repeating this process for all cylinders and adding the contributions yields the engine's total indicated torque. The difference between total indicated torque and brake torque is taken as the engine's friction torque. A disadvantage of this method is that changes in temperature and intake/exhaust flow due to the deactivation of a cylinder might affect the remaining cylinders. Additionally, this method is based on motoring one cylinder at a time, so the indicated torque is not directly comparable to fired conditions. Instead, it bears resemblance to a motored test and shares its disadvantages in terms of temperature and pressure limitations.

7.3 Motored Tests

In a motored test the engine is driven by an external electric motor, and the torque required to do so is measured. The measured torque represents the "lost output torque" due to internal engine friction. Different engine speeds can be explored, and the engine does not necessarily need to have all parts installed. This is a major advantage compared to a fired test, and enables isolating contributions from different components by performing a strip or teardown test. This is performed by measuring the torque for the engine assembly, removing the part of interest and measuring the torque again. The difference between the two measurements indicates the removed part's contribution. This testing can be successively performed all the way from a full engine assembly down to only the crankshaft. The influence of part design can be investigated in a motored test by swapping parts instead of removing them. No irreversible engine modifications are needed, but in many cases the temperatures, pressures, and forces are of great interest, so modifications are still performed.

In a full assembly, the pumping losses related to intake and exhaust will be included in the measured torque, and can be hard to separate from the losses related to the valve train operation in a strip/teardown test. As noted by Daniels and Braun [5], if the spark plug (or possibly also a valve) is removed but the cylinder head is kept, the torque required to run the engine might increase due to extensive pumping of air through the open orifice. This is an unrealistic loss during normal operation, and should be avoided or accounted for.

The major disadvantage of a motored test is that it does not mimic the actual engine operating conditions as well as a fired test does. Cylinder pressures are either too low (compression, but no combustion) or non-existent (valves or cylinder head removed), and the fluctuating temperature due to combustion is not considered. This has implications for the piston transverse force, oil film contact pressure, and Poiseuille oil shear in the piston-liner interaction [12]. No combustion means that the only heat generated is by friction and oil shearing, so oil and coolant might need external heating to secure correct thermal expansion, clearances, and oil viscosity.

The engine's friction losses in a fired test and a motored test are quite similar. The exception being in the piston assembly during the power stroke, where the pressure and temperature differences are significant [14, 18]. The high combustion pressure (causing high ring-liner contact pressure) and high temperature (reducing local oil viscosity) encountered in a fired test result in a larger degree of boundary lubrication for the piston rings, increasing the loss compared to a motored test. On the other hand, increased liner oil temperature is advantageous for the piston skirt friction, as hydrodynamic lubrication benefits from reduced viscosity. Through carefully controlling the liner surface temperature, similar lubrication conditions to fired operation can be approximated and used to deduct more precise friction results [18].

7.4 Chosen Test Method

As previously mentioned, the main parts of interest in this thesis are the piston assembly, connecting rod, and crankshaft. This means that losses related to the valve train and transmission are not applicable in this case. A motored test on a partial engine assembly is chosen to investigate the relevant mechanisms of loss, as fired testing can not be performed without the valve train. The electric motor is connected to the crankshaft, eliminating contributions from the transmission and clutch. The partial engine assembly used is described in section 8.1.

Since all testing is performed on a single engine configuration (Honda OEM piston assembly, connecting rod, and crankshaft), directly isolating contributions from various friction and damping effects is not possible. Assigning friction contributions to different mechanisms with the help of previously written literature is therefore used instead.

The test procedure chosen does not involve running the engine under its own power, but rather turning the crank through external influence. Because of this, the pressures and temperatures normally encountered in a running engine is not present. As mentioned earlier, this influences engine operating conditions, particularly during the power stroke where the lack of combustion pressure and local temperature will reduce the piston assembly losses. Less transverse force and piston ring contact pressure, together with a higher local viscosity (lower oil temperature), improves the lubrication conditions causing the piston assembly to operate closer to mixed/hydrodynamic lubrication than boundary/mixed. Since the engine is tested without the cylinder head and valves, the piston top operates in atmospheric pressure at all times. The underside of the piston however, does not. Because the crankcase is sealed, some compression of the air in the crankcase will occur for each stroke, and add to the torque required to run the engine.

Despite the differences between motored and fired operation, the motored results are accurate enough to provide relevant friction data. To ensure correct thermal expansion, clearances, and oil viscosity, heating the engine oil is necessary. The engine test rig is described in section 8.2, and the execution of the test in section 8.3.

Chapter 8

Engine Test Setup

8.1   Honda CRF 250 R Engine

Honda CRF 250 R engine	
Displacement volume	250 cm^3
Minimum operating speed	2500 rpm
Maximum operating speed	14500 rpm
Maximum brake torque	24.8 Nm (9000 rpm)

Table 8.1: Honda CRF 250 R engine specifications

The engine used for testing and modeling is a single-cylinder four-stroke Honda CRF 250 R motocross engine. It is liquid cooled and runs on gasoline. Engine specifications can be seen in table 8.1. In ready-to-run configuration, the engine includes intake, exhaust, valve train, valves, piston, piston rings, piston pin, connecting rod, balance shaft, flywheel, crankshaft, clutch, gearbox, oil pump, bearings, and seals. As mentioned earlier, not all of these parts are required to run a motored test, and not necessary to include in the modeling since they are not currently a part of the FVTB configuration. The engine assembly used for testing consists of the Honda engine block with cylinder/liner, OEM piston and piston rings, OEM connecting rod, and OEM crankshaft with bearings and seals. Since motored testing is performed, no combustion heat issues are expected. Plumbing, radiator, water pump, and coolant are therefore not included in the test setup.

The oil pump is not installed in the engine during testing. It is mainly responsible for pumping oil to the cylinder head (which has been removed) and the connecting rod big end (through channels in the crankshaft). At high engine speeds, the oil pressure is sufficient to cause the big end needle bearing to operate in the hydrodynamic regime. Since a motored test without any cylinder pressure is performed, the load on the big end bearing is small compared to fired engine operation. It is assumed that the big end bearing will have sufficient lubrication from the oil sump alone. The crankshaft rotates in the oil bath in the sump, lubricating the connecting rod through dipping and the cylinder liner through oil splashing. Motorex Cross Power 4T 10W-50 engine oil is used during engine break-in and testing. The engine features two separate oil sumps, one for the crankshaft/connecting rod assembly and one for the gearbox (which is an integrated part of the engine block). Since the gearbox is empty (internal parts are removed), only the crankshaft sump is filled with oil. Approximately 0.7 L of oil is used to fill the sump to the maximum line on the oil dip-stick.

Since oil temperature significantly affects friction and clearance in the engine, it is necessary to heat the engine oil to its normal operating temperature of 80 - 85 °C in order to get reliable test results. This is done by mounting a Norske Backer 400 W heat cartridge in the oil sump. A Sunvic Simmerstat Type TYJ 7202 is used to control the output of the heat cartridge from level 1 to 5 (controlling the relation between on- and off-time). Both the Simmerstat and the heat cartridge are designed to operate on 230 V AC, and therefore plugged directly into a wall socket. A TES 1300 thermometer is used to monitor the oil temperature in the sump. The temperature sensor is mounted in a separate chamber from the heat cartridge to reduce the impact of the cartridge temperature on the measurements. Custom aluminum brackets were made to keep the heat cartridge and temperature sensor in the desired areas, while keeping the wires away from rotating parts. The heat cartridge and temperature sensor arrangement

can be seen in figure 8.1. The heat cartridge is shown in the green rectangle, the temperature sensor in the yellow circle, and the red line indicates the approximate oil level in the sump.
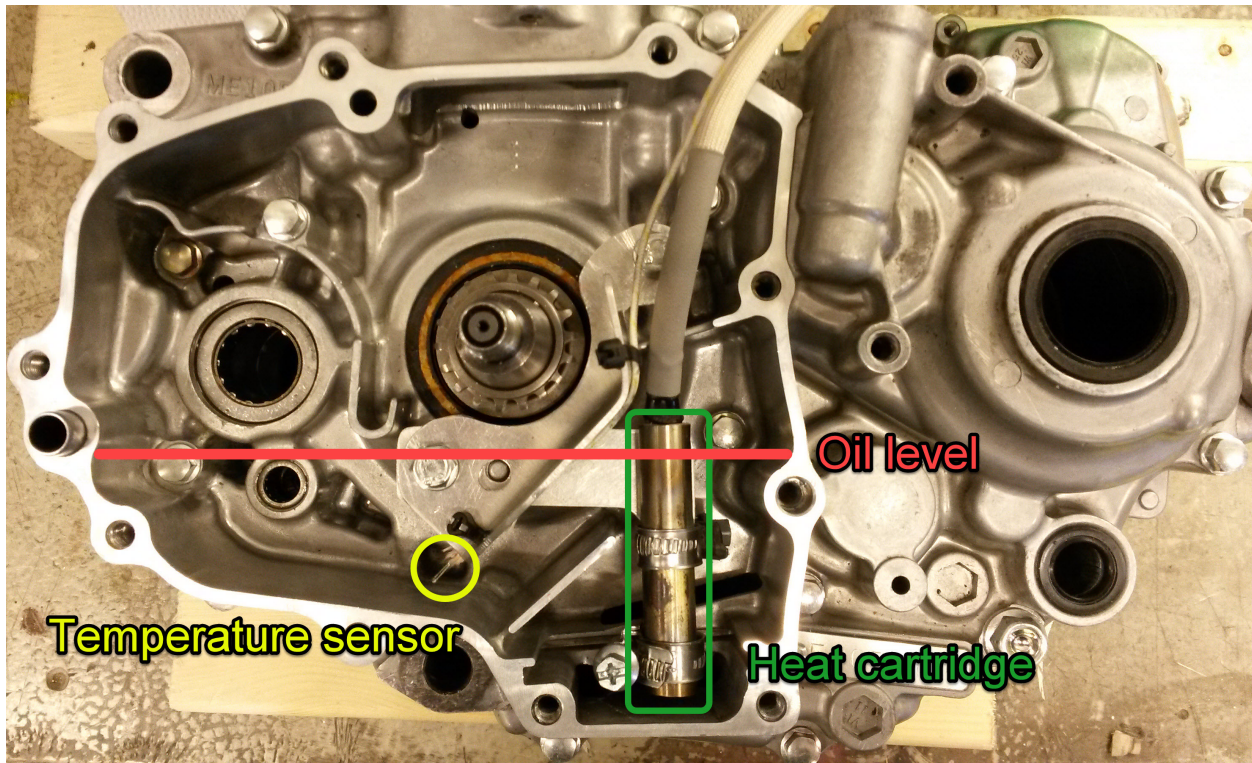

Figure 8.1: Engine oil heating arrangement

Since the engine is tested without the cylinder head, four 60 mm long steel tube spacers with outer dimensions Ø20 mm and inner dimensions Ø10 mm were made to allow the cylinder head bolts to securely fasten the cylinder/liner. Specified bolt torque is 40 Nm. A 8 mm thick steel plate with a center hole is used as a safety measure, absorbing the piston's kinetic energy in the event of engine failure during testing. The center hole is Ø68 mm and the piston is Ø76.8 mm. Since the difference between diameters is relatively small, the safety plate will not cause substantial airflow resistance (pumping loss) when the piston reciprocates. The bottom side of the safety plate center hole has a 4 mm deep cut-out of Ø80 mm to avoid piston collision (see figure 8.2). Because the piston is slightly dome/wedge shaped at the top, the piston center travels approximately 3 mm above the cylinder/liner in the center hole, but the edge of the piston stays in the cylinder/liner at all times. The engine cylinder assembly setup is shown in figure 8.3.
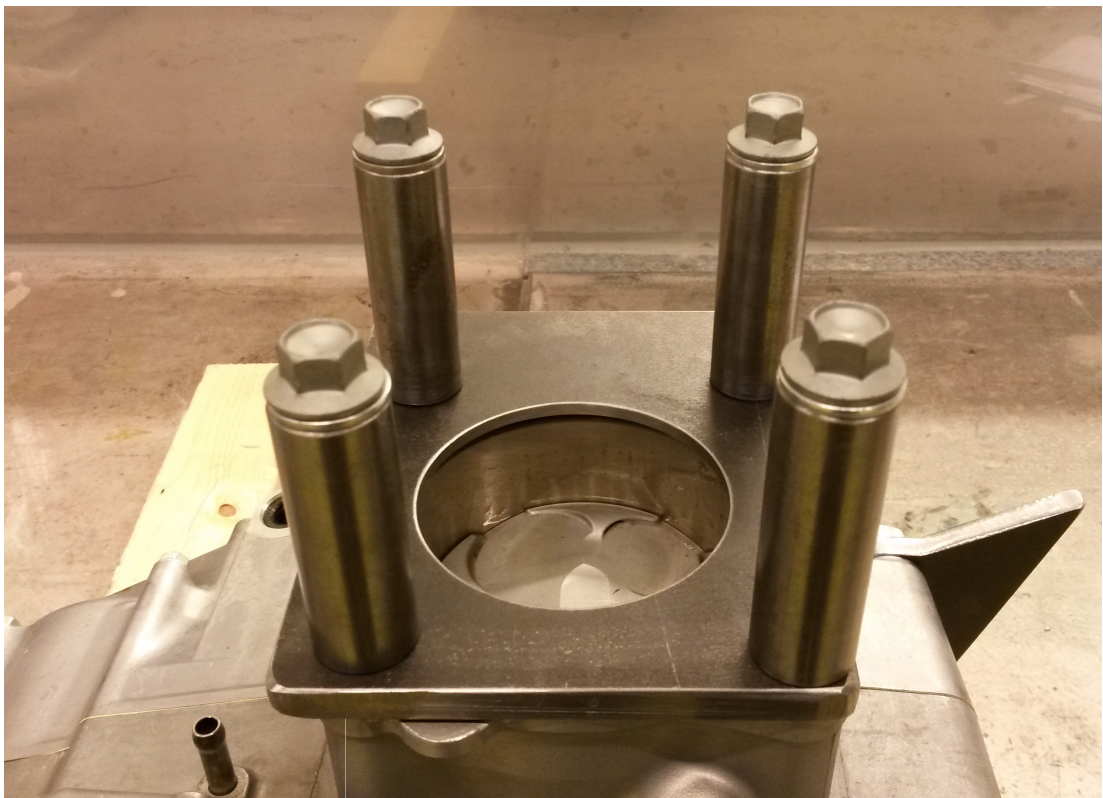
Figure 8.2: Safety plate

Figure 8.3: Engine cylinder assembly

8.2   Engine Test Rig Design
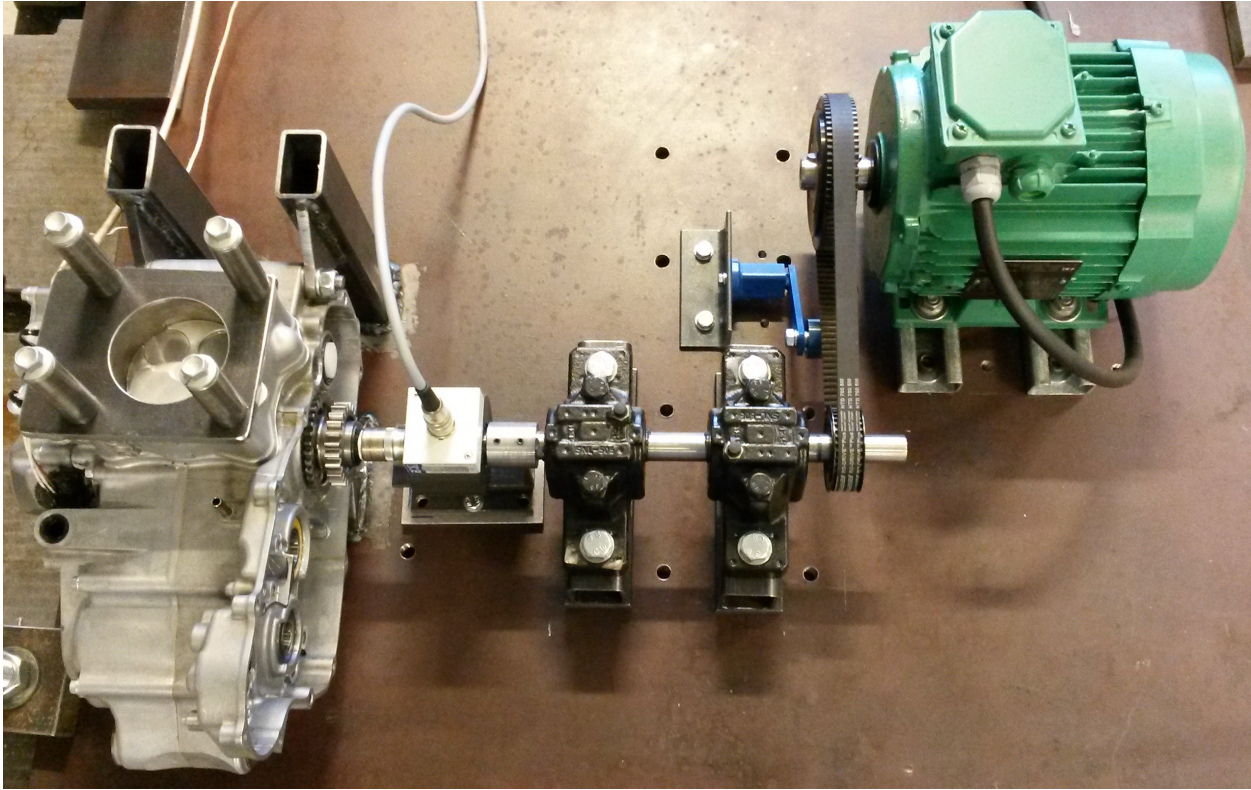
8.2.1   Mechanical Aspects

Figure 8.4: Engine test rig

The engine test rig can be seen in figures 8.4 and 8.5. A 15 mm wide belt is used to connect a Leroy Somer LSES 90 S electric motor with a 72-tooth pulley to a Ø20 mm steel axle with a 36-tooth pulley, to double the rotational speed. The electric motor is mounted on rails with four M10 bolts to allow adjustments of the belt tension and angle. A Rosta SE 11 belt tensioner with a Rosta R11 roll is used to keep the belt from oscillating during testing. It is bolted to the 20 mm thick steel base plate with a bracket and two M8 bolts.

The axle is mounted to the base plate through two FAG 1205-K-TVH-C3 ball bearings, with FAG H205 adapter sleeves, mounted in SKF SNL 505 plummer block housings. The housings are bolted to the base plate with two long M12 bolts each, running through steel spacers and square profile beams (to get the correct height).

Steel engine mounts were fabricated and welded to the base plate. A detailed view of the mounts before welding is seen in figure 8.6. The engine mounts are connected to the engine's OEM attachment points with two M10 bolts running through both the engine block and the mounts.
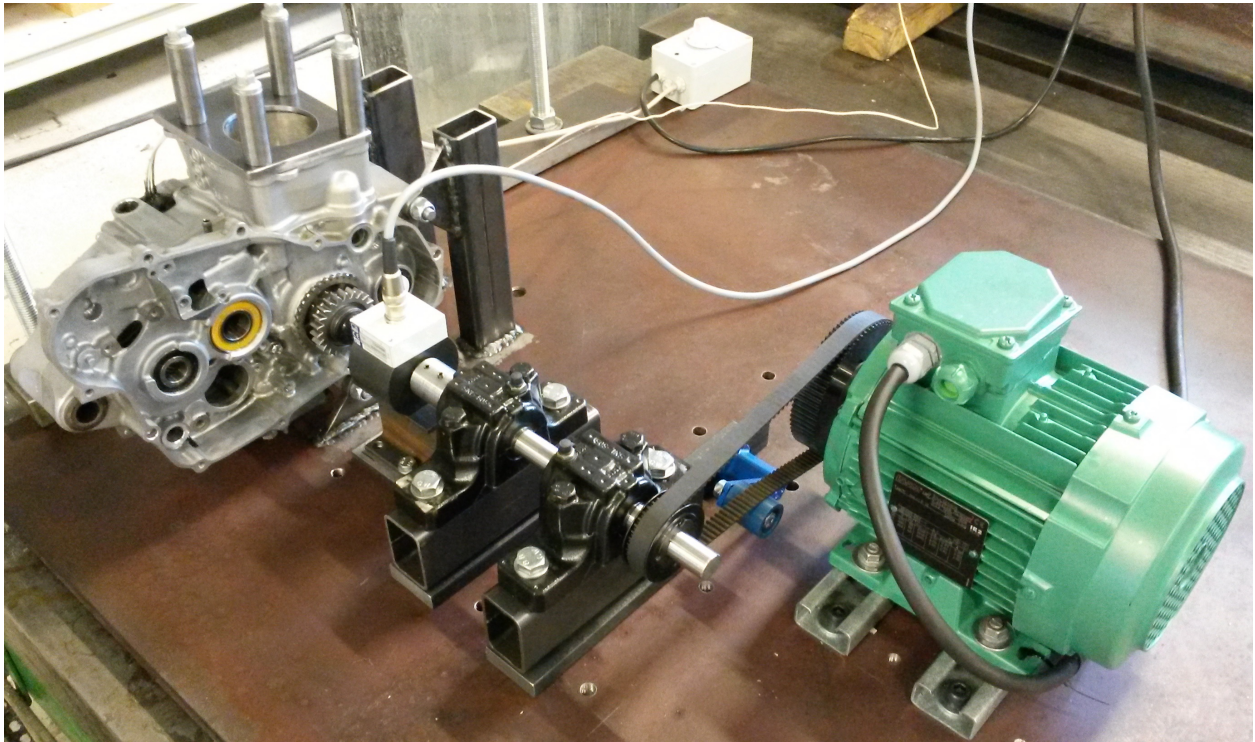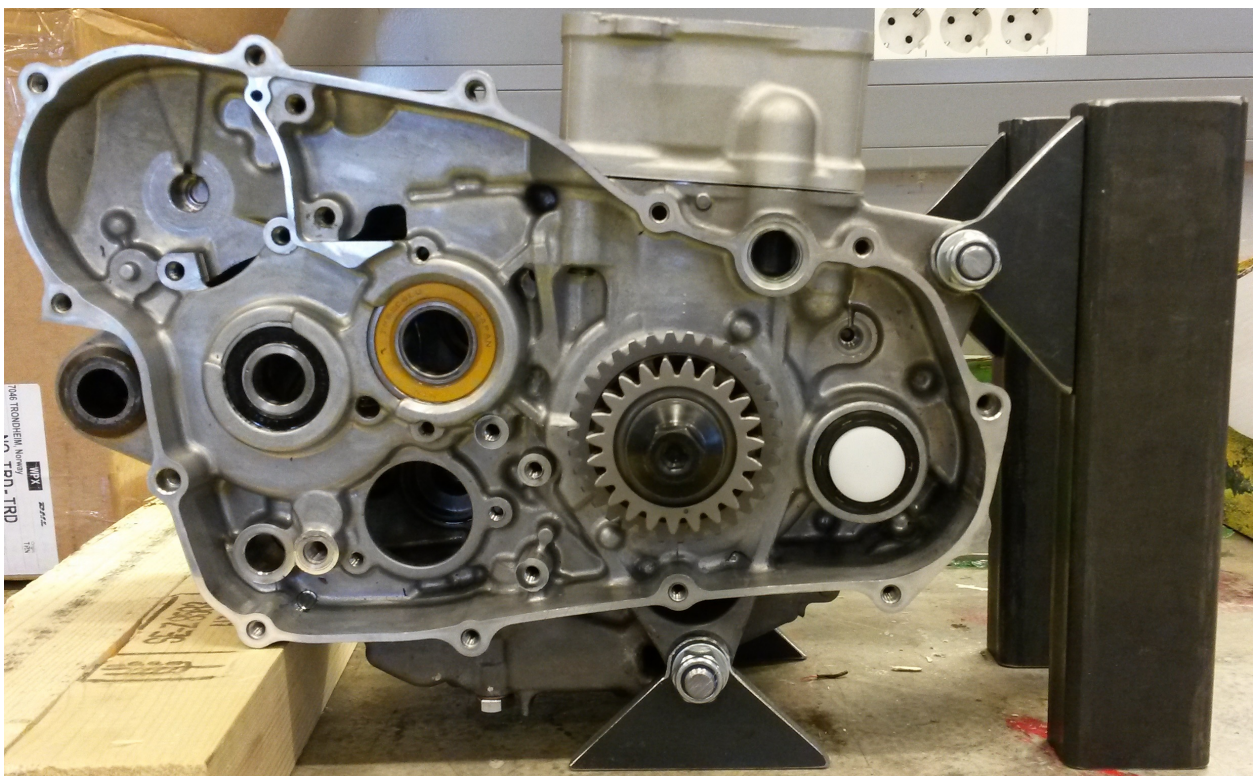
Figure 8.5: Engine test rig

Figure 8.6: Engine mounts

The axle is connected to a HBM T22 in-line torque transducer by a steel sleeve with set screws. Both entering axles were ground flat on one side for the set screws. The transducer is kept from rotating with the axle by an I-beam support. The support is bolted to the base plate with two M8 bolts, but the transducer is free to translate on top of the support. The torque transducer is connected to the engine by a 17 mm steel socket, modified with a 0.02 mm shrink-fit on the transducer side. Figure 8.7 shows the connections between the axle, torque transducer and the engine.
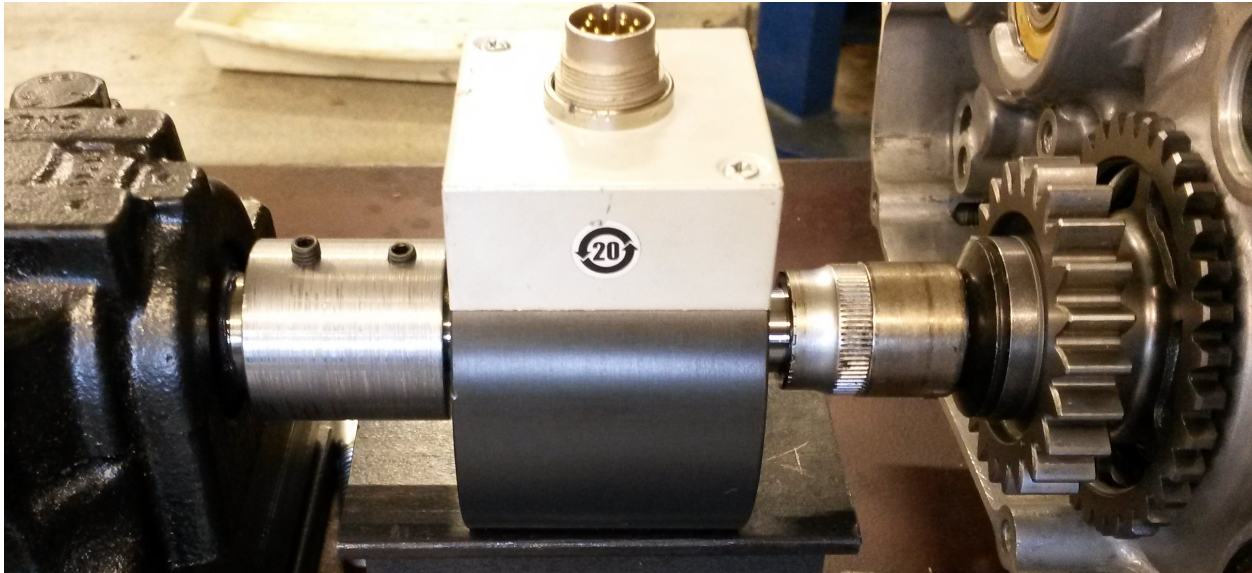
Figure 8.7: Connections between axle, torque transducer and engine

Using the modified socket (figure 8.8) allows the OEM bolt in the crankshaft to remain in place, along with the two cogs usually present on the crankshaft spline (figure 8.9). This is an advantage, as the crankshaft oil seal depends on the inner cog sleeve (see figure 8.10), and tightening the bolt to 40 Nm assures correct axial play in the crankshaft assembly. The white plastic plug seen in the figures is used to seal the hole where the balance shaft normally sits.

Because of thermal expansion, some axial play in the crankshaft assembly is expected. Using the modified socket to connect the torque transducer to the engine crankshaft bolt, allows for some axial sliding between the two without introducing axial forces in the transducer or the engine. The shape and size of a 17 mm socket also allows some play against a 17 mm bolt head, permitting a small misalignment of the two rotating axes without introducing large bending moments. However, the play in the socket and bolt connection introduces rattling and vibrations, so a thin layer of tape is attached to the hexagonal bolt head before the socket is introduced. This reduces the rattling significantly, but the tape is compliant enough to avoid the introduction of large bending moments.

Figure 8.8: Modified socket connection

Figure 8.9: Crankshaft with cogs and bolt
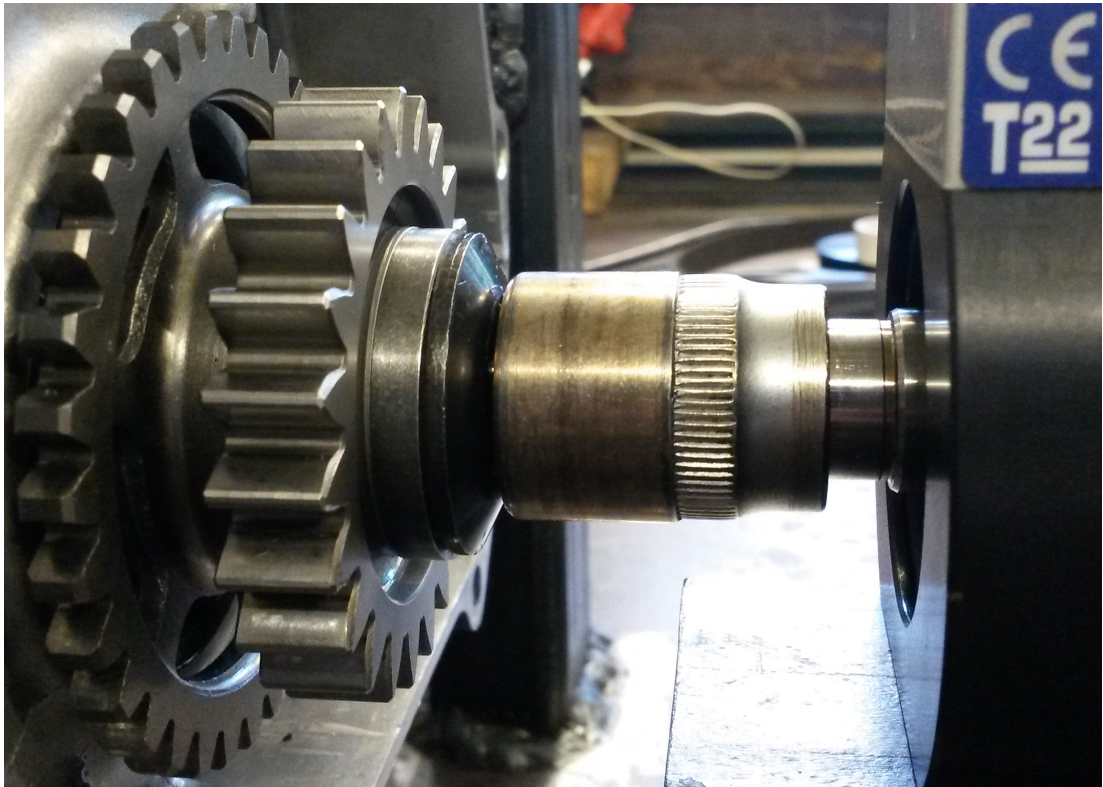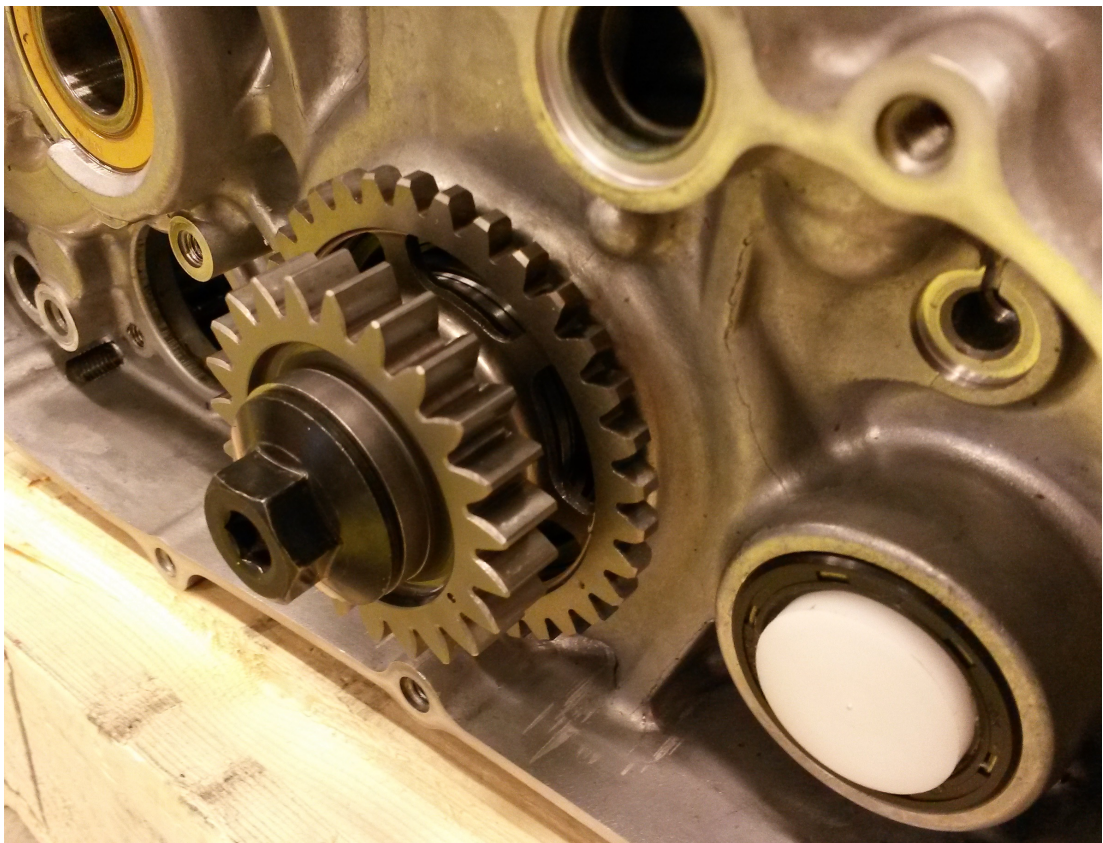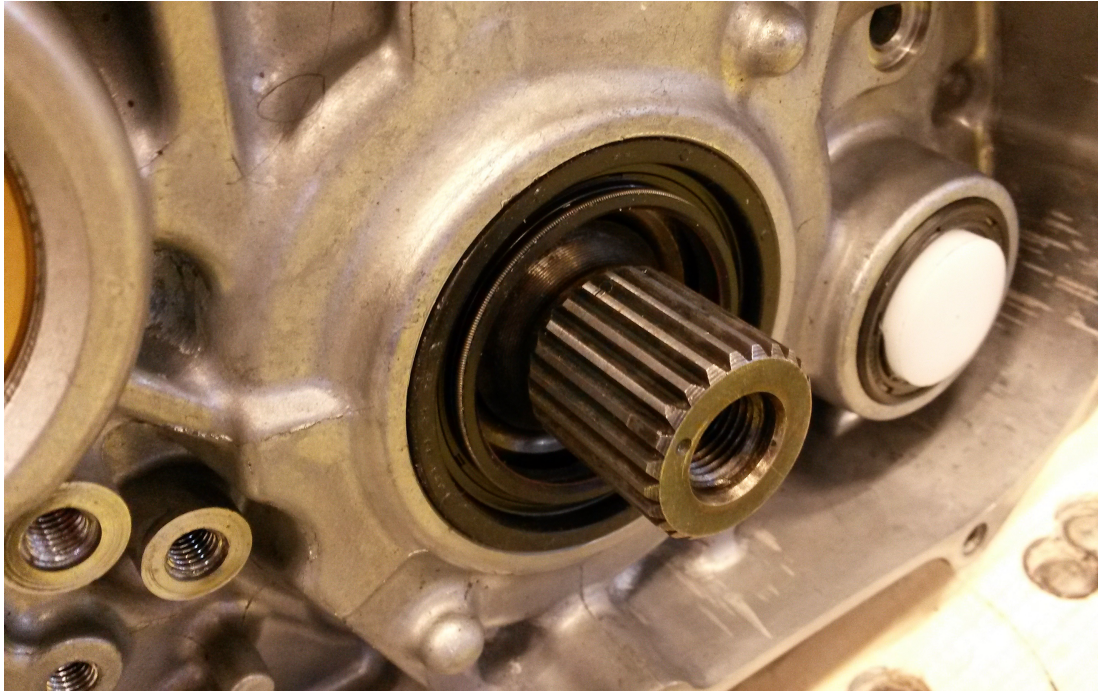
Figure 8.10: Crankshaft oil seal

8.2.2 Electrical Aspects

The electric motor is controlled through a SEW Eurodrive Movitrac B frequency inverter, connected to a computer running SEW Eurodrive Movitools MotionStudio software. This enables the motoring speed to be set and controlled precisely. The torque transducer is connected to a HBM Spider 8 universal amplifier and data acquisition system. The spider is connected to a computer running Catman AP V3.5.1 data acquisition software. A sampling frequency of 1200 Hz is used to obtain a sufficient number of representative measurements at high engine speeds. At 9000 rpm, a sampling frequency of 1200 Hz results in 8 measurements per crankshaft revolution.

As already mentioned, the friction torque is a function of piston position (crankshaft angle) due to varying piston speed and lubrication regimes. Taking a sufficient number of measurements during each crankshaft revolution at constant engine speed, and then calculating the mean value, provides an average friction torque at that speed. It does not provide information on instantaneous friction as a function of crankshaft angle or piston position. Such information requires a more elaborate test setup, and is not needed for the chosen friction modeling in the virtual test bench. The mean value calculation of the torque measurements are performed over both one second intervals and five second intervals to get a better picture of trends and fluctuations in the values. This also reduces the influence of outliers, in the event that more measurements are taken closer to the maximum friction value than the minimum (or vice versa) during a crankshaft revolution.

Technical specifications for the torque transducer, frequency inverter and motor can be seen in tables 8.2, 8.3 and 8.4 respectively. As seen from table 8.2, the transducer output voltage approximately equals the measured torque. This makes interpreting the measured results quite easy: 1 V equals 1 Nm. Some inconsistency in this relation might still be expected, due to specified deviations in linearity, sensitivity and zero value.

HBM T22 in-line torque transducer	
Nominal torque	5 Nm
Nominal sensitivity (zero to rated torque)	5 V
Nominal sensitivity linearity error (including hysteresis)	$\leq \pm 0.3\%$
Sensitivity tolerance (output deviation at rated torque)	$\pm 0.2\%$
Output change per 10 K in nominal temperature range	$\leq \pm 0.2\%$
Output at zero torque	0 ± 0.2 V
Zero torque output change per 10 K in nominal temperature range	$\leq \pm 0.5\%$
Nominal temperature range	+5...+45 °C
Operating temperature range	0...+60 °C
Nominal rotational speed	16000 rpm
Nominal supply voltage (DC)	11.5...30 V

Table 8.2: Torque transducer specifications

SEW Eurodrive Movitrac B MC07B0015-2B1-4-00 frequency inverter	
Nominal line voltage and frequency (AC)	1x200...240 V, 50...60 Hz
Nominal line current (AC)	16.7 A (230 V)
Output voltage and frequency	3x0...Line voltage, 0...599 Hz
Output current (AC)	7.3 A (230 V)
Output power	1.5 kW
Temperature range	-10...+50 °C

Table 8.3: Frequency inverter specifications

Leroy Somer LSES 90 S motor	
Rated power	1.5 kW
Rated speed	2860 rpm
Rated torque	4.9 Nm
Start torque	16.66 Nm
Maximum torque	22.05 Nm
Rated voltage and frequency	230...400 V, 50 Hz
Rated current (230 V)	5.5 A
$\cos \varphi$	0.84

Table 8.4: Motor specifications

8.3 Engine Test Procedure

8.3.1 Engine Break-in

Before performing physical testing, the engine needs to be broken-in. As mentioned by Fadel et al. [8], the engine's friction properties changes significantly during break-in of engine parts, and performing a break-in before testing is therefore essential.

This is done by heating the engine oil to 75 - 80 °C while running the engine at 300 rpm. When the correct oil temperature is reached, the engine is run at a constant speed of 4000 rpm while monitoring the torque transducer output. When a steady state output is obtained, and the measurements show no change in engine friction, the engine break-in is considered complete. The result of the engine break-in procedure is found in section 10.2.

8.3.2 Engine Friction Torque Testing

Since the engine's minimum operating speed is 2500 rpm, 3000 rpm was chosen as the lowest engine speed for testing. The engine is tested without the balance shaft and cylinder head, and this has implications for engine forces and vibrations. In the interest of health and safety, it was decided not to run the engine in the test rig faster than 9000 rpm. Vibrations and forces at higher speeds would be severe, and might result in failure of the engine or the test rig. Testing the engine at 9000 rpm still provides important data on engine performance, as this is the speed where maximum brake torque is delivered during normal fired operation. Testing is performed on the engine configuration described in section 8.1 using the following procedure:

1. Heat the engine oil to 75 - 80 °C while running the engine at 300 rpm

2. Run the engine at 3000 rpm until the torque transducer output stabilizes

3. Increase engine speed by 1000 rpm, run until the torque transducer output stabilizes

4. Repeat step 3. until a speed of 9000 rpm is achieved

5. Decrease engine speed by 1000 rpm, run until the torque transducer output stabilizes

6. Repeat step 5. until a speed of 3000 rpm is achieved

Using this test procedure results in data for steady state cycle-averaged friction torque as a function of rpm. It does not include torque needed for acceleration or how the friction torque changes with crankshaft angle. Performing torque measurements during both increasing and decreasing rpm test schemes is done to investigate hysteresis. Repeating the test procedure several times, and averaging the measurements across tests, ensures reliable results. The speeds referred to in this test procedure are the engine speeds (after the belt transmission) and not the electric motor's speeds (which would be half). The engine friction torque results can be found in section 10.3.

Chapter 9

Modeling and Tuning Approach

9.1 Virtual Test Bench Modeling

9.1.1 Reference Test Bench Model

A reference test bench model is established as a base for incorporating friction and damping effects. This is done in order to obtain a model behaving exactly as expected before any friction and damping effects are accounted for. The FVTB from section 3.2 is used as a starting point. Firstly, one of the engines is removed from the model to save simulation time and to make the model easier to work with. The flywheel and balance shaft are also removed to leave only the piston, piston pin, connecting rod and crankshaft, replicating the physical test setup. The reference test bench model can be seen in figure 9.1.
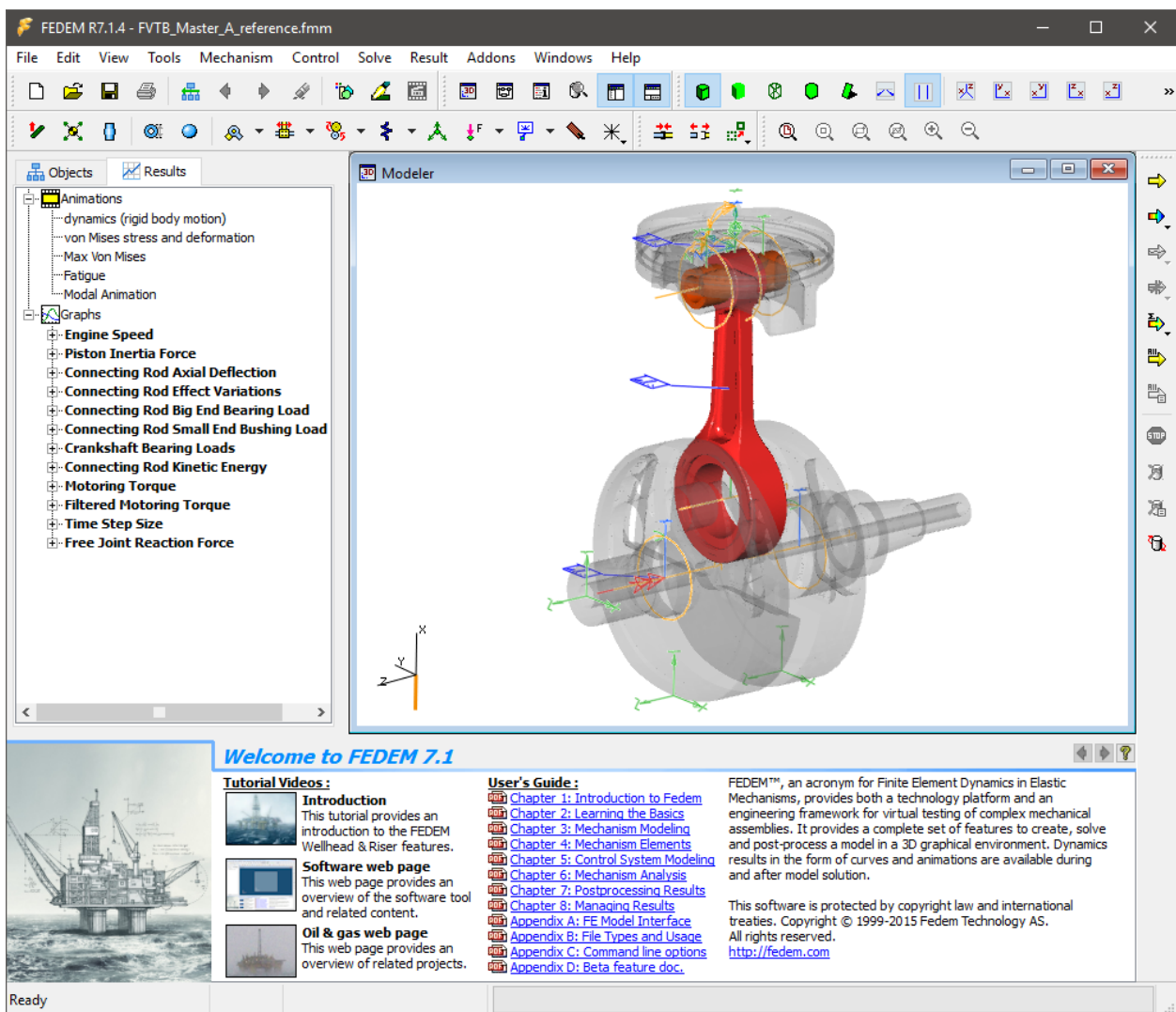

Figure 9.1: Reference test bench model

The original FVTB used an electric starter motor to bring the engine up to speed, before powering the engine through a cylinder pressure cycle function. Because physical testing is done without the cylinder head, no cylinder pressure is present, so the pressure cycle is removed

from the model. So is the dynamometer load, used to measure torque during operation. All friction and damping definitions imposed on the various joints in the model, along with part mass proportional damping, are also removed. The remaining engine model is therefore an ideal representation, free from friction and drag losses. This is utilized to fine-tune the model's numerical damping and time steps.
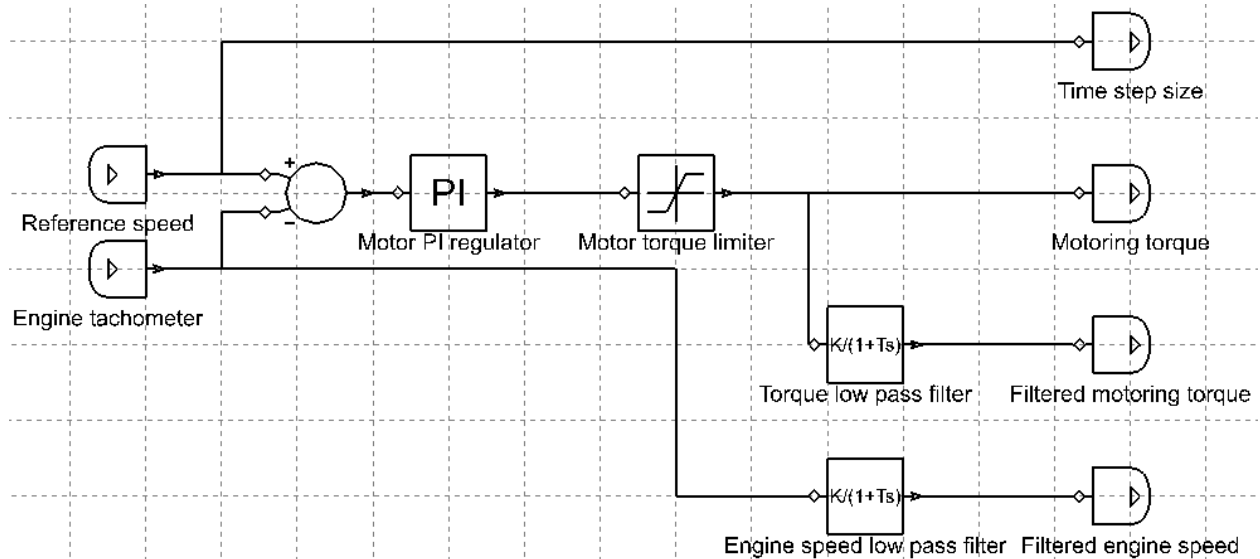

Figure 9.2: Control system

A control system (figure 9.2) is implemented to regulate the engine model simulation. The model test cycle is 11.5 seconds long and uses a poly line with linear ramping to control the reference speed from 3000 rpm to 9000 rpm. The reference speed is brought from zero to 3000 rpm in 1.5 seconds, and held at that speed for 1 second. Then the speed is increased by 1000 rpm in 0.5 seconds, and held at the new speed for 1 second. This is repeated all the way up to 9000 rpm. The resulting simulation reference speed is seen in figure 9.3. The magnitude of the acceleration between the reference speed plateaus is not of particular interest in the simulation. The reason being that torque measurements are being read at the end of each 1 second hold, to obtain a friction torque for steady state speed only. Longer simulation runs (both slower acceleration and longer holds) for a total of 125 seconds were also explored, but they provided the same result as the shorter simulations, with no indication of additional numerical drift. The major increase the time required to solve the simulation, was however a significant drawback.

The difference between the reference speed and the actual engine speed is used to determine the motoring torque supplied to the engine crankshaft. This is done using a Proportional-Integral (PI) controller. The piston assembly and connecting rod's motion and inertia affects the instantaneous rotational velocity of the crankshaft. This phenomenon combined with the nature of the PI controller, causes both the engine speed and motoring torque to oscillate. Low-pass filters are used for additional plotting of the engine speed and motoring torque, to provide a clearer picture of the average values occurring. The control system also includes a torque limiter for the electric motor, enabling maximum output motoring torque to be set.
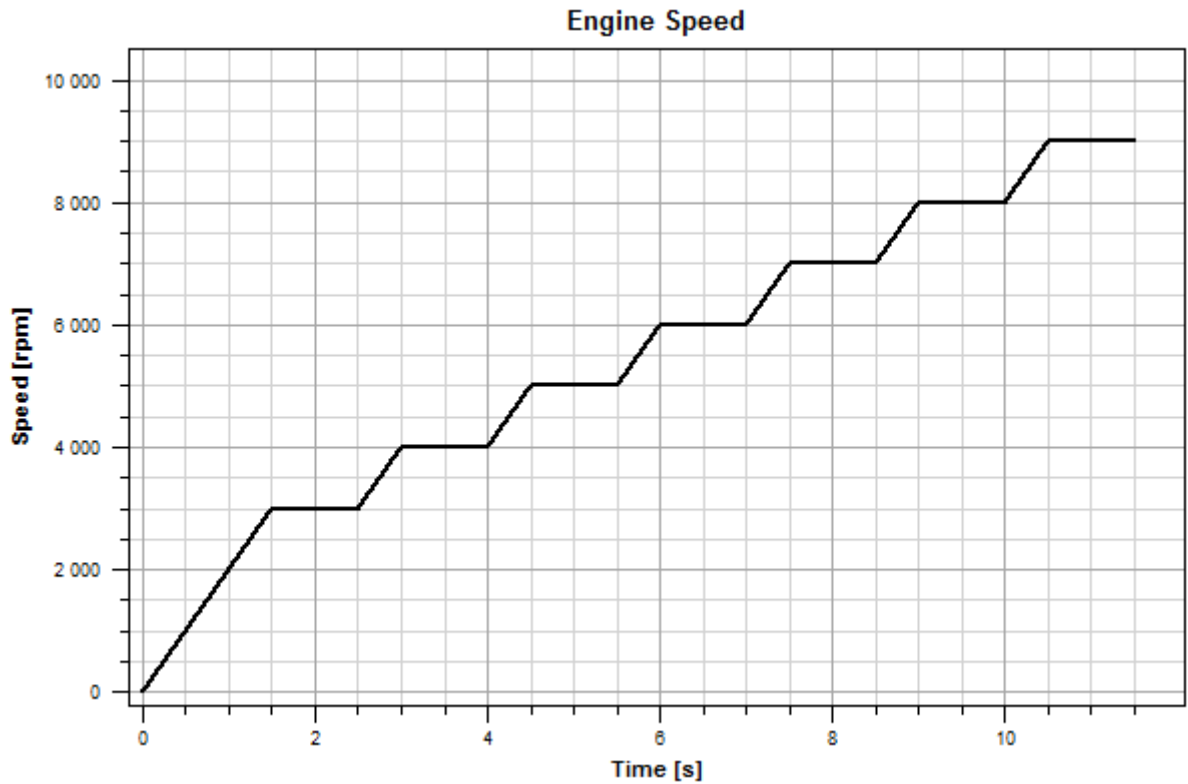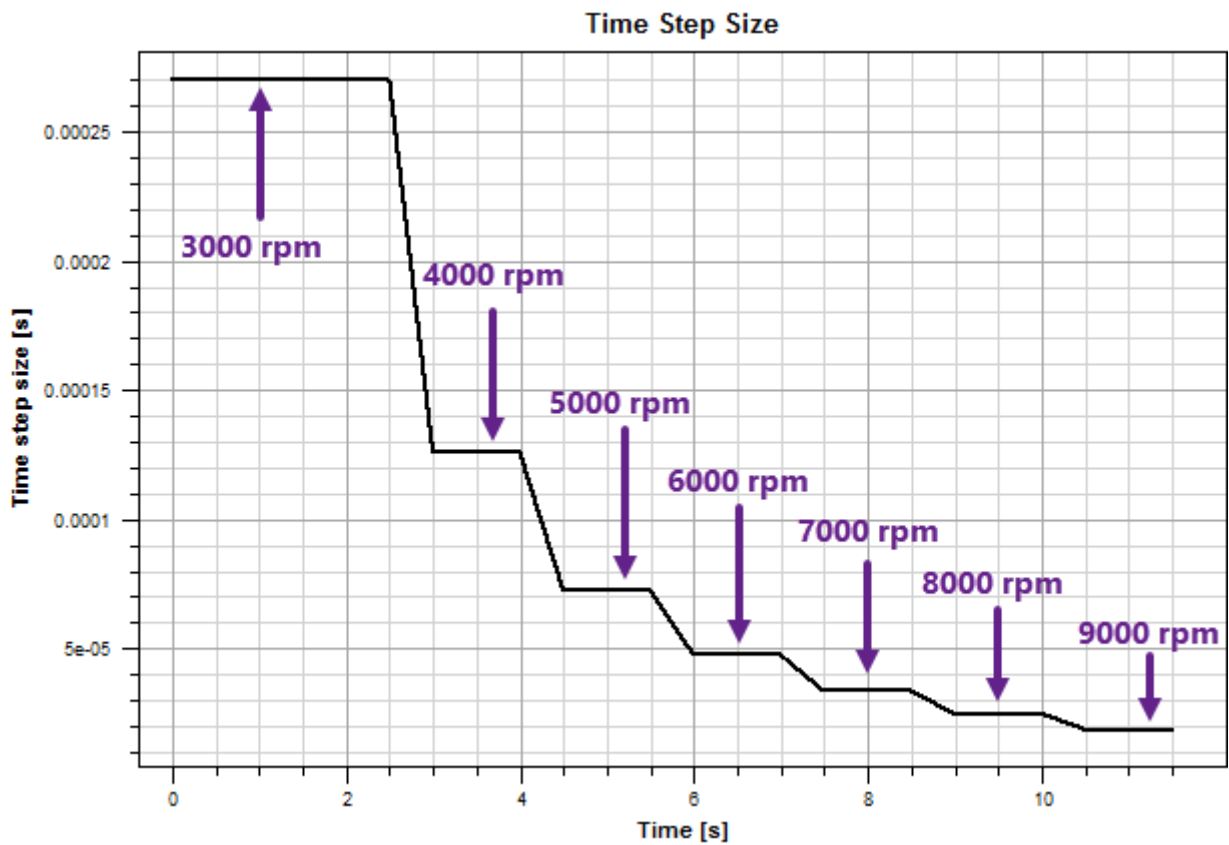
Figure 9.3: Simulation reference speed

Figure 9.4: Simulation time step size

Engine speed	Time step size
3000 rpm	2.700×10^{-4} s
4000 rpm	1.260×10^{-4} s
5000 rpm	7.260×10^{-5} s
6000 rpm	4.772×10^{-5} s
7000 rpm	3.360×10^{-5} s
8000 rpm	2.483×10^{-5} s
9000 rpm	1.871×10^{-5} s

Table 9.1: Time step size

FEDEM uses the Newmark-β and HHT-α time integration algorithm to solve the dynamic equation. This causes the numerical damping and the error to increase with the frequency ω (rotational velocity) if the time step h is constant, as seen in figures 9.5 and 9.6. To counteract this, variable time step size is employed. Adding stiffness proportional damping (refer to subsection 6.2.1) to the parts in the model adds some numerical stability, without introducing artificial damping against rigid body motion [9].

Trial and error is used to zero in on values for the numerical damping, and the optimal time step size for each step in engine reference speed. This is done though monitoring the motoring torque required at each of the reference speed plateaus. When the engine without any losses is held at a constant speed, no motoring torque is required to keep it operating at that speed. Tweaking time steps and numerical damping until zero average torque is required to keep the engine at the different reference speeds, yielded the time step sizes seen in figure 9.4 and table 9.1. A poly line function is defined in the control system, decreasing the time step size as reference speed increases. The rest of the model and simulation parameters are listed in table 9.2, and the reference model motoring torque (from the low-pass filter) is seen in figure 9.7.

Simulation parameters	
Electric motor torque limit	5 Nm
PI controller proportional term	0.05
PI controller integral term	1000
HHT-α factor	0.0031
Stiffness proportional damping (all parts)	8.0×10^{-5}
Max. number of iterations	50
Min. number of iterations	3
Geometric stiffness contribution	On
Centripetal force correction	On
Time between each print to result file	0.001 s

Table 9.2: Simulation parameters
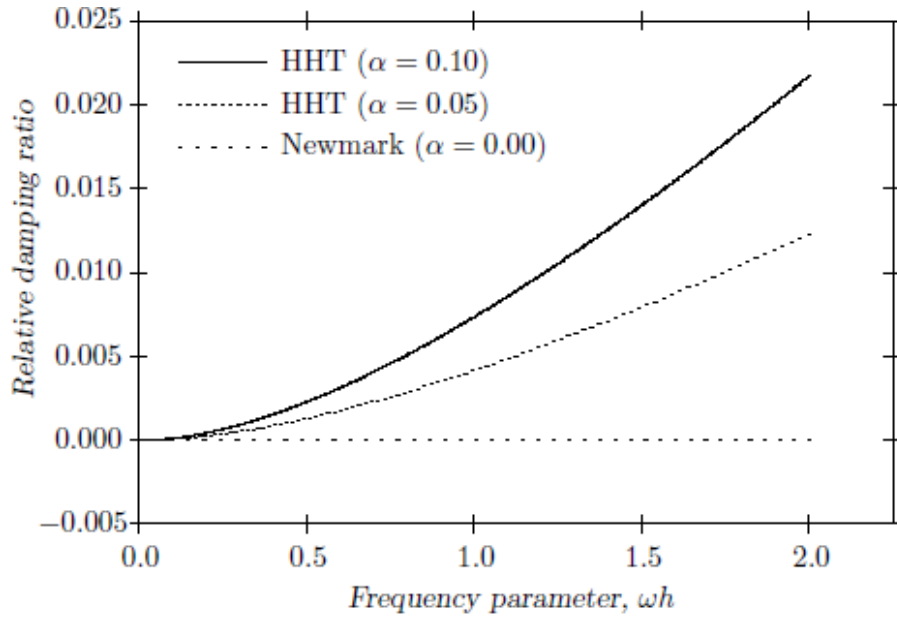
Figure 9.5: Numerical damping ratio [9]
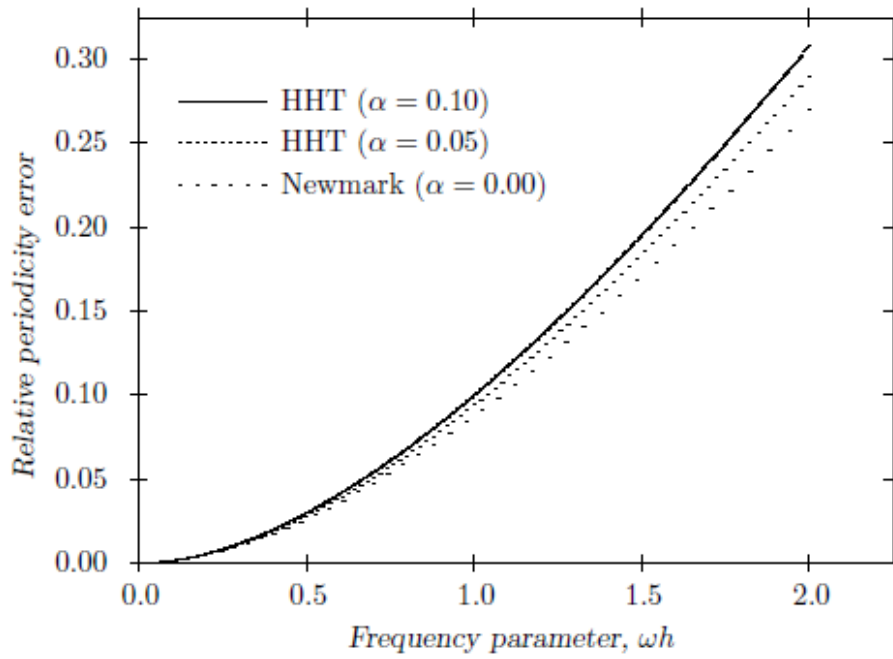
Figure 9.6: Numerical damping error [9]
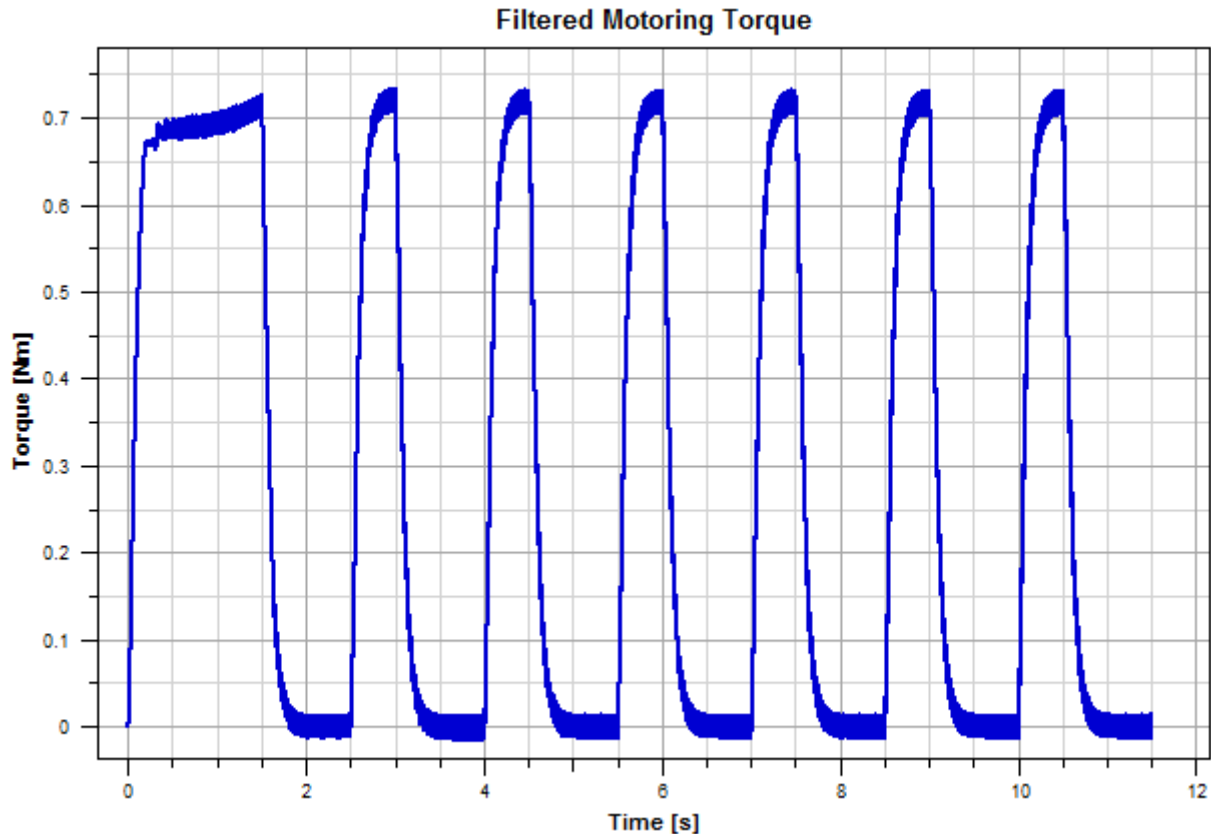
Figure 9.7: Reference model filtered motoring torque

9.1.2 Modeling and Meshing of OEM Connecting Rod

The piston, piston pin, and crankshaft were already modeled, imported and reduced in the FVTB (being used as basis for the reference test bench model), so the only part needing preparation is the connecting rod. The connecting rod with its small end bushing and big end bearing is modeled and meshed in Siemens NX before being exported as a Nastran data file to FEDEM. A dummy piston pin is also present in the model to include its stiffness contribution to the small end.

A quarter of the parts are modeled before being mirrored twice to create the full model. This ensures that the model is 100% symmetric in both directions about the center axis, and also makes symmetric meshing easier. The big end bearing is modeled using a simple approximation: A solid ring with the same physical size as the actual bearing is modeled using steel as the material. The actual bearing has some hollow space inside (due to the bearing function), so the total volume of the material is less than the solid ring. The stiffness of the material in the approximated bearing is reduced in accordance with the volume fraction of the real bearing compared to the approximated solid ring. The bearing and dummy piston pin are modeled with a "massless" material $(\rho = 10^{-10} \frac{kg}{m^3})$ to exclude their influence on the simulation, but the actual weight is accounted for in the FVTB.

The mesh chosen is CTETRA10 elements with a mesh size of 2 mm, and mesh mating with the setting "Glue-Coincident" is used to control the transitions between the connecting rod quarter parts and pin/bearing/bushing parts. Two RBE3 one-dimensional connection elements are added. One in the center of the big end bearing and one in the center of the dummy piston pin. These elements are connected to the neighboring surface nodes and used as connection points for the joints in the assembly in FVTB.

Table 9.3 shows the properties of the OEM steel connecting rod. The connecting rod and its FE model can be seen in figure 9.8. The piston pin is purple, the green color identifies the big end bearing and oil channels are seen in red.

Property	Value
Volume	22419.39 mm^3
Mass	174.80 g
Centroidal moments of inertia	$I_{xc} = 235.61$ kg mm^2 $I_{yc} = 33.19$ kg mm^2 $I_{zc} = 261.80$ kg mm^2
Root radius	30 mm
Width small end	15 mm
Transversal width	6.80 mm

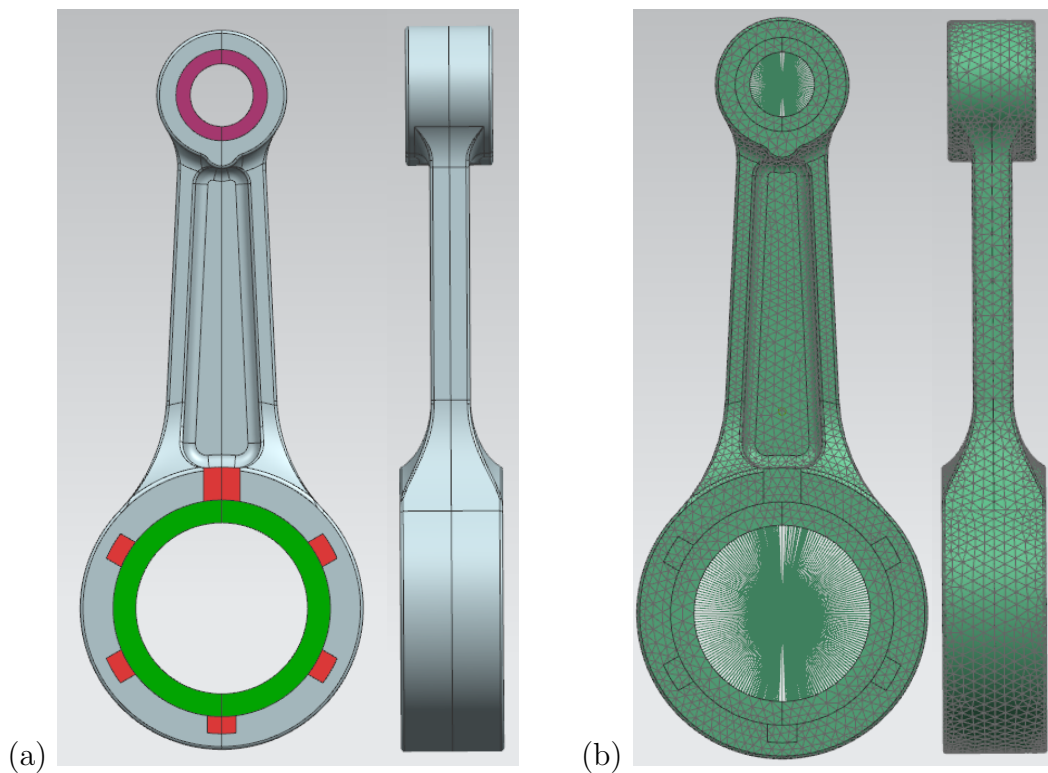Table 9.3: OEM connecting rod properties

Figure 9.8: OEM connecting rod: (a) CAD model (b) Meshed FE model

9.2 Virtual Test Bench Tuning

Using test results and establishing the reference test bench model from subsection 9.1.1 as a starting point, tuning of the virtual test bench can be performed. The goal is to recreate the friction behavior observed during testing. As already mentioned, the friction torque obtained during testing is an average friction torque at a chosen steady state speed, not instantaneous friction torque. The friction behavior in the virtual test bench is therefore also tuned according to average friction torque. Based on the findings in chapter 5, it is decided to apply the friction torque distribution in table 9.4 to the partial engine assembly in the virtual test bench. The piston assembly is responsible for approximately three times the friction torque of either the crankshaft or the connecting rod system. Looking at the percentages in the table alone, might lead one to believe that the friction from the crankshaft and connecting rod deceases as engine speed is increased. This is not the case, as the total friction torque equating to 100% varies with engine speed.

Mechanism	Friction torque distribution	
	Low engine speed	High engine speed
Piston assembly	56%	59%
Crankshaft system	23%	21%
Connecting rod system	21%	20%

Table 9.4: Friction torque distribution

In the virtual test bench, 3000 rpm is considered low engine speed, and 9000 rpm is considered high engine speed. Using the measured test data at 3000 and 9000 rpm to calculate the friction torque distribution at low and high engine speeds, provides two reference points for both the crankshaft and connecting rod systems. Adapting 2nd degree polynomial curves between the two points for each of the two systems, result in their friction contributions across the speed range. By using 2nd degree polynomials, it is assumed that the bearing friction and oil drag in these systems depend on engine speed in such a manner. This assumption is justified by considering that bearing friction depends on the acting normal force to some extent, and the normal force is a result of the inertia forces occurring in the piston and connecting rod assembly. Referring to equations 4.9, 4.10, and 4.11, it can be seen that both reciprocating and rotating forces depend on the square of the engine speed, thereby causing a 2nd degree dependency. The oil drag is basically viscous friction loss, and therefore follows the relation in equation 6.6, adding a linear component to the dependency on engine speed.

Modeling the friction loss caused by the connecting rod system is done by defining a rotational friction with the total friction model from equation 6.11, and a torque-angular velocity viscous damper (equation 6.6), on the joint in the connecting rod big end bearing. It is desired to make the virtual test bench model able to reflect change in friction as a result of changes in component mass and moments of inertia. Since the friction model shows dependency on the inertia force (through normal force), as much as possible of the 2nd degree polynomial friction torque is modeled using this approach. Without introducing too much friction at certain engine speeds, this approach results in too little friction at some speeds. The viscous damper is used to compensate for this, utilizing a poly line scaling function for the viscous coefficient (which is defined as 1). Tuning this scaling function until the combined friction and damping coincides

with the 2nd degree polynomial friction torque, produces the total connecting rod system friction. No friction is modeled in the small end of the connecting rod, as the friction loss from the small end bearing is negligible compared to the big end and the crankshaft bearings [18].

The same approach as the one just described for the connecting rod, is used to model the crankshaft system friction loss. The main difference is that there are two bearing joints in the crankshaft system. This means that the rotational friction is applied to two bearings, but the normal force each bearing sees is half of the total. The viscous dampers on each joint only depend on rotational velocity, so the parameters in the scaling function needs to be half of what would be the case for a single-joint setup.

The situation for the piston assembly is a bit more complex, because the coefficient of friction changes with the lubrication regime, oil viscosity, piston speed, and load, as seen in the Stribeck diagram (figure 5.1). It is also affected by the compression of the air on the underside of the piston. A translational friction with the total friction model is applied to the free joint representing the piston/cylinder interaction. The friction model in FEDEM does not support a variable coefficient of friction, which would have been the appropriate way of modeling changes in lubrication regime. Analogous to the approach for the connecting rod, as much friction as possible is introduced through the translational friction. The rest is compensated for by adding a viscous damper with a coefficient of 1, and using a scaling function to obtain the desired response.

Adding the viscous damper to the reciprocating cylinder free joint, causes the motoring torque to get out of control. The suspected reason is discussed in chapter 11. The viscous damping is instead applied as an addition to the scaling function for the damping already in place on the connecting rod big end bearing joint, and tuned until total friction behavior matches the test data for the whole speed range. While this might not be an completely accurate approach, the error resulting from the translational friction's inability to account for changes in the coefficient of friction (lubrication regime), is suspected to be of greater concern. It is worth mentioning that the compression of crankcase air by the reciprocating piston is not modeled as a separate phenomenon. It is included in the overall piston assembly loss.

The parameters used in the rotational and translational frictions are seen in table 9.5, and the poly line scaling functions for the viscous damping are presented in table 9.6.

Parameter	Connecting rod	Crankshaft	Piston
Force caused by pre-stress	X	X	0
Coulomb coefficient	0.0025	0.00245	0.08
Magnitude of Stribeck effect, S	0	0	0
Critical Stribeck speed, V_{slip}	0	0	0
Radius of contact surface, R	0.017	0.02	X
Torque caused by pre-stress	0	0	X

Table 9.5: Friction parameters

Regarding the operation of both the connecting rod and the crankshaft bearings, no Stribeck (stick-slip) effects are expected. The bearings only turn in one direction and are constantly turning at speeds far greater than what is associated with the Stribeck effect. A parameter

study of S and V_{slip} was performed for the translational piston friction, as the piston reaches zero velocity at both TDC and BDC. Stribeck friction captures the transition from static to kinetic friction as sliding velocity is increased, but in the case of the piston friction, this effect was negligible. This is thought to be because the extreme acceleration experienced by the piston near the dead centers causes piston velocity to increase past the critical Stribeck speed over a very short distance. This means that the Stribeck effect is only active in a relatively small part of total piston travel, resulting in a minuscule impact on the total average friction.

Function X-value (argument is engine speed)	Function Y-value (crankshaft)	Function Y-value (connecting rod)	Function Y-value (connecting rod + piston)
314.159 rad/s	0.091	0.180	0.655
418.879 rad/s	0.085	0.160	1.157
523.599 rad/s	0.073	0.140	0.972
628.319 rad/s	0.060	0.115	0.582
733.038 rad/s	0.040	0.085	0.303
837.758 rad/s	0.020	0.045	0.110
942.478 rad/s	0	0	0.032

Table 9.6: Viscous damping poly line scaling functions

A simplified flowchart describing the tuning process can be seen in figure 9.9. Temporary results from the tuning procedure, before and after the introduction of piston friction, can be seen in figures 9.10 and 9.11 respectively. The result from the engine testing was plotted in the same graphs for easy comparison. The final result is presented in section 10.4.
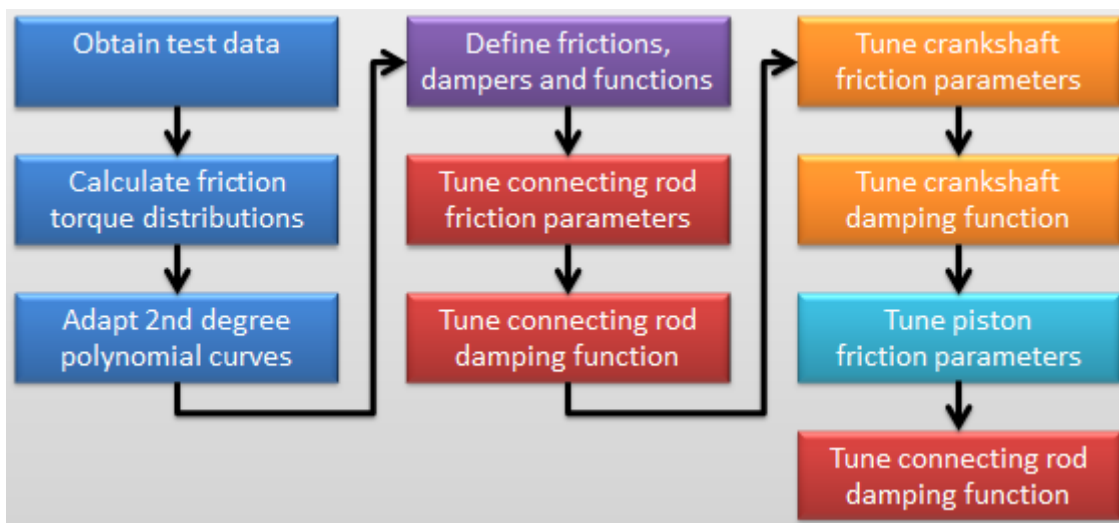

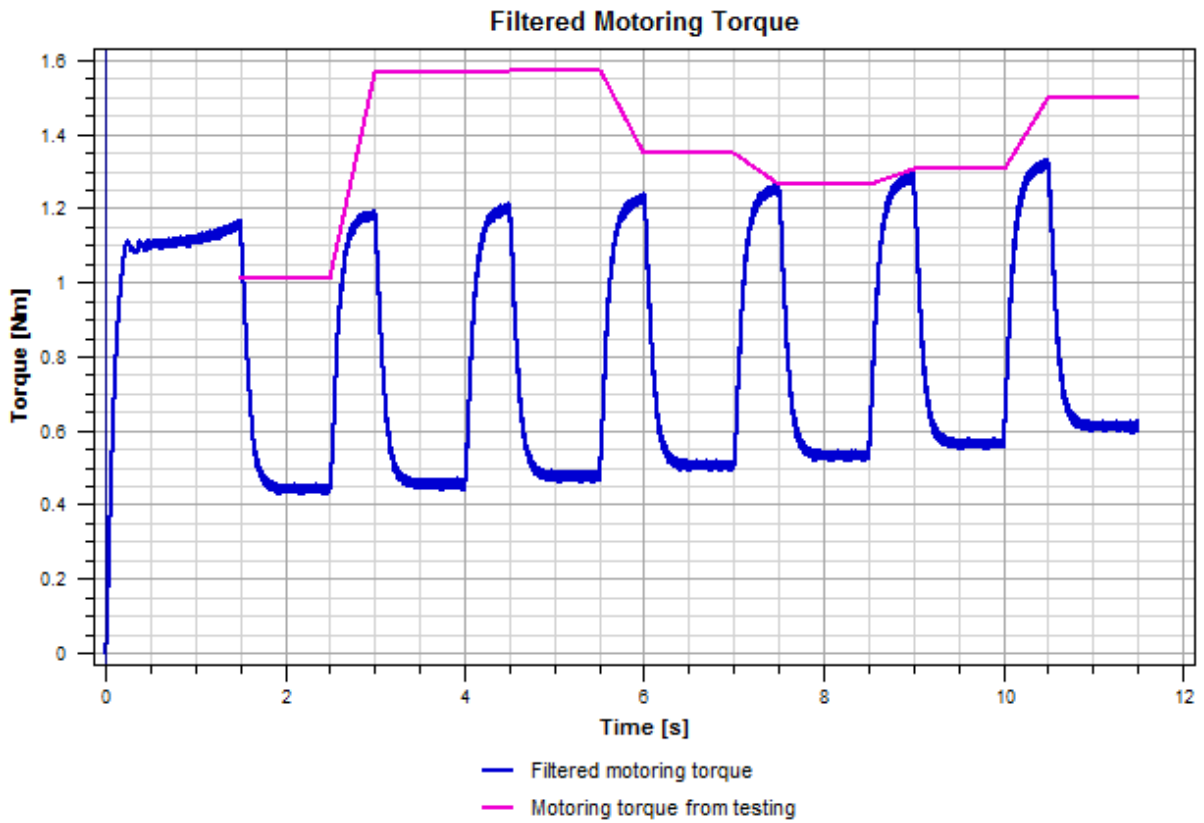Figure 9.9: Simplified flowchart for virtual test bench tuning

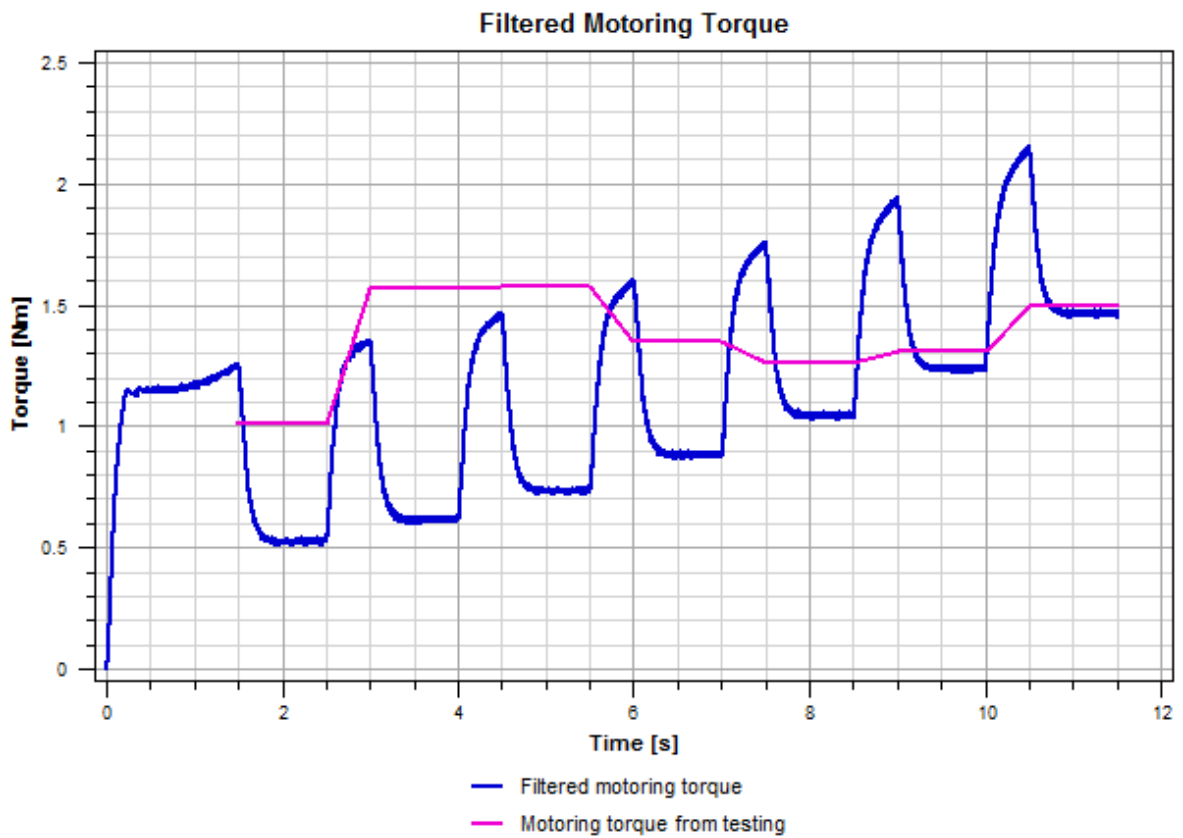Figure 9.10: Temporary result with only bearing friction and damping

Figure 9.11: Temporary result with bearing friction and damping plus piston friction

Chapter 10

Results

10.1   Modifications and Challenges Regarding the Test Setup

During testing it was observed that some engine oil seemed to squeeze past the piston rings, and ended up on the upper side of the piston. This flow of oil through the piston ring pack might change the lubrication conditions for the piston compared to during fired operation. A soft-box made from an oil-absorbing mat was placed on top of the four cylinder head bolts (not completely around the engine top), catching the oil flinging off the piston without restricting the air flow into the cylinder.

The wires for the oil temperature sensor and the heat cartridge entered the engine block through an existing sensor passage in the engine block cover. A custom rubber seal was fabricated to prevent oil and air from escaping due to compression of the crankcase air by piston reciprocation. The rubber seal did not perform 100%, so Sikaflex-11FC polyurethane adhesive was used to improve the seal's function. It turned out that the crankcase pressure combined with high oil temperature made it difficult to get the seal to work properly. It did perform well enough for testing, but some oil leakage was encountered during the test runs.

Considerable set-up time was spent getting correct alignment of the axle, bearings, torque transducer, and the belt drive. Even the smallest misalignment in terms of belt angle would cause the belt to travel to one side of the pulleys, with the risk of wearing it out against the edges or jumping off the pulley system.

The initial plan for connecting the axle, transducer, and engine was to use bellows couplings. After assembling the test rig for the first time, it was clear that the bellows couplings had too much run-out to ensure proper alignment of the rotating axes. The next idea was to replace the bellows couplings with 0.02 mm shrink-fits on both sides of the transducer. The connection against the engine (modified socket) performed excellent, but the aluminum sleeve between the axle and the transducer (figure 10.1) showed signs of slipping after the initial function test. A new sleeve made from steel was fabricated, but it turned out to be difficult to align properly. In the process of improving the alignment, the torque transducer was damaged by excessive heat and/or mechanical force, which resulted in a bent transducer axle.
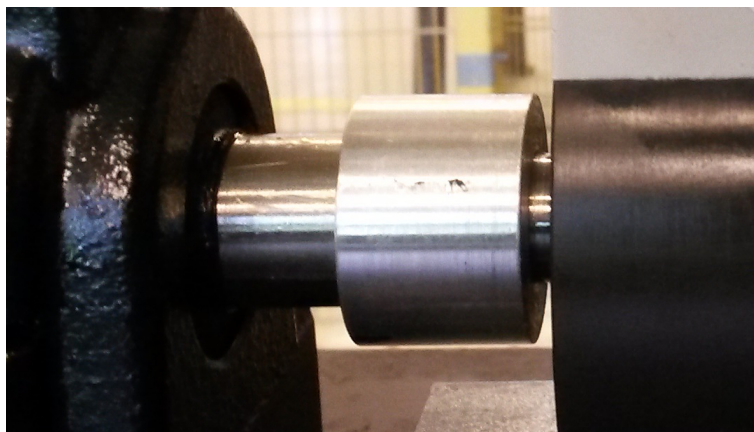
Figure 10.1: Old shrink-fit aluminum sleeve

Due to the high cost and delivery time associated with obtaining a new transducer, it was decided to first investigate if the transducer already in hand could be repaired. The torque transducer was disassembled and the axle straightened. After reassembly, the torque transducer seemed to function properly, but the output at zero torque had shifted. Not an unexpected result, as plastic deformation of the axle would naturally affect the transducer's strain gauges.

To investigate if the transducer could still be used, it was connected to the data acquisition system and calibrated in such a way that a zero reading in Catman coincided with zero transducer torque. Then, one side of the transducer was held stationary while a precision torque wrench was used on the socket-side to apply torque in 0.5 Nm increments from 1 Nm to 5 Nm. The transducer's response can be seen in figure 10.2, and it revealed a predictable and relatively linear response. From the specifications in subsection 8.2.2, each volt of transducer output equals one Nm. The output did not match the torque wrench settings precisely, which could be explained by the transducer's tolerances in terms of linearity, sensitivity and zero value. Also, the accuracy of the torque wrench settings was unknown.

After considering these uncertainties and reviewing the result of the test, it was decided to perform the engine testing with the repaired transducer. It is important to bear in mind that the accuracy and reliability was most likely reduced as a consequence of plastic deformation where the strain gauges were placed. It was decided to use a steel sleeve with set screws to connect the axle to the transducer, to avoid damaging the transducer further. Both axles entering the sleeve were ground flat on one side to give better conditions for the set screws.
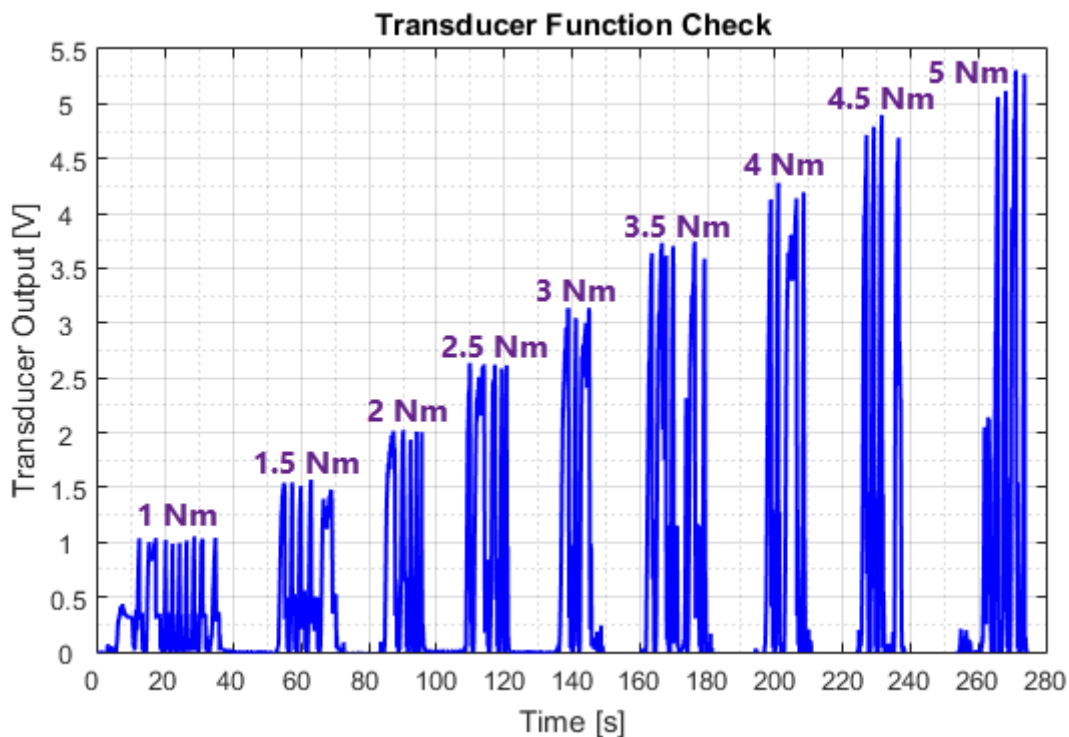
Figure 10.2: Transducer function check

10.2 Engine Break-in Results
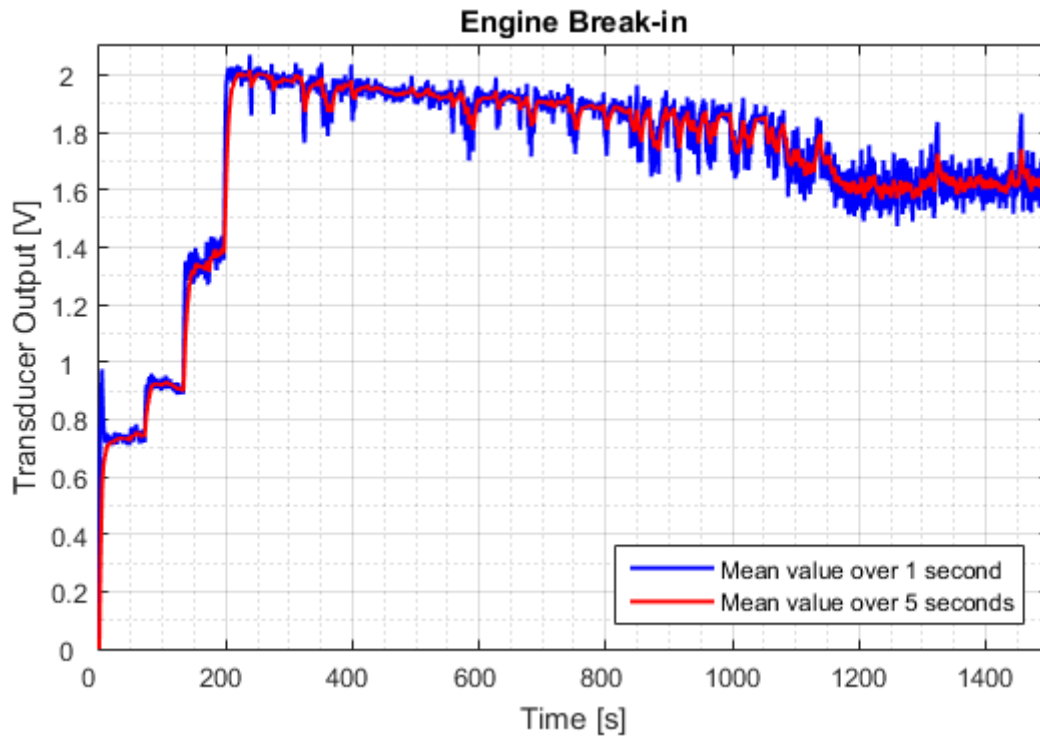
Figure 10.3: Engine break-in

The engine was broken in using the procedure described in subsection 8.3.1, with the Simmerstat heat cartridge regulator set to level 3. The engine speed was stepped up from zero, and reached 4000 rpm 200 seconds into the test. It was held at 4000 rpm for approximately 22 minutes. After reaching an oil temperature of 85 °C, the oil heating was turned off. It was observed that the engine produced enough heat on its own at 4000 rpm to keep the oil temperature at 87 °C for the remainder of the test. The transducer output (equivalent to friction torque) showed a steady decrease from approximately 2 V to 1.6 V over the course of 17 minutes, before stabilizing (see figure 10.3). With no substantial change in measured value for the last 5 minutes, the break-in was considered complete.

10.3 Engine Test Results

10.3.1 Initial Function Test

After assembling the test rig for the first time, a function test was performed. The test data was recorded and can be seen in figure 10.4. Extracted representative results are shown in table 10.1. Since this was an early function test, the complete test procedure was not fully developed and followed. Despite only providing mean value calculation over one second intervals, using different engine speed steps, and being performed on the engine before break-in, the results

are still usable for comparison purposes. After the initial function test was completed, it was discovered that the aluminum sleeve between the axle and the transducer (figure 10.1) showed signs of slipping. This was solved as described in section 10.1.

Figure 10.4: Function test results

Approximate test cycle time	Engine speed	Transducer output	Oil temperature	Oil heating setting
0 - 40 s	1000 rpm	0.73 V	78 °C	3
50 - 75 s	2000 rpm	0.94 V	77 °C	3
85 - 150 s	3000 rpm	1.37 V	75 °C	3
185 - 210 s	4000 rpm	2.04 V	74 °C	3
220 - 250 s	5000 rpm	2.07 V	77 °C	3
290 - 325 s	6000 rpm	1.82 V	80 °C	3
350 - 390 s	7000 rpm	1.75 V	82 °C	3
400 - 420 s	8000 rpm	1.76 V	86 °C	3

Table 10.1: Function test representative results

10.3.2   Full Test Cycle

Before any further testing was performed, the engine oil used during the initial test and engine break-in was replaced. This was done to make sure that the engine oil used for testing did not contain any any debris or impurities from the break-in procedure. A full test cycle was performed according to the procedure described in subsection 8.3.2, and the results can be seen

in figure 10.5. Extracted representative results (using the five second mean values) are shown in table 10.2.

It looks like the first 6000 rpm plateau (between 235 and 275 seconds) was held a bit to short, since the values did not stabilize completely before continuing with the test. The dip in output between 275 and 300 seconds appears because the test speed was reduced for a short period of time, to approach and inspect the test rig before continuing.
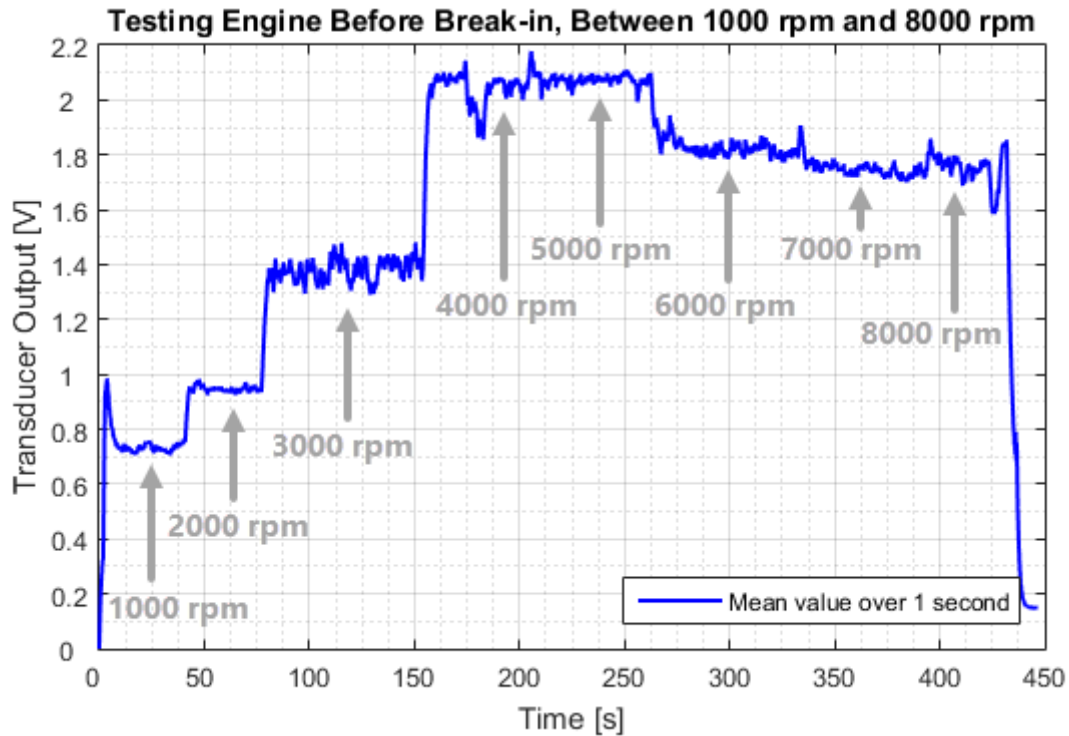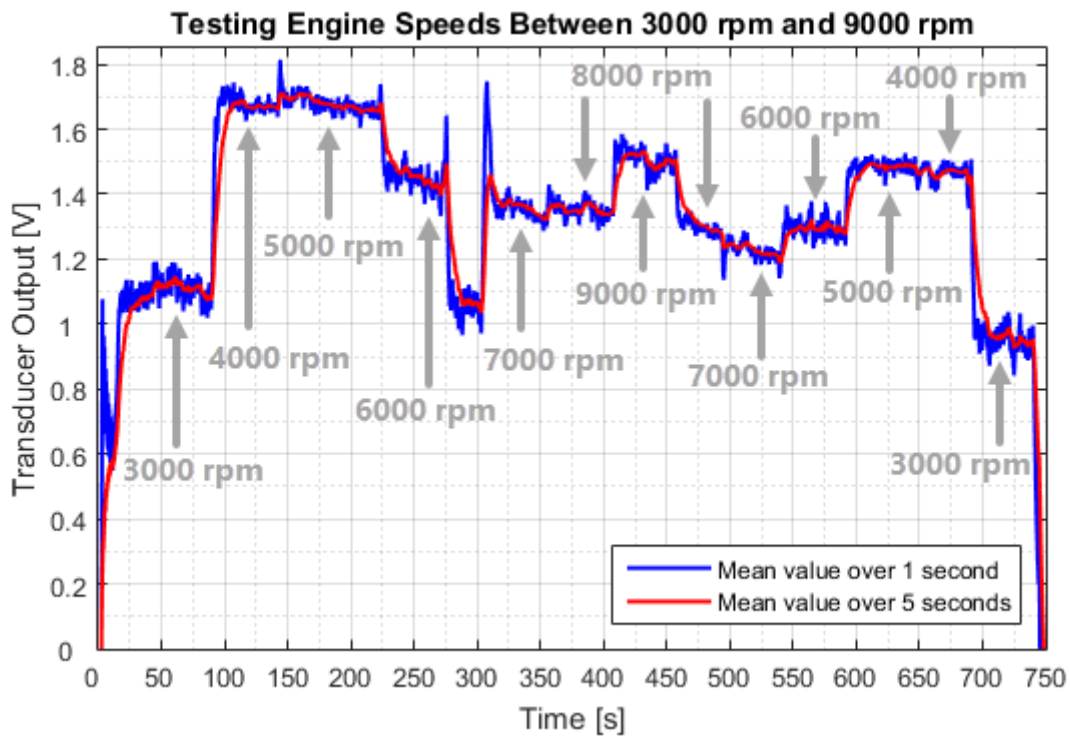

Figure 10.5: Full test results

Approximate test cycle time	Engine speed	Transducer output	Oil temperature	Oil heating setting
15 - 90 s	3000 rpm	1.08 V	75 °C	3
100 - 140 s	4000 rpm	1.67 V	75 °C	3
150 - 225 s	5000 rpm	1.66 V	77 °C	3
235 - 275 s	6000 rpm	1.41 V	80 °C	3
310 - 350 s	7000 rpm	1.32 V	79 °C	0
360 - 400 s	8000 rpm	1.34 V	80 °C	0
410 - 450 s	9000 rpm	1.50 V	82 °C	0
460 - 490 s	8000 rpm	1.28 V	82 °C	0
500 - 540 s	7000 rpm	1.21 V	83 °C	0
550 - 590 s	6000 rpm	1.29 V	84 °C	0
600 - 640 s	5000 rpm	1.49 V	85 °C	0
650 - 690 s	4000 rpm	1.47 V	85 °C	0
700 - 740 s	3000 rpm	0.94 V	84 °C	0

Table 10.2: Full test representative results

10.3.3   Test with Transducer Failure

After the first full test cycle, the plan was to run more to get several sets of test data for comparisons and averaging. Early in the second test (4000 rpm), it was discovered that the output did not behave as expected. The measured values did not appear to stabilize, and the problem became more pronounced at 5000 rpm. The measured output continued to increase until transducer failure occurred. The results can be seen in figure 10.6. Extracted representative results (using the five second mean values) are shown in table 10.3.

After the transducer was damaged and repaired (see section 10.1), there were some concerns regarding its accuracy and reliability following the plastic deformation that had occurred. Additional damage accumulated through high frequency torsion cycling (varying torque over each crankshaft revolution), and possibly also bending (misalignment), caused fatigue failure of the axle inside the transducer.
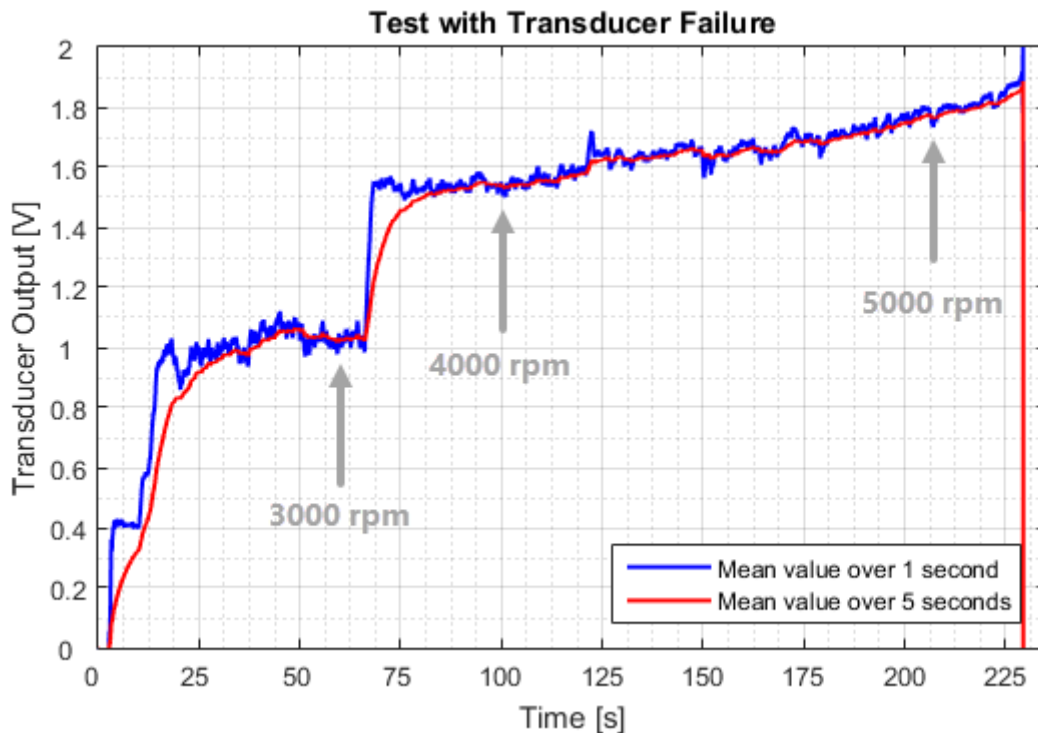
Figure 10.6: Transducer failure test results

Approximate test cycle time	Engine speed	Transducer output	Oil temperature	Oil heating setting
50 - 65 s	3000 rpm	1.03 V	82 °C	2
75 - 120 s	4000 rpm	1.57 V	83 °C	2
130 - 225 s	5000 rpm	1.86 V	83 °C	0

Table 10.3: Transducer failure test representative results

10.3.4 Test Results Summary

From the specifications in subsection 8.2.2, each volt of transducer output equals one Nm. A summary of the test results is presented in figures 10.7 and 10.8. The average values of the tests with rising and falling rpm steps were used as representative values in tuning of the virtual test bench. These values are found in table 10.4.
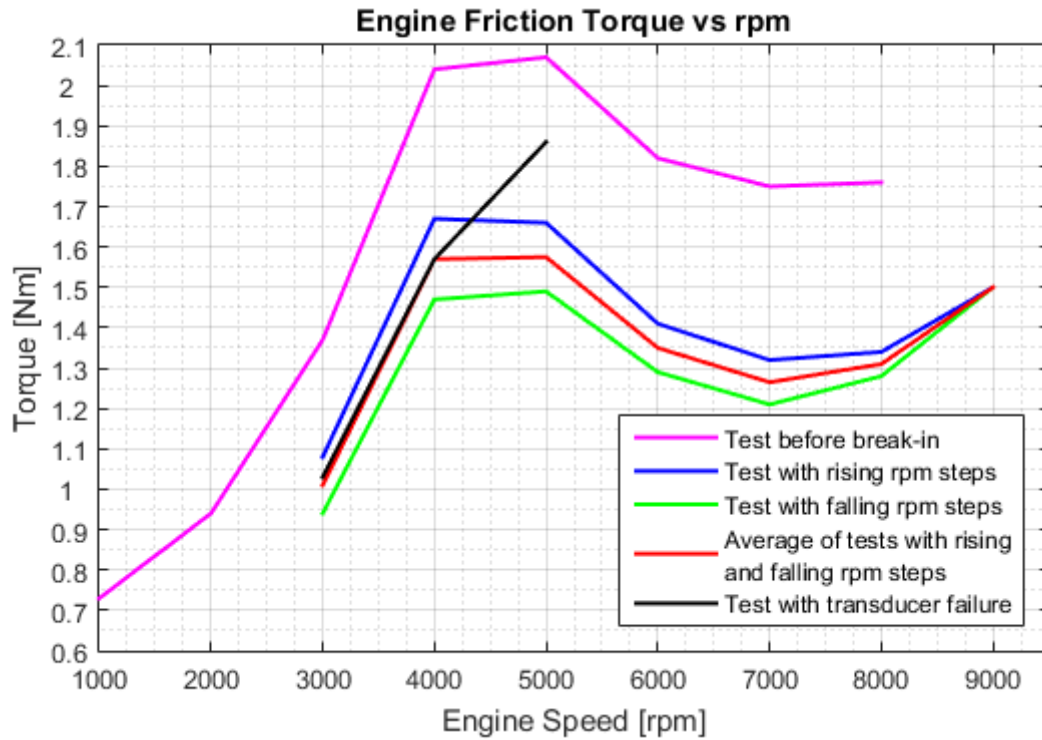
Figure 10.7: Friction torque vs. engine speed

Engine speed	Friction torque	Oil temperature
3000 rpm	1.01 Nm	80 °C
4000 rpm	1.57 Nm	80 °C
5000 rpm	1.58 Nm	81 °C
6000 rpm	1.35 Nm	82 °C
7000 rpm	1.27 Nm	81 °C
8000 rpm	1.31 Nm	81 °C
9000 rpm	1.50 Nm	82 °C

Table 10.4: Averaged results summary
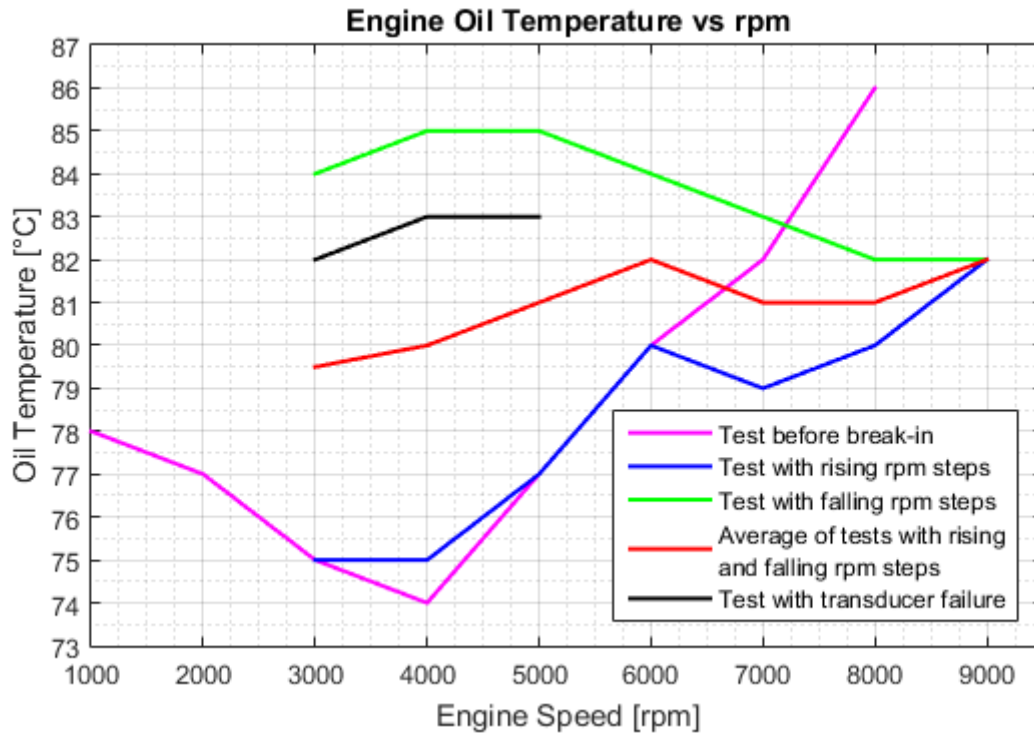
Figure 10.8: Oil temperature vs. engine speed

10.4 Virtual Test Bench Results

The final result from the virtual test bench tuning in section 9.2 is presented in figure 10.9 and table 10.5. The values were extracted from the filtered motoring torque using the mean value from the curve statistics in FEDEM. The mean was taken over 0.1 seconds at the end of each engine speed plateau. The result from the engine testing was plotted in the same graph for easy comparison. A simulation run in the virtual test bench is completed in approximately 20 minutes.

As a result of introducing resistance in the test bench model, the parameters for the PI controller established in the reference test bench model caused the simulation engine speed to be too low. To remedy this, the PI controller integral term was reduced to 3. As seen from both figure 10.10 and the results in table 10.5, the engine speed from the simulation still deviated slightly from the set points from the reference speed curve. At some speeds it was too low, and at others too high. On average, the new PI controller setting performed acceptably well.

To investigate the virtual test bench's response to weight changes in a part, a simulation was set up where the connecting rod's mass was scaled down to 60%. FEDEM provides options for scaling mass and stiffness of individual parts, without changing the FE model. The result can be seen in table 10.6.

Filtered Motoring Torque
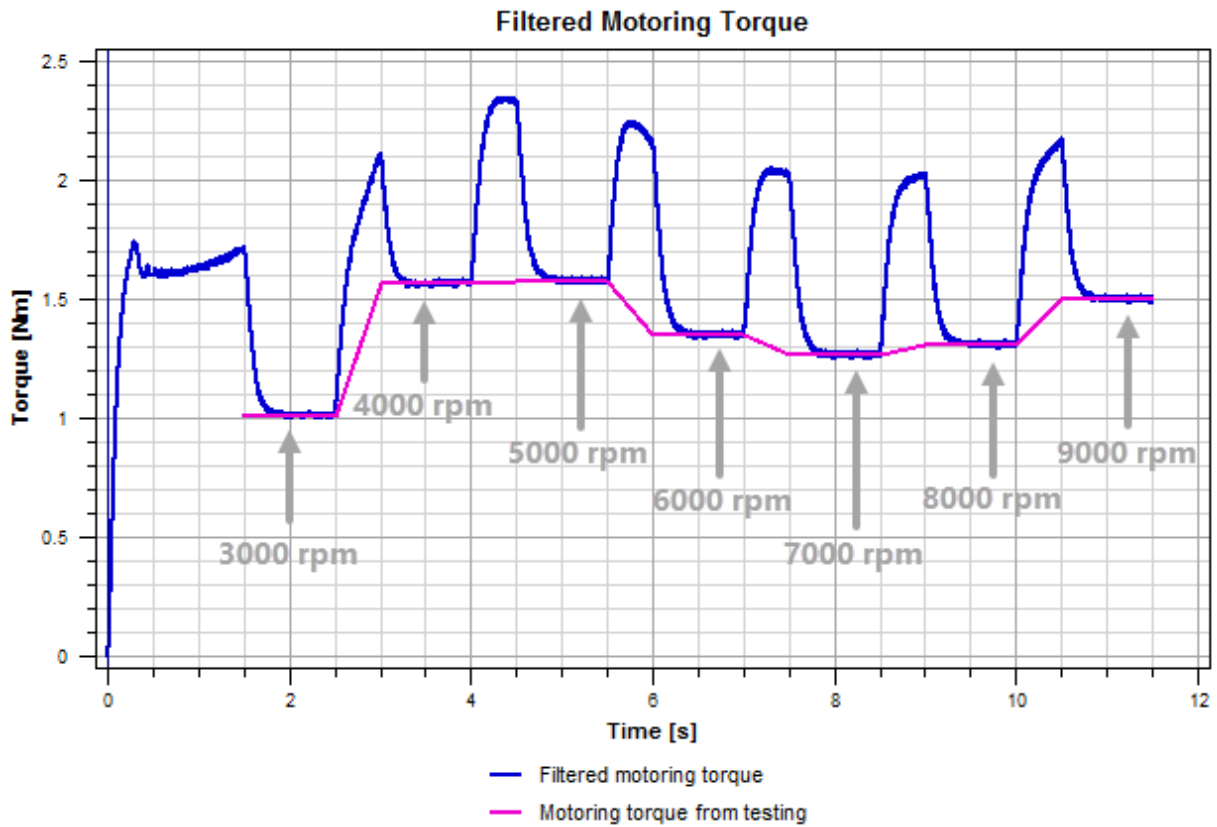
Figure 10.9: Graphic representation of final result
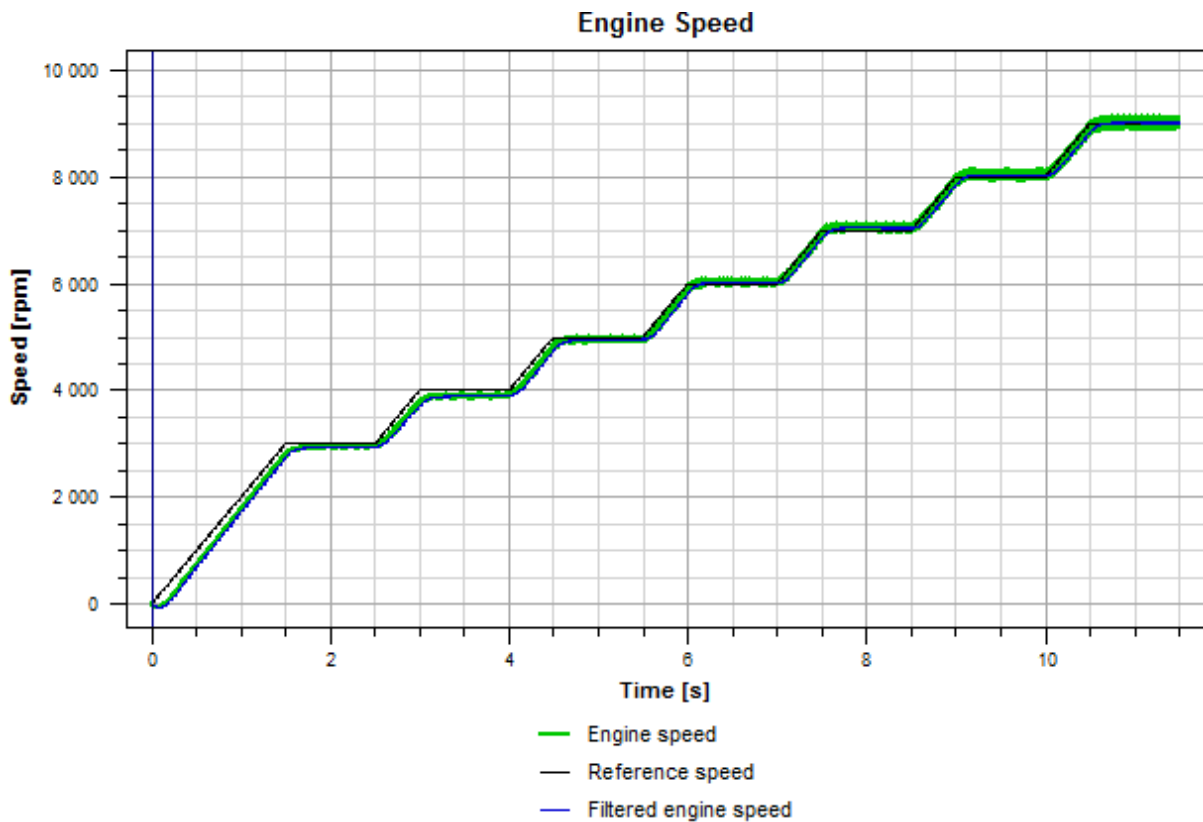
Engine Speed

Figure 10.10: Engine speed from final result

Engine speed		Simulation speed	Simulation torque
3000 rpm	314.159 rad/s	308.786 rad/s	1.01 Nm
4000 rpm	418.879 rad/s	409.308 rad/s	1.57 Nm
5000 rpm	523.599 rad/s	519.495 rad/s	1.58 Nm
6000 rpm	628.319 rad/s	630.735 rad/s	1.35 Nm
7000 rpm	733.038 rad/s	737.388 rad/s	1.27 Nm
8000 rpm	837.758 rad/s	841.448 rad/s	1.31 Nm
9000 rpm	942.478 rad/s	943.699 rad/s	1.50 Nm

Table 10.5: Results from the virtual test bench tuning

Engine speed		Simulation speed	Simulation torque
3000 rpm	314.159 rad/s	308.775 rad/s	1.01 Nm
4000 rpm	418.879 rad/s	409.298 rad/s	1.57 Nm
5000 rpm	523.599 rad/s	519.486 rad/s	1.57 Nm
6000 rpm	628.319 rad/s	630.747 rad/s	1.34 Nm
7000 rpm	733.038 rad/s	737.416 rad/s	1.25 Nm
8000 rpm	837.758 rad/s	841.498 rad/s	1.29 Nm
9000 rpm	942.478 rad/s	943.774 rad/s	1.48 Nm

Table 10.6: Results from connecting rod with reduced mass

Chapter 11

Discussion

As mentioned in section 10.1, oil was seen to squeeze past the piston rings during testing. It is suspected that this issue occurred as a consequence of motored testing without the cylinder head. As the engine rotates, oil is splashed onto the cylinder wall by the crankshaft. Each time the piston moves down, some oil is scraped off and accumulated near the bottom of the piston rings, and pressure is built up under the piston due to compression of the crankcase air. Since no combustion pressure was present during testing, there was no back-pressure helping the piston rings seal during the power stroke. Any oil managing to squeeze past the oil control ring during the intake stroke under fired operation would most likely be squeezed back before passing the compression ring, by the pressure during the compression stroke and the blow-by of combustion gases during the power stroke.

Resolving this issue while maintaining atmospheric pressure in the cylinder would mean introducing a pumping loss through venting of the crankcase. Instead, it was decided to perform the tests with some oil squeezing past the piston rings, being aware that this might change the lubrication conditions for the piston compared to during fired operation. The absence of back-pressure (due to motored testing) to push the piston rings towards the liner reduces the normal force between them, resulting in a thicker oil film in the piston-liner interaction. This reduces the friction from the scraping action of the piston rings. However, the lack of back-pressure also reduces the sealing capability of the piston rings, causing a higher pressure gradient across the rings, and increases Poiseuille shear of the oil film compared to fired tests. Whether these two effects cancel each outer out, or if one of them dominates, is hard to decide without performing additional specific tests.

After the torque transducer was damaged and repaired, it seemed to work satisfactorily. While the shift in zero torque output revealed that some damage had occurred, the transducer function check (figure 10.2) showed a predictable and relatively linear response. The accuracy of the output values compared to the torque wrench settings seemed to be sufficient.

It would have been an advantage to get data from more tests, particularly to avoid variations due to measurement values not stabilizing entirely before moving on to the next engine speed. Performing the break-in procedure once again at a higher engine speed could have been done to make sure that the engine was properly broken-in. Due to the torque transducer failure, this was however not possible. One might speculate in the validity and accuracy of the test data obtained with the repaired transducer, but the results in figure 10.7 show that the same trend is present and repeatable in all of the test runs. Even in the test where the transducer ultimately failed, the first measurements closely match the average from the test with rising and falling rpm steps. This gives credibility to the test results.

Questions might be raised as-to whether the test results from motored testing are representative for a normally running engine. Since no combustion is encountered, the temperature of the cylinder liner is lower than what would be the case if the engine was firing normally, and this has implications for oil viscosity and piston friction, particularly during the power stroke. While heating and precisely measuring the cylinder liner is a possible approach to approximate fired operation, this requires extensive modifications to the engine and was therefore not performed at this time. The lack of cylinder pressure is also an influencing factor, affecting both Poiseuille shear and piston ring back-pressure. According to Hoshi [14] and Mufti [18], the results from motored and fired testing are relatively similar. The power stroke is where most of the differences lie. This means that motored testing can still provide relevant friction data,

but comparison with fired operation would be beneficial.

In figure 10.7 it can be observed that all of the tests show the same behavior of the friction torque. It is interesting to note that even the test performed before engine break-in shows the same behavior, but at higher friction values. This highlights the importance of engine break-in on the friction properties, in agreement with the findings of Fadel et al. [8].

The curves from the test with rising and falling rpm steps both show the same behavior, but the values are different. This can be explained by looking at the corresponding oil temperatures in figure 10.8. Since oil viscosity is sensitive to temperature, the friction losses are too. This applies to both the bearings and the piston assembly. The work by Daniels and Braun [5] confirms this relation between temperature and losses. As the oil temperature increases, the viscosity is reduced, resulting in lower friction for the hydrodynamic part of the stroke. The temperatures from the falling rpm steps measurements were higher than from the rising rpm steps measurements, and this explains why the friction torque from the measurements during falling rpm steps were lower.

The reason for the higher temperatures was that the test schemes were run in succession, so the oil temperature was higher from the start. Even though the oil heating system was turned off, oil temperature continued to rise as the test proceeded. Since no heat was supplied from combustion, this must mean that bearing and piston friction, together with oil shearing, were responsible for the temperature rise. This is further exemplified by the results from the engine break-in, where it was observed that the engine produced enough heat on its own at 4000 rpm to keep the oil temperature at 87 °C, despite the whole engine acting as a heat sink. The engine is normally liquid cooled, but the testing was performed without plumbing, radiator, water pump and coolant. Including this in the test rig would most likely keep the oil temperature more stable.

Assuming that bearing friction is strictly increasing with engine speed (viscous damping, inertia forces), means that the piston assembly friction is responsible for the shape of the curves in figure 10.7. An interesting observation is that the overall shape of the curves resemble the Stribeck diagram (figure 5.1). The Stribeck diagram shows the friction coefficient as a function of the duty parameter $\left(\frac{viscosity \times speed}{load}\right)$. This explains the test data's curves to some extent, seeing as the mean piston velocity increases with engine speed. (This assumes that the oil viscosity and normal load from inertia forces behave in such a manner that the duty parameter is strictly increasing with engine speed). When the engine speed is below 4000 rpm, the dominating piston assembly lubrication regime appears to be boundary. Between 4000 rpm and 5000 rpm, the dominating lubrication regime seems to shift to mixed, and gradually transition towards hydrodynamic at 7000 rpm. From there and up, hydrodynamic lubrication appears to be the dominating regime. It is important to note that even if a specific regime is seen to "dominate" the friction behavior, this does not mean that it is the only one in effect. Different regimes still occur during a piston stroke (as described in chapter 5), but which one contributes the most, changes.

The results from the virtual test bench shows that it was successfully able to recreate the measurements from the engine testing. Engine speed stays fairly accurate, and the motoring torque for each engine speed plateau matches the test data. The results from the simulation run with a lighter connecting rod were however not as expected. Even with the connecting

rod weighing in at 60% of the OEM rod, the reduction in required motoring torque was barely noticeable (0.02 Nm at the most). A larger reduction is expected when comparing to the experimental findings by Johnson et al. [15].

The reason for this discrepancy is suspected to be that the modeling approach does not replicate the actual friction behavior in the engine. In particular, the modeling of piston assembly friction is of concern. It has already been mentioned that the FEDEM friction model for translational friction is not comprehensive enough to capture the changes in lubrication regime for the piston assembly. It does not support a variable coefficient of friction, but requires the Coulomb coefficient to have a constant value. This limitation is unfortunate, as it can not represent the complex piston assembly friction in an accurate manner. Working around this limitation meant modeling the lubrication regime changes by viscous damping with a variable viscous coefficient. This causes the friction behavior to be less dependent on the weight of the engine components (through inertia forces).

An additional challenge was adding the viscous damping to translation of the piston assembly. In order to get the desired effect, the magnitude of the viscous coefficient would have to be fairly large, and this caused the motoring torque to get out of control. The reason is suspected to be the varying piston velocity, and the fact that viscous damping depends on this. As the piston reaches maximum velocity (and viscous damping force) mid-stroke, the PI controller ramps up the torque to keep the engine speed constant. As the piston starts to slow towards dead center, the viscous damping force decreases, causing the engine speed to increase while the PI controller tries to slow it down. The PI controller is not able to react fast enough to the viscous damping changes during the course of a stroke, and therefore causes motoring torque overshoot. This problem could possibly be solved by implementing a different control strategy for the engine speed, but this would mean starting from scratch with both modeling of the reference test bench and the tuning. Since this issue was discovered rather close to the thesis deadline, it was decided to work around this problem to see if viable results could be produced with the existing model. The workaround by adding the viscous damping to the scaling function for the connecting rod damping seemed to work, but is not an accurate representation of real engine friction behavior.

When introducing friction in the virtual test bench, it was noted that the existing parameters for the PI controller caused the simulation engine speed to be too low. Reducing the PI controller integral term was seen to acceptably remedy the issue, but the simulation engine speeds still deviated slightly from the reference speed curve. To implement this change of a control system parameter perfectly, the modeling of the reference test bench (with time steps) and the tuning should have been performed from scratch. This would have been too time consuming considering the thesis deadline, but is something that should be considered in future work.

The modeling performed in the virtual test bench only considers one piston assembly loss, encompassing piston rings, piston skirt, and crankcase air compression losses. This approach does not consider the separate effects of piston rings and piston skirt, and secondary motion is not accounted for. The piston friction is applied to the free joint, representing the piston/cylinder interaction in the virtual test bench. A more detailed approach would be to employ contact formulations for the piston rings and skirt, and apply the friction through these. This approach would necessarily increase the model complexity and computational cost, but whether it is necessary in terms of result accuracy is difficult to answer without more detailed testing and

simulation.

A possible solution to improve the friction and damping modeling could be utilizing an external .dll file for this task. This would be analogous to the cylinder pressure cycle .dll file from section 3.2. By using this approach, better control over the parameters (such as variable Coulomb coefficients) and friction behavior is possible, at the expense of a more complex modeling procedure. Exploring this option would be a natural step in improving the accuracy of the virtual test bench.

The general approach used during modeling was to add as much as possible of the piston, crankshaft, and connecting rod contributions as either translational or rotational frictions. The remaining parts were added as viscous damping. This choice was based on possibilities and limitations in FEDEM. The unfortunate impact on the modeling of piston assembly friction has already been discussed. For the crankshaft and connecting rod systems, it is difficult to tell if this was an appropriate way to distribute the contributions from fiction and viscous drag. Some test data on the matter would be beneficial to improve the model. The final choice of Coulomb coefficients for the rotational (bearing) frictions was typically 0.0025, and the coefficient for the translational (piston) friction was 0.08. Both values are very low, but a higher friction for lubricated translational friction than bearing friction makes good sense. The choice of coefficients was limited by the desired friction contribution at certain engine speeds, and this means that their values might not be exact compared to real life measurements.

To further investigate the accuracy of the virtual test bench simulations, more test data is needed. By performing physical testing with different engine parts (piston, connecting rod, crankshaft), and comparing the results to the virtual test bench simulations with the same parts, information on the accuracy and impact on friction behavior can be obtained. This also opens up for studies on the influence of the connecting rod shank design (O-, I- or H-beam). Strip/teardown tests would be beneficial in determining the exact friction contribution of the crankshaft.

Chapter 12

Summary and Conclusion

A customized engine test rig was designed, and motored testing was performed to measure the friction torque of a partial assembly of a Honda CRF 250 R motocross engine in the speed range from 3000 rpm to 9000 rpm. The end result of the work performed in this thesis is a virtual test bench modeled in FEDEM, capable of recreating the results from physical engine testing.

Concerns were raised regarding the accuracy of the test data obtained with a damaged and repaired torque transducer. A function check revealed that the transducer showed a predictable and relatively linear response, with sufficient accuracy. Despite this, the transducer failed relatively early in the testing phase, resulting in only one complete test run (with both increasing and decreasing rpm steps) after engine break-in. The results showed that the same trend was present and repeatable in all of the test runs, both complete and partial, adding credibility to the test results.

It was noted that motored testing without a cylinder head can be problematic in terms of piston ring sealing and oil film behavior. The test results showed that the dominating piston assembly lubrication regime changes from boundary, via mixed, to hydrodynamic with increasing engine speed. This caused the measured friction torque to go from 1 Nm (3000 rpm), via a peak of 1.6 Nm (5000 rpm), to 1.5 Nm (9000 rpm). The engine friction's sensitivity to oil temperature was noted, as a higher oil temperature leads to reduced viscosity, affecting the friction losses. Engine friction and oil shearing produced enough heat to keep the oil temperature at 87 °C at 4000 rpm, exemplifying the need for liquid cooling to control engine temperature accurately. Comparing test results from before and after engine break-in clearly shows the break-in's impact on the engine's friction losses.

The virtual test bench was successfully able to recreate the measurements from the engine testing, with both fairly accurate engine speeds, and a matching motoring torque for each investigated engine speed. A simulation run with reduced connecting rod mass did not produce the expected friction reduction, and it was suspected that a weakness in the modeling approach was responsible.

The friction modeling formulation in FEDEM did not have the capability to capture the changes in lubrication regime for the piston assembly. It does not support a variable coefficient of friction, but requires the Coulomb coefficient to have a constant value. This meant working around the problem by adding additional viscous damping with a variable viscous coefficient, resulting in a less realistic model behavior. High levels of translational viscous damping was also seen to cause problems with the PI controller responsible for keeping the desired motoring speeds. Using an external .dll file for friction and damping modeling was mentioned as a possible solution to the friction modeling problem.

It is concluded that more test data and improved friction modeling in FEDEM is required to obtain a virtual test bench accurate enough to predict real engine behavior, when inertia and mass properties of critical engine components are changed. Additional physical testing and simulation with different engine parts would provide information on the simulation accuracy and the impact of different parts on the engine's total friction behavior.

Chapter 13

Recommendations for Further Work

Based on issues discussed in chapter 11, the following recommendations are made for further improvement and validation:

- Improve the friction modeling in the virtual test bench, possibly through the use of an external .dll file including variable Coulomb coefficients

- Re-tune the PI controller and time steps to better match the desired engine speed during load

- Add liquid cooling to the test setup to gain better control over oil temperatures

- Perform additional tests with a fully functional and calibrated torque transducer to obtain more data

  – Tests with different engine parts to chart the impact on friction behavior and similarity to simulations

  – Test with cylinder head and compression, try to isolate the effect on piston ring lubrication from pumping work

  – Additional break-in procedure at higher engine speed to make sure no time-dependent friction effects are present

Bibliography

[1] Abu-Nada, Al-Hinti, Al-Sarkhi, and Akash. Effect of piston friction on the performance of si engine: A new thermodynamic approach. *ASME Journal of Engineering for Gas Turbines and Power*, 130(2), 2008.

[2] Ozgen Akalin and Golam M. Newaz. Piston ring-cylinder bore friction modeling in mixed lubrication regime: Part i-analytical results. *Journal of Tribology*, 123(1):211–218, 1999.

[3] Ozgen Akalin and Golam M. Newaz. Piston ring-cylinder bore friction modeling in mixed lubrication regime: Part ii-correlation with bench test data. *Journal of Tribology*, 123(1):219–223, 1999.

[4] H. Allmaier, C. Priestner, D.E. Sander, and F.M. Reich. *Tribology in Engineering*, chapter 9 Friction in Automotive Engines, pages 149–184. InTech, 2013.

[5] C. C. Daniels and M. J. Braun. The friction behavior of individual components of a spark-ignition engine during warm-up. *Tribology Transactions*, 49(2):166–173, 2006.

[6] P S Dellis. Effect of friction force between piston rings and liner: A parametric study of speed, load, temperature, piston-ring curvature, and high-temperature, high-shear viscosity. *Proceedings of the Institution of Mechanical Engineers, Part J: Journal of Engineering Tribology*, 224(5):411–426, 2010.

[7] Encyclopædia Britannica Inc. Internal-combustion engine. http://media.web.britannica.com/eb-media/72/93572-034-26C16785.jpg. Accessed 9. April, 2016.

[8] C. Fadel, N. G. Chalhoub, G. A. Kfoury, and N. A. Henein. Direct measurement of the piston-assembly friction force in a single cylinder engine under motoring conditions. In *ASME 2008 Dynamic Systems and Control Conference*, number DSCC2008-2173, pages 505–512, 2008.

[9] Fedem Technology AS. *Fedem Release 7.1 Theory Guide*, October 2014.

[10] Fedem Technology AS. *Fedem Release 7.1 User's Guide*, October 2014.

[11] M Gore, R Rahmani, H Rahnejat, and PD King. Assessment of friction from compression ring conjunction of a high-performance internal combustion engine: A combined numerical and experimental study. *Proceedings of the Institution of Mechanical Engineers, Part C: Journal of Mechanical Engineering Science*, 2015.

[12] Michael Gore, Michael Theaker, Sebastian Howell-Smith, Homer Rahnejat, and Paul D King. Direct measurement of piston friction of internal-combustion engines using the floating-liner principle. *Proceedings of the Institution of Mechanical Engineers, Part D: Journal of Automobile Engineering*, 228(3):344–354, 2014.

[13] Kenneth Holmberg, Peter Andersson, and Ali Erdemir. Global energy consumption due to friction in passenger cars. *Tribology International*, 47:221–234, 2012.

[14] M. Hoshi. Reducing friction losses in automobile engines. *Tribology International*, 17(4):185–189, 1984.

[15] T. Johnson, B. Campbell, G. Gibson, and B. Jawad. Impact of reduced rotating mass to throttle response in a cbr600f4i engine. *SAE Technical Paper 2005-01-3448*, 2005.

[16] D. K. W. Leong, P. J. Shayler, I. G. Pegg, and M Murphy. Characterizing the effect of viscosity on friction in the piston assembly of internal combustion engines. *Proceedings of the Institution of Mechanical Engineers, Part J: Journal of Engineering Tribology*, 221(4):469–478, 2007.

[17] Xianghui Meng, Lipu Ning, Youbai Xie, and Victor W Wong. Effects of the connecting-rod-related design parameters on the piston dynamics and the skirt-liner lubrication. *Proceedings of the Institution of Mechanical Engineers, Part D: Journal of Automobile Engineering*, 227(6):885–898, 2013.

[18] Riaz Ahmad Mufti. *Total and Component Friction in a Motored and Firing Engine*. PhD thesis, The University of Leeds School of Mechanical Engineering, 2004.

[19] Terje Rølvåg and Matteo Bella. Dynamic test bench for motocross engines. Unpublished, submitted to the International Journal of Automotive and Mechanical Engineering on 2. June, 2015.

[20] William F. Rohr, Ke Nguyen, Bruce G. Bunting, and Jun Qu. Feasibility of observing small differences in friction mean effective pressure between different lubricating oil formulations using a small, single-cylinder motored engine rig. *Tribology Transactions*, 58(6):1067–1075, 2015.

[21] Qianfan Xin. *Diesel Engine System Design*, chapter 10 Friction and lubrication in diesel engine system design, pages 651–758. Woodhead Publishing, 2011.

Appendix

Kartlegging av risikofylt aktivitet

Dato: 25.01.2016

Enhet:

Linjeleder:

Deltakere ved kartleggingen (m/ funksjon): Jøran Melby (Student), Terje Rølvåg (Ansvarlig veileder)
(Ansv. veileder, student, evt. medveiledere, evt. andre m. kompetanse)

Kort beskrivelse av hovedaktivitet: Masteroppgave Jøran Melby: Internal Combustion Engine Friction Testing and Virtual Modeling

Er oppgaven rent teoretisk? *(JA/NEI)*:   **NEI**   «JA» betyr at veileder innestår for at oppgaven ikke inneholder noen aktiviteter som krever
risikovurdering. Dersom «JA»: Beskriv kort aktiviteten i kartleggingskjemaet under. Risikovurdering trenger ikke å fylles ut.

Signaturer: *Ansvarlig veileder:*   *Student:* Jøran Melby

ID nr.	Aktivitet/prosess	Ansvarlig	Eksisterende dokumentasjon	Eksisterende sikringstiltak	Lov, forskrift o.l.	Kommentar
1	Konstruksjon og montering av testrig for motorer	JM				Arbeid i verksted, bruk av maskiner og verktøy.
2	Fysiske tester av motor	JM				Roterende deler, muligens elektrisitet involvert.

NTNU
HMS

Utarbeidet av	Nummer	Dato
HMS-avd.	HMSRV2601	22.03.2011
Godkjent av		Erstatter
Rektor		01.12.2006

Risikovurdering

Dato: 25.01.2016

Enhet:

Linjeleder:

Deltakere ved kartleggingen (m/ funksjon): Jøran Melby (Student), Terje Rølvåg (Ansvarlig veileder)
(Ansv. Veileder, student, evt. medveiledere, evt. andre m. kompetanse)

Risikovurderingen gjelder hovedaktivitet: Masteroppgave Jøran Melby: Internal Combustion Engine Friction Testing and Virtual Modeling

Signaturer: *Ansvarlig veileder:* [signatur]   *Student:* [signatur] Jøran Melby

ID nr	Aktivitet fra kartleggings-skjemaet	Mulig uønsket hendelse/belastning	Vurdering av sannsyn-lighet (1-5)	Vurdering av konsekvens: Menneske (A-E)	Ytre miljø (A-E)	Øk/ materiell (A-E)	Om-dømme (A-E)	Risiko-Verdi (menn-eske)	Kommentarer/status Forslag til tiltak
1	Konstruksjon og montering av testbenk for motorer	Personskade eller materiell skade som følge av verktøybruk	3	A	A	A	B	A3	Bruk av personlig verneutstyr (briller, hansker hørselsvern). Sørge for nødvendig opplæring.
2	Fysiske tester av motor	Personskade eller materiell skade som følge av feil ved testoppsett	2	B	A	C	C	B2	God planlegging og gjennomføring av oppsett. Synspunkt fra flere personer. Bruk av barrierer, verneutstyr og sikkerhetsavstand.
2	Fysiske tester av motor	Personskade eller materiell skade som følge av nærkontakt med testbenk (roterende deler)	2	C	A	A	B	C2	Bruk av barrierer, verneutstyr og sikkerhetsavstand.
2	Fysiske tester av motor	Strømgjennomgang i forbindelse med bruk av elektrisk motor og måleutstyr	3	C	A	B	C	C3	Bruk av barrierer, verneutstyr og sikkerhetsavstand. Måling av elektriske kretser før fysisk berøring.

Risikovurdering

Sannsynlighet vurderes etter følgende kriterier:

Svært liten 1	Liten 2	Middels 3	Stor 4	Svært stor 5
1 gang pr 50 år eller sjeldnere	1 gang pr 10 år eller sjeldnere	1 gang pr år eller sjeldnere	1 gang pr måned eller sjeldnere	Skjer ukentlig

Konsekvens vurderes etter følgende kriterier:

Gradering	Menneske	Ytre miljø Vann, jord og luft	Øk/materiell	Omdømme
E Svært Alvorlig	Død	Svært langvarig og ikke reversibel skade	Drifts- eller aktivitetsstans >1 år.	Troverdighet og respekt betydelig og varig svekket
D Alvorlig	Alvorlig personskade. Mulig uførhet.	Langvarig skade. Lang restitusjonstid	Driftsstans > ½ år Aktivitetsstans i opp til 1 år	Troverdighet og respekt betydelig svekket
C Moderat	Alvorlig personskade.	Mindre skade og lang restitusjonstid	Drifts- eller aktivitetsstans < 1 mnd	Troverdighet og respekt svekket
B Liten	Skade som krever medisinsk behandling	Mindre skade og kort restitusjonstid	Drifts- eller aktivitetsstans < 1uke	Negativ påvirkning på troverdighet og respekt
A Svært liten	Skade som krever førstehjelp	Ubetydelig skade og kort restitusjonstid	Drifts- eller aktivitetsstans < 1dag	Liten påvirkning på troverdighet og respekt

Risikoverdi = Sannsynlighet x Konsekvens
Beregn risikoverdi for Menneske. Enheten vurderer selv om de i tillegg vil beregne risikoverdi for Ytre miljø, Økonomi/materiell og Omdømme. I så fall beregnes disse hver for seg.

Til kolonnen "Kommentarer/status, forslag til forebyggende og korrigerende tiltak":
Tiltak kan påvirke både sannsynlighet og konsekvens. Prioriter tiltak som kan forhindre at hendelsen inntreffer, dvs. sannsynlighetsreduserende tiltak foran skjerpet beredskap, dvs. konsekvensreduserende tiltak.

NTNU		utarbeidet av	Nummer	Dato
	Risikomatrise	HMS-avd.	HMSRV2604	08.03.2010
		godkjent av		Erstatter
HMS/KS		Rektor		09.02.2010

MATRISE FOR RISIKOVURDERINGER ved NTNU

		Svært liten	Liten	Middels	Stor	Svært stor
KONSEKVENS	Svært alvorlig	E1	E2	E3	E4	E5
	Alvorlig	D1	D2	D3	D4	D5
	Moderat	C1	C2	C3	C4	C5
	Liten	B1	B2	B3	B4	B5
	Svært liten	A1	A2	A3	A4	A5
		SANNSYNLIGHET				

Prinsipp over akseptkriterium. Forklaring av fargene som er brukt i risikomatrisen.

Farge		Beskrivelse
Rød		Uakseptabel risiko. Tiltak skal gjennomføres for å redusere risikoen.
Gul		Vurderingsområde. Tiltak skal vurderes.
Grønn		Akseptabel risiko. Tiltak kan vurderes ut fra andre hensyn.

First draft for paper

Internal Combustion Engine Friction Testing and Virtual Modeling

Jøran Melby

Abstract

A virtual test bench capable of performing integrity analysis of internal engine components has previously been developed in FEDEM. It does however not include any damping and friction effects. As a result, engine performance is overestimated and shows little dependency on the inertia and mass of engine components. In this paper, the friction and damping effects related to the piston assembly, connecting rod, and crankshaft of an engine were identified. A customized engine test rig was designed, and motored testing performed from 3000 rpm to 9000 rpm to measure the friction torque of a partial assembly of a Honda CRF 250 R engine. A virtual test bench representing the physical testing was developed and tuned in FEDEM.

Problems were encountered with a damaged torque transducer, possibly affecting the accuracy of the measurements, and resulting in less experimental data than desired. Engine oil was found to squeeze past the piston rings as a consequence of testing without cylinder pressure, possibly affecting lubrication conditions. Test results showed that the dominating piston assembly lubrication regime changes from boundary, via mixed, to hydrodynamic with increasing engine speed. This caused the measured friction torque to go from 1 Nm (3000 rpm), via a peak of 1.6 Nm (5000 rpm), to 1.5 Nm (9000 rpm). The engine friction's sensitivity to oil temperature was noted. Engine friction and oil shearing produced enough heat to keep the oil temperature at 87 °C at 4000 rpm, exemplifying the need for cooling systems, even in motored testing. Measurements taken before and after engine break-in clearly showed the importance of break-in on the engine's friction losses.

The virtual test bench was successfully able to recreate the measurements from physical engine testing. Simulation with reduced connecting rod mass did not produce the expected friction reduction, and it was suspected that a weakness in the modeling approach was responsible. The friction modeling formulation in FEDEM did not have the capability to capture the changes in lubrication regime for the piston assembly. It did not support a variable coefficient of friction, but required the Coulomb coefficient to have a constant value. Compensating for this weakness by adding additional viscous damping resulted in a less realistic model behavior.

It is concluded that more test data and improved friction modeling in FEDEM is required to obtain a virtual test bench accurate enough to predict real engine behavior, when inertia and mass properties of critical engine components are changed.

Introduction

Internal combustion engines are in widespread use for a large number of applications. They are relatively complex machines subjected to a range of phenomena such as inertia forces, temperature fluctuations, pressure cycling, varying load, friction, wear, and fluid mechanic related losses. In motor vehicle applications, the engine's main purpose is to convert the chemical energy in the fuel into mechanical energy used to propel the vehicle. Some of the fuel energy is lost in the engine through various effects such as as incomplete combustion, heat transfer, pumping losses, viscous drag, and friction. These effects do not contribute to propulsion. In other words, some fuel is being used for other purposes than what is desired.

1

It is estimated that 1/3 of the fuel energy in passenger cars is used to overcome friction in the engine, transmission, tires, and brakes. In 2009 this corresponded to a worldwide consumption of 208 000 million liters of fuel to overcome friction [10]. This means that reducing the losses is beneficial in terms of both fuel consumption and performance. Since an engine contains a lot of moving parts, friction and drag effects (between parts and air or oil) are present throughout the whole system and contribute to the total losses. Friction losses also contribute to increased operating temperatures and component wear. As a consequence of this, less friction loss means less heat generation and thereby requires less cooling. Reducing friction can also be beneficial for component life and durability.

As a step towards improving existing engine designs, or designing new highly efficient engines, computer modeling and simulation is used to predict engine behavior prior to the production and assembly of the engine itself. This reduces both time and cost compared to successive prototyping, testing and modification. In order to successfully apply the modeling and simulation approach, knowledge of an engine's losses and friction effects is required. Engines contain a lot of moving parts, which are all subjected to friction of varying significance. Due to the vast number of moving parts, combined with their varying speed, load, thermal expansion, dynamic modes and inertia effects, calculation of friction and prediction of losses are complicated. Performing measurements directly on the parts is also difficult. Both from a practical point of view, and due to the fact that many parts are interconnected and affected by other parts in addition to the aforementioned effects.

Professor Terje Rølvåg, in cooperation with MX Real Racing (MXRR) and Fedem Technology AS, has developed a virtual test bench for internal combustion engines. The virtual test bench is built in the FEDEM computer software environment and is capable of performing integrity analysis of the internal engine components, while providing extensive control over the virtual engine test cycle. This enables dynamic simulation of the engine (including flexible body models), providing information about stress, strain, displacement, fatigue, etc. In addition to this, the virtual test bench allows for engine characteristics such as speed, torque, and power to be virtually measured. These characteristics are highly dependent on the numerous damping and friction losses occurring in the engine, and the virtual test bench does not include these effects in the simulation. As a result, the engine performance is overestimated and shows little dependency on changes in the inertia and mass of critical engine components.

In this paper, the overall objective is to identify the friction and damping effects related to the piston assembly, connecting rod, and crankshaft, and model a virtual testing tool that accounts for these. This allows for more accurate predictions of engine performance, while enabling comparative studies of different connecting rod designs and their effect on engine behavior. To identify the effects in question, a customized engine test rig is designed and a test scheme developed and executed. A virtual model representing the engine test is made and tuned in FEDEM. The basis for the work performed in this paper is a single-cylinder four-stroke Honda CRF 250 R motocross engine.

Engine Friction and Damping

The piston assembly is the largest source of engine friction. Exact numbers depend on engine configuration, operating speed, load, and temperature, but the relative contributions of different mechanisms in a complete, representative, four-cylinder engine can be seen in table 1. The table summarize the findings from various papers. Contributions in the lower end of the percentage spans are expected for low engine speeds and loads, whereas higher contributions are expected when the engine is subjected to high speeds and loads. Due to differences in engine configurations between these sources, and the fact that the percentages given here are only the largest contributors, the numbers might not add up to 100% for all available choices of values. The values presented are meant to give an indication of the various systems contributions as opposed to exact values.

Mechanism	Percentage of total engine friction	
Piston assembly	38% - 60%	[4, 10, 11]
Crankshaft system	16% - 19%	[5, 11]
Connecting rod system	14% - 18%	[11]

Table 1: Friction loss contributions in four-cylinder engines

The piston assembly experiences the most complex lubrication conditions, and it is estimated that 80% is hydrodynamic lubrication (including squeeze film effect at dead centers), 10% is mixed lubrication, and 10% is boundary lubrication [10]. The varying piston velocity and acceleration over the course of a stroke, combined with several changes in the lubrication regime during each revolution of the crankshaft, causes the engine's instantaneous friction to be a function of piston position (or crankshaft angle). Adding the fact that engine speed (or mean piston velocity) and effective oil viscosity also influence the friction behavior, further complicates the situation.

The piston rings experience boundary and mixed lubrication around the dead centers, where the piston velocity is low, and hydrodynamic lubrication around the mid-strokes, where the piston velocity is high [4, 7, 9, 11]. The piston skirt operates mostly under hydrodynamic lubrication [12]. Under mixed lubrication, the coefficient of friction decreases with increasing engine speed, as higher piston velocity results in a thicker oil film and a larger hydrodynamic lubrication effect. For the piston skirt, operating in the hydrodynamic regime, an increase in engine speed will result in increased losses [12]. This can be observed in a Stribeck diagram (figure 1) where the friction coefficient is plotted as a function of the "duty parameter", $\frac{viscosity \times speed}{load}$.
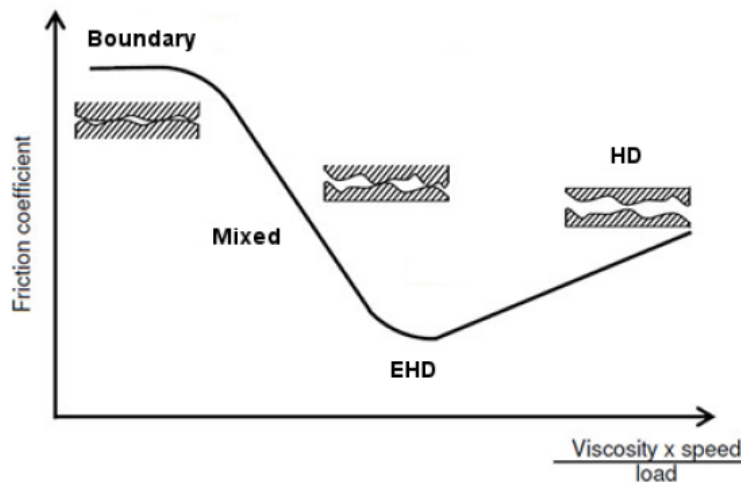

Figure 1: Stribeck diagram [4]

In hydrodynamic lubrication, the friction loss is mainly accredited shearing of the oil film and is therefore proportional to the engine speed [5]. In addition to shearing of the oil film through relative movement of the parts (Couette flow), pressure gradient driven shearing (Poiseuille flow) is also involved for the piston when the cylinder pressure increases due to compression or combustion. This increased pressure pushes against the oil film and piston rings, causing an oil shearing effect [9]. It is worth noting that the maximum friction force under hydrodynamic lubrication is significantly lower than the forces in boundary and mixed regimes [7]. Despite this, hydrodynamic lubrication is responsible for a substantial part of the total engine losses, the reason being that boundary and mixed lubrication usually dominate near the dead centers, a relatively small portion of the engine cycle compared to the hydrodynamic region.

The friction force between the piston rings and the cylinder liner has contributions from viscous shearing of the oil film, asperity contact, and the stroke-direction component of the asperity contact pressure [2].

During the engine's power stroke, the friction between piston rings and cylinder liner increases significantly. The connecting rod's angle during the power stroke and the piston's restricted movement (stroke-direction only) dictates that some of the force transferred from the piston to the connecting rod is directed towards the cylinder wall. The reaction force between the cylinder wall and the piston rings is a normal force acting in the radial direction, causing friction as the piston moves down. As the normal load on the piston rings is increased, the oil film thickness decreases [2, 3]. This is important to consider to avoid a breakdown of the oil film and a change in lubrication regime during the power stroke. Under fired engine operation, the combustion pressure also increases the back-pressure of the compression ring, pushing it harder against the liner [7, 9]. This causes better sealing and thereby a lower pressure gradient across the ring, reducing Poiseuille shear. Piston ring friction is relatively small compared to piston skirt friction [1], but the piston skirt is found to contribute the least to the total friction loss of the piston assembly [7]. Piston ring friction acts over a large portion of the engine cycle, whereas piston skirt contact primarily occurs near dead centers, a relatively small portion of the total engine cycle.

Oil viscosity is reduced as temperature is increased. A consequence of the viscosity reduction is that the Minimum Oil Film Thickness (MOFT) and its load carrying capacity is reduced. This might lead to a mixed lubrication regime throughout the stroke, increasing friction loss and component wear [3, 4, 6, 11]. As long as lubrication stays in the hydrodynamic regime, reduced viscosity is beneficial for reducing losses. However, as soon as the transition towards mixed lubrication starts, reduced viscosity will increase losses (refer to the Stribeck diagram in figure 1). In general, the higher the viscosity, the more the lubrication regime shifts from boundary/mixed towards mixed/hydrodynamic [7].

The direct connecting rod losses are mainly friction in the big end bearing and oil drag. The friction loss from the small end bearing is negligible compared to the losses in the big end and the crankshaft bearings [12]. The OEM connecting rod in the Honda CRF 250 R engine uses a needle bearing in its big end. As the engine speed increases, so does the pressure of the oil being forced through the crankshaft and into the bearing. The effect of this is that the bearing transitions from needle bearing operation towards hydrodynamic operation as the engine speed is increased. The connecting rod can indirectly have an impact on engine friction through the transverse inertia force transferred to the piston assembly as the connecting rod moves. The crankshaft is connected to the engine block through bearings, and rotates through the engine oil contained in the oil sump. The dominating losses related to the crankshaft is therefore bearing friction and oil drag. The OEM crankshaft in the Honda CRF 250 R engine uses two roller bearings.

Engine Testing

A motored test does not mimic the actual engine operating conditions as well as a fired test does. Cylinder pressures are either too low or non-existent, and the fluctuating temperature due to combustion is not considered. This has implications for the piston transverse force, oil film contact pressure, and Poiseuille oil shear in the piston-liner interaction [9]. Despite this, the friction losses in a fired test and a motored test are quite similar. The exception being in the piston assembly during the power stroke, where the pressure and temperature differences are significant [11, 12]. The high combustion pressure (causing high ring-liner contact pressure) and high temperature (reducing local oil viscosity) encountered in a fired test result in a larger degree of boundary lubrication for the piston rings, increasing the loss compared to a motored test. On the other hand, increased liner oil temperature is advantageous for the piston skirt friction, as hydrodynamic lubrication benefits from reduced viscosity.

The engine used for testing and modeling is a single-cylinder four-stroke Honda CRF 250 R motocross engine. The engine assembly used for testing consists of the Honda engine block with cylinder/liner, OEM piston and piston rings, OEM connecting rod, and OEM crankshaft with bearings and seals. Since motored testing is performed, liquid cooling is not included in the test setup. The engine is tested without the cylinder head and valves, so the piston top operates in atmospheric pressure at all times. The underside of the piston however, does not. Because the crankcase is sealed, some compression of the air in the crankcase will occur for each stroke, and add to the torque required to run the engine. The oil pump is not installed

in the engine during testing. It is mainly responsible for pumping oil to the cylinder head (which has been removed) and the connecting rod big end. Since a motored test without any cylinder pressure is performed, the load on the big end bearing is small compared to fired engine operation. It is assumed that the big end bearing will have sufficient lubrication from the oil sump alone. The crankshaft rotates in the oil bath in the sump, lubricating the connecting rod through dipping and the cylinder liner through oil splashing. Motorex Cross Power 4T 10W-50 engine oil is used during engine break-in and testing.

Since oil temperature significantly affects friction and clearance in the engine, it is necessary to heat the engine oil to its normal operating temperature of 80 - 85 °C. This is done by mounting a Norske Backer 400 W heat cartridge in the oil sump. A Sunvic Simmerstat Type TYJ 7202 is used to control the output of the heat cartridge from level 1 to 5. A TES 1300 thermometer is used to monitor the oil temperature in the sump. The temperature sensor is mounted in a separate chamber from the heat cartridge to reduce the impact of the cartridge temperature on the measurements. Custom aluminum brackets were made to keep the heat cartridge and temperature sensor in the desired areas, while keeping the wires away from rotating parts. The heat cartridge and temperature sensor arrangement can be seen in figure 2. The heat cartridge is shown in the green rectangle, the temperature sensor in the yellow circle, and the red line indicates the approximate oil level in the sump.
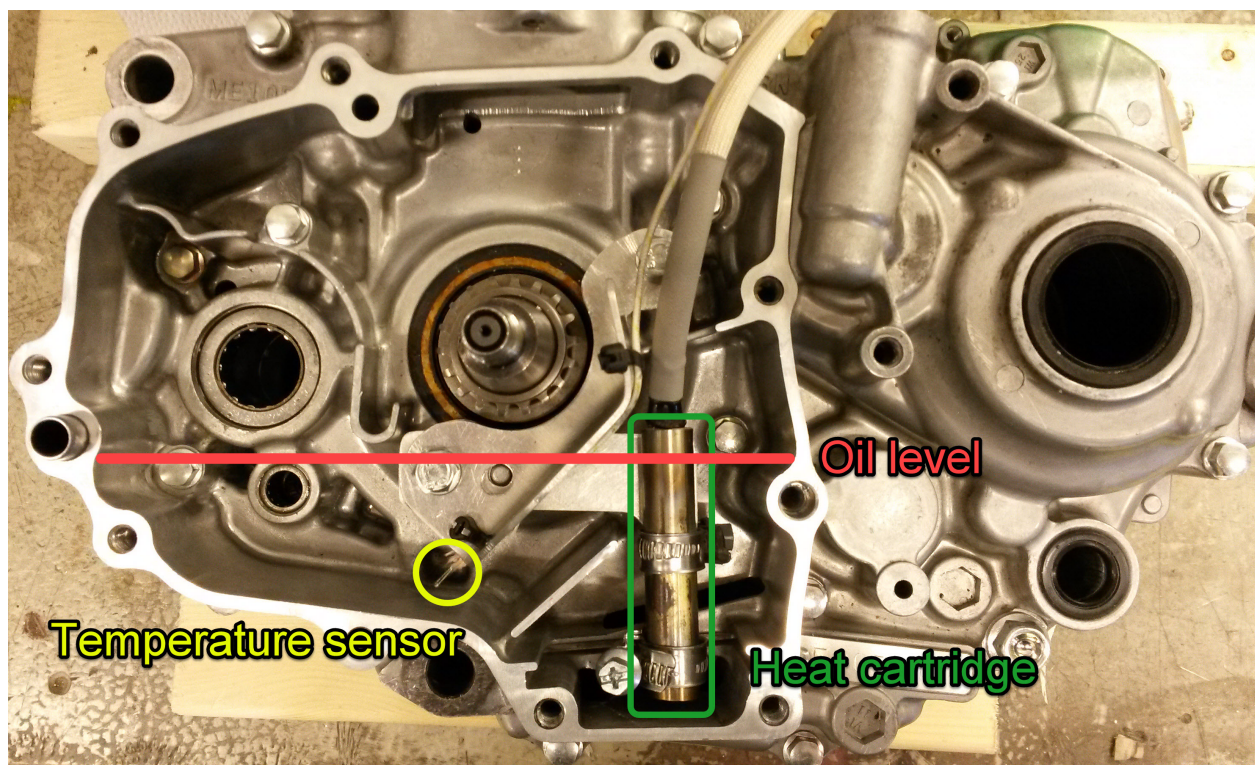

Figure 2: Engine oil heating arrangement

Since the engine is tested without the cylinder head, four 60 mm long steel tube spacers with outer dimensions Ø20 mm and inner dimensions Ø10 mm were made to allow the cylinder head bolts to securely fasten the cylinder/liner. A 8 mm thick steel plate with a center hole is used as a safety measure, absorbing the piston's kinetic energy in the event of engine failure during testing. The center hole is Ø68 mm and the piston is Ø76.8 mm. Since the difference between diameters is relatively small, the safety plate will not cause substantial airflow resistance (pumping loss) when the piston reciprocates. The bottom side of the safety plate center hole has a 4 mm deep cut-out of Ø80 mm to avoid piston collision. Because the piston is slightly dome/wedge shaped at the top, the piston center travels approximately 3 mm above the cylinder/liner in the center hole, but the edge of the piston stays in the cylinder/liner at all times. The engine cylinder assembly setup is shown in figure 3.

Figure 3: Engine cylinder assembly
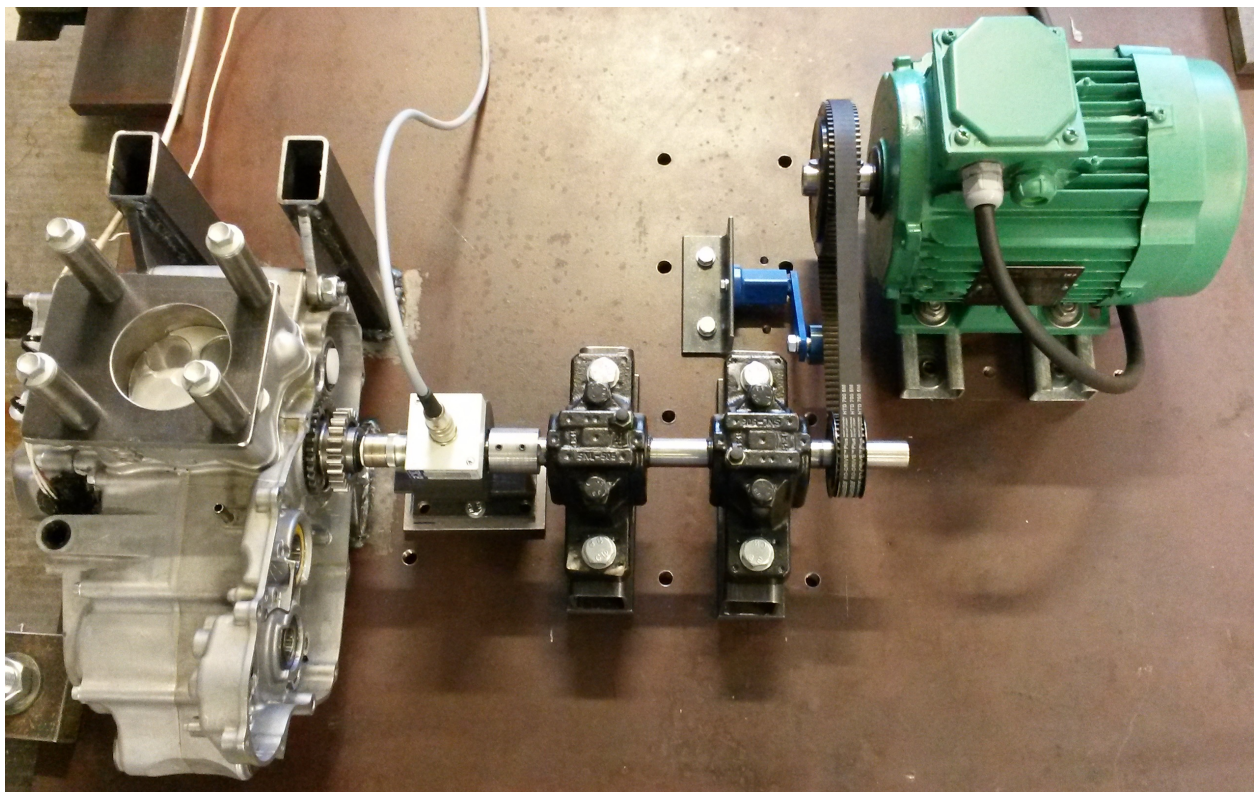
Figure 4: Engine test rig

The engine test rig can be seen in figure 4. A 15 mm wide belt is used to connect a Leroy Somer LSES 90 S 1.5 kW electric motor with a 72-tooth pulley to a Ø20 mm steel axle with a 36-tooth pulley, to double the rotational speed. The electric motor is mounted on rails with four M10 bolts to allow adjustments of the belt tension and angle. A Rosta SE 11 belt tensioner with a Rosta R11 roll is used to keep the belt from oscillating during testing. It is bolted to the 20 mm thick steel base plate with a bracket and two M8 bolts.

The axle is mounted to the base plate through two FAG 1205-K-TVH-C3 ball bearings, with FAG H205 adapter sleeves, mounted in SKF SNL 505 plummer block housings. The housings are bolted to the base plate with two long M12 bolts each, running through steel spacers and square profile beams. Steel engine mounts were fabricated and welded to the base plate. The engine mounts are connected to the engine's OEM attachment points with two M10 bolts running through both the engine block and the mounts. The axle is connected to a HBM T22 in-line torque transducer by a steel sleeve with set screws. Both entering axles were ground flat on one side for the set screws. The transducer is kept from rotating with the axle by an I-beam support. The support is bolted to the base plate with two M8 bolts, but the transducer is free to translate on top of the support. The torque transducer is connected to the engine by a 17 mm steel socket, modified with a 0.02 mm shrink-fit on the transducer side. Figure 5 shows the connections between the axle, torque transducer and the engine.
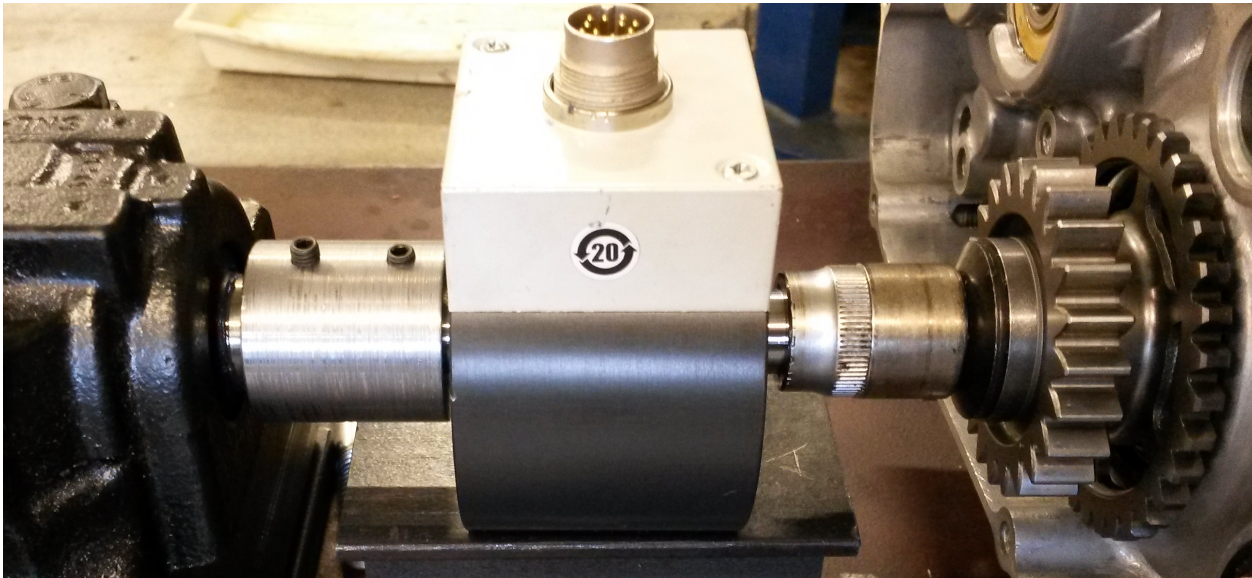

Figure 5: Connections between axle, torque transducer and engine

Using the modified socket allows the OEM bolt in the crankshaft to remain in place, along with the two cogs usually present on the crankshaft spline. This is an advantage, as the crankshaft oil seal depends on the inner cog sleeve, and tightening the bolt to 40 Nm assures correct axial play in the crankshaft assembly. Because of thermal expansion, some axial play in the crankshaft assembly is expected. Using the modified socket to connect the torque transducer to the engine crankshaft bolt, allows for some axial sliding between the two without introducing axial forces in the transducer or the engine. The shape and size of a 17 mm socket also allows some play against a 17 mm bolt head, permitting a small misalignment of the two rotating axes without introducing large bending moments. However, the play in the socket and bolt connection introduces rattling and vibrations, so a thin layer of tape is attached to the hexagonal bolt head before the socket is introduced. This reduces the rattling significantly, but the tape is compliant enough to avoid the introduction of large bending moments.

The electric motor is controlled through a SEW Eurodrive Movitrac B frequency inverter, connected to a computer running SEW Eurodrive Movitools MotionStudio software. This enables the motoring speed to be set and controlled precisely. The torque transducer is connected to a HBM Spider 8 universal amplifier and data acquisition system. The spider is connected to a computer running Catman AP V3.5.1 data acquisition software. A sampling frequency of 1200 Hz is used to obtain a sufficient number of representative measurements at high engine speeds. At 9000 rpm, a sampling frequency of 1200 Hz results in 8 measurements per crankshaft revolution. Taking a sufficient number of measurements during each crankshaft revolution at constant engine speed, and then calculating the mean value, provides an average friction torque at that speed. It does not provide information on instantaneous friction as a function of crankshaft angle or piston position. The mean value calculation of the torque measurements are performed over both one second intervals and five second intervals to get a better picture of trends and fluctuations in the values. This also reduces the influence of outliers. The transducer output voltage approximately equals the measured torque.

This makes interpreting the measured results quite easy: 1 V equals 1 Nm. Some inconsistency in this relation might still be expected, due to specified deviations in linearity, sensitivity and zero value.

Break-in of the engine is done by first heating the engine oil to 75 - 80 °C while running the engine at 300 rpm, then running it at a constant speed of 4000 rpm while monitoring the torque transducer output. When a steady state output is obtained, and the measurements show no change in engine friction, the break-in is considered complete.

Since the engine's minimum operating speed is 2500 rpm, 3000 rpm was chosen as the lowest engine speed for testing. The engine is tested without the balance shaft, and this has implications for engine forces and vibrations. In the interest of health and safety, it was decided not to run the engine in the test rig faster than 9000 rpm. Testing the engine at 9000 rpm still provides important data on engine performance, as this is the speed where maximum brake torque is delivered during normal fired operation. Testing is performed using the following procedure:

1. Heat the engine oil to 75 - 80 °C while running the engine at 300 rpm

2. Run the engine at 3000 rpm until the torque transducer output stabilizes

3. Increase engine speed by 1000 rpm, run until the torque transducer output stabilizes

4. Repeat step 3. until a speed of 9000 rpm is achieved

5. Decrease engine speed by 1000 rpm, run until the torque transducer output stabilizes

6. Repeat step 5. until a speed of 3000 rpm is achieved

Using this test procedure results in data for steady state cycle-averaged friction torque as a function of rpm. Performing torque measurements during both increasing and decreasing rpm test schemes is done to investigate hysteresis.

Engine Modeling

FEDEM (Finite Element Dynamics in Elastic Mechanisms) is a software package capable of virtual testing of complex mechanical assemblies. FEDEM includes tools for model creation, simulation solving, and post processing of results. Plots and animations are generated and can be viewed both during and after solution. The post processor enables full stress analysis, eigenmode calculations, strain gage solutions, and fatigue analysis for selected time steps. FEDEM solutions assume elements with linear material parameters (no yielding effects are considered), but the problem is solved as a nonlinear case due to the dynamic effects and the large geometric variations. The parts used in a FEDEM simulation can be made in the integrated modeler or imported as FE models. Each part is reduced (by FEDEM) to a superelement with a co-rotated frame, for separation of elastic and rigid body movement. The mass matrix is Component Mode Synthesis (CMS) reduced, and therefore remains fully populated. This allows gyro effects to be correctly represented. FEDEM uses the Newmark-β and HHT-α (Hilbert Hughes Taylor) time integration algorithm to solve the dynamic equation with respect to displacement increments. Iteration with the Newton-Raphson method is used to correct nodal displacements and modal amplitudes towards equilibrium before the next increment is solved [8, 13]. Control parameter equations are solved with Runge-Kutta methods. Friction between parts connected by a joint is in FEDEM calculated from forces, moments, and relative joint velocity. Viscous friction is effectively modeled as a damper, and the friction force (or torque) depends on a viscous coefficient c and the velocity of the damper V [8]:

$$F_{viscous} = cV \tag{1}$$

The total friction model in FEDEM is [8]:

$$F_{total} = F_{viscous} + \left[F_0 + \mu_{Coulomb} F_e \left(1 + S e^{-\left(\frac{V}{V_{slip}} \right)^2} \right) \right] sgn(V) \tag{2}$$

$\mu_{Coulomb}$ is the Coulomb friction coefficient, F_e is the equivalent normal load, $sgn(V)$ is the sign of the velocity (± 1, direction of movement), and F_0 is the friction force resulting from any pre-stress of components. S is the stick-slip factor, describing the magnitude of the Stribeck effect, and V_{slip} is the critical velocity for the Stribeck effect. The magnitude of the Stribeck friction force depends on velocity, and is in that regard a more complete friction model than Coulomb friction. Stribeck friction captures the transition from static (higher) to kinetic (lower) friction when the sliding velocity is increased. Parts in FEDEM are connected by joints with various Degrees Of Freedom (DOF). In addition to controlling the available DOF and their range, it is also possible to impose spring and damper behavior on each joint. This makes it possible to add damping directly to a joint connection.
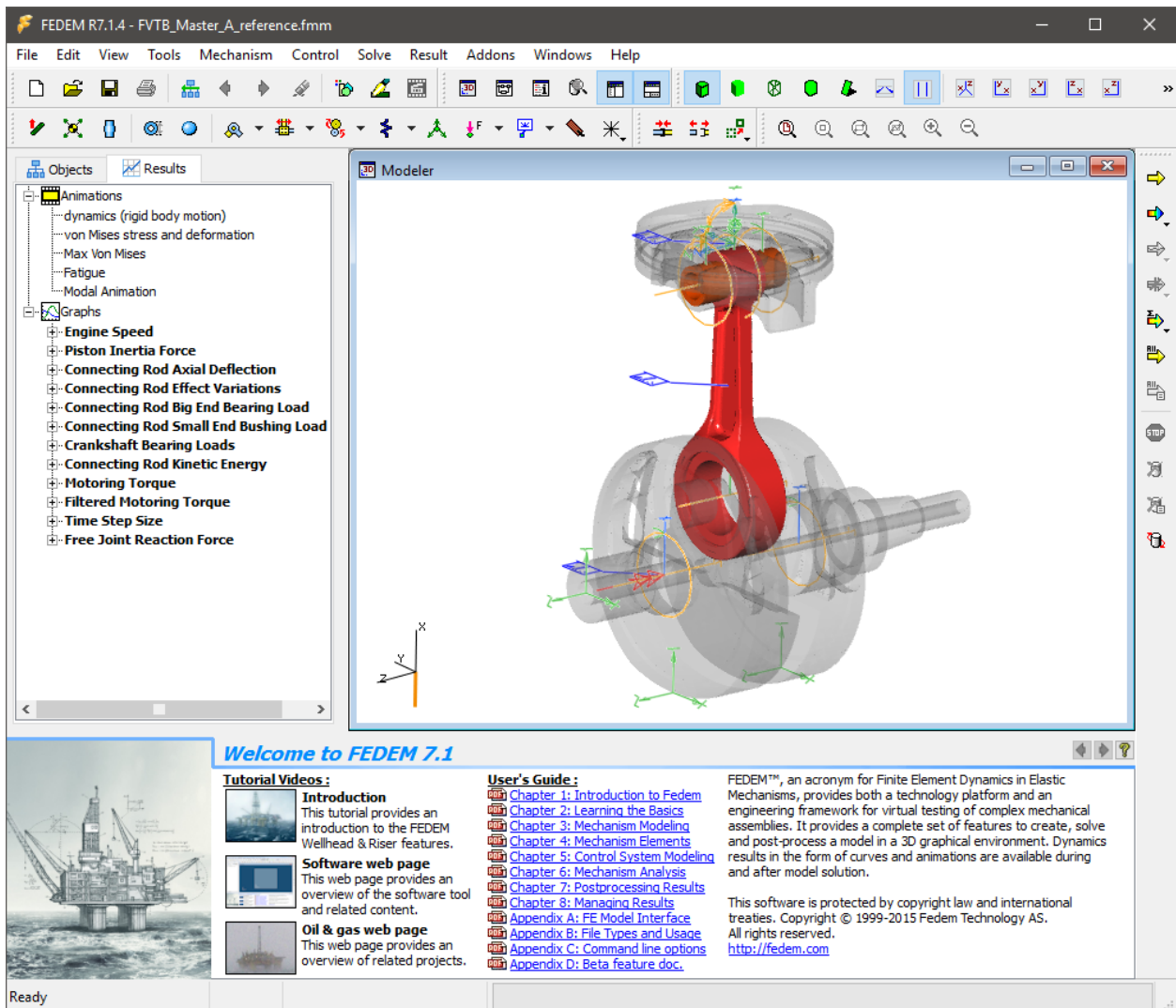
Figure 6: Reference test bench model

A reference test bench model is established as a base for incorporating friction and damping effects. This is done in order to obtain a model behaving exactly as expected before any friction and damping effects are accounted for. The reference model only contains the piston, piston pin, connecting rod, and crankshaft (see figure 6). The reference model is an ideal representation, free from friction and drag losses. FEDEM uses the Newmark-β and HHT-α time integration algorithm to solve the dynamic equation. This causes the

9

numerical damping and the error to increase with the rotational velocity if the time step is constant. To counteract this, variable time step size is employed. Adding stiffness proportional damping to the parts in the model adds some numerical stability, without introducing artificial damping against rigid body motion [8].

A control system is implemented to regulate the engine model simulation. The model test cycle is 11.5 seconds long and uses a function to control the reference speed from 3000 rpm to 9000 rpm. The reference speed is brought from zero to 3000 rpm in 1.5 seconds, and held at that speed for 1 second. Then the speed is increased by 1000 rpm in 0.5 seconds, and held at the new speed for 1 second. This is repeated all the way up to 9000 rpm. The magnitude of the acceleration between the reference speed plateaus is not of particular interest in the simulation. The reason being that torque measurements are being read at the end of each 1 second hold, to obtain a friction torque for steady state speed only. Longer simulation runs (both slower acceleration and longer holds) for a total of 125 seconds were also explored, but they provided the same result as the shorter simulations, with no indication of additional numerical drift. The difference between the reference speed and the actual engine speed is used to determine the motoring torque supplied to the engine crankshaft. This is done using a Proportional-Integral (PI) controller. The piston assembly and connecting rod's motion and inertia affects the instantaneous rotational velocity of the crankshaft. This phenomenon combined with the nature of the PI controller, causes both the engine speed and motoring torque to oscillate. Low-pass filters are used for additional plotting of the engine speed and motoring torque, to provide a clearer picture of the average values occurring.

Trial and error is used to zero in on values for the numerical damping, and the optimal time step size for each step in engine reference speed. This is done though monitoring the motoring torque required at each of the reference speed plateaus. When the engine without any losses is held at a constant speed, no motoring torque is required to keep it operating at that speed. Tweaking time steps and numerical damping until zero average torque is required to keep the engine at the different reference speeds, yielded the time step sizes seen in table 2. A function is defined in the control system, decreasing the time step size as reference speed increases. The rest of the model and simulation parameters are listed in table 3.

Engine speed	Time step size
3000 rpm	2.700×10^{-4} s
4000 rpm	1.260×10^{-4} s
5000 rpm	7.260×10^{-5} s
6000 rpm	4.772×10^{-5} s
7000 rpm	3.360×10^{-5} s
8000 rpm	2.483×10^{-5} s
9000 rpm	1.871×10^{-5} s

Table 2: Time step size

Simulation parameters	
Electric motor torque limit	5 Nm
PI controller proportional term	0.05
PI controller integral term	1000
HHT-α factor	0.0031
Stiffness proportional damping (all parts)	8.0×10^{-5}
Max. number of iterations	50
Min. number of iterations	3
Geometric stiffness contribution	On
Centripetal force correction	On
Time between each print to result file	0.001 s

Table 3: Simulation parameters

Using test results and establishing the reference test bench model as a starting point, tuning of the virtual test bench can be performed. Since all testing is performed on a single engine configuration, directly isolating contributions from various friction and damping effects is not possible. Assigning friction contributions to different mechanisms with the help of previously written literature is therefore used instead. It is decided to apply the friction torque distribution in table 4 to the partial engine assembly in the virtual test bench. Looking at the percentages in the table alone, might lead one to believe that the friction from the crankshaft and connecting rod deceases as engine speed is increased. This is not the case, as the total friction torque equating to 100% varies with engine speed.

Mechanism	Friction torque distribution	
	Low engine speed	High engine speed
Piston assembly	56%	59%
Crankshaft system	23%	21%
Connecting rod system	21%	20%

Table 4: Friction torque distribution

In the virtual test bench, 3000 rpm is considered low engine speed, and 9000 rpm is considered high engine speed. Using the measured test data at 3000 and 9000 rpm to calculate the friction torque distribution at low and high engine speeds, provides two reference points for both the crankshaft and connecting rod systems. Adapting 2nd degree polynomial curves between the two points for each of the two systems, result in their friction contributions across the speed range. By using 2nd degree polynomials, it is assumed that the bearing friction and oil drag in these systems depend on engine speed in such a manner. This assumption is justified by considering that bearing friction depends on the acting normal force to some extent, and the normal force is a result of the inertia forces occurring in the piston and connecting rod assembly. Referring to equations 3, 4, and 5, it can be seen that both reciprocating and rotating forces depend on the square of the engine speed, thereby causing a 2nd degree dependency. The oil drag is basically viscous friction loss, and therefore follows the relation in equation 1, adding a linear component to the dependency on engine speed.

If the connecting rod is considered as a two-point mass system (big end and small end), and it is assumed that the small and big ends are responsible for $\frac{1}{3}$ and $\frac{2}{3}$ of the connecting rod's mass m_c, the reciprocating mass can be considered as the mass of the piston assembly plus $\frac{1}{3}$ of the connecting rod's mass. The rotating mass is considered to be the remaining $\frac{2}{3}$ of the connecting rod's mass. This means that the reciprocating and rotating inertia force can be calculated as [12]:

$$F_{rec} = \left(m_p + \frac{1}{3}m_c\right) a_a \qquad (3)$$

$$a_a = -R_a\omega^2 \left(\cos(\theta) + \frac{\lambda\cos(2\theta) + \lambda^3 \sin^4(\theta)}{\sqrt{\left(1 - \lambda^2 \sin^2(\theta)\right)^3}}\right) \qquad (5)$$

$$F_{rot} = \frac{2}{3}m_c R_a \omega^2 \qquad (4)$$

The acceleration of the piston can be found using kinematic relations [12], where $\lambda = \frac{R_a}{L}$, L being the length of the connecting rod, R_a is the radius of the crankshaft, θ is the crank angle, and ω is the engine's angular velocity. As a result of changes in the connecting rod angle during the stroke, the piston will move more per crank angle near the TDC ($\pm 90°$) than near the BDC ($\pm 90°$). The explanation of this behavior lies in the shortening and lengthening of the connecting rod's projected length along the cylinder axis. As the big end of the connecting rod moves away from the cylinder vertical axis it effectively pulls the piston down, in addition to the downwards movement already imposed by crankshaft rotation. The opposite effect is observed near BDC, where the connecting rod's projected vertical length is increased, moving the piston up (counteracting some of the downwards movement from the crankshaft rotation). The largest piston acceleration occurs at TDC, where the piston changes direction the fastest. This can be observed in figure 7, where percent-wise piston acceleration is plotted as a function of crankshaft angle (for chosen values of L and R_a). 0 and 360 degrees correspond to TDC, and 180 degrees is BDC.

The primary contribution (first term of eq. 5) is the acceleration resulting from the rotation of the crankshaft. It has a sinusoidal shape, and occurs once for each crankshaft revolution. The secondary contribution (second term of eq. 5) is the acceleration resulting from the shortening and lengthening of the connecting rod's projected length along the cylinder axis. This contribution also has a sinusoidal shape, but occurs twice for each crankshaft revolution. The combination of these contributions gives the total acceleration. Piston (and connecting rod) acceleration is the source of reciprocating forces and vibrations in the engine assembly, and therefore needs to be balanced out as much as possible. For a single-cylinder engine, counterweights on the crankshaft are used to balance the primary forces, and one or two balance shafts (spinning at twice the speed of the crankshaft) are used to balance the secondary forces.
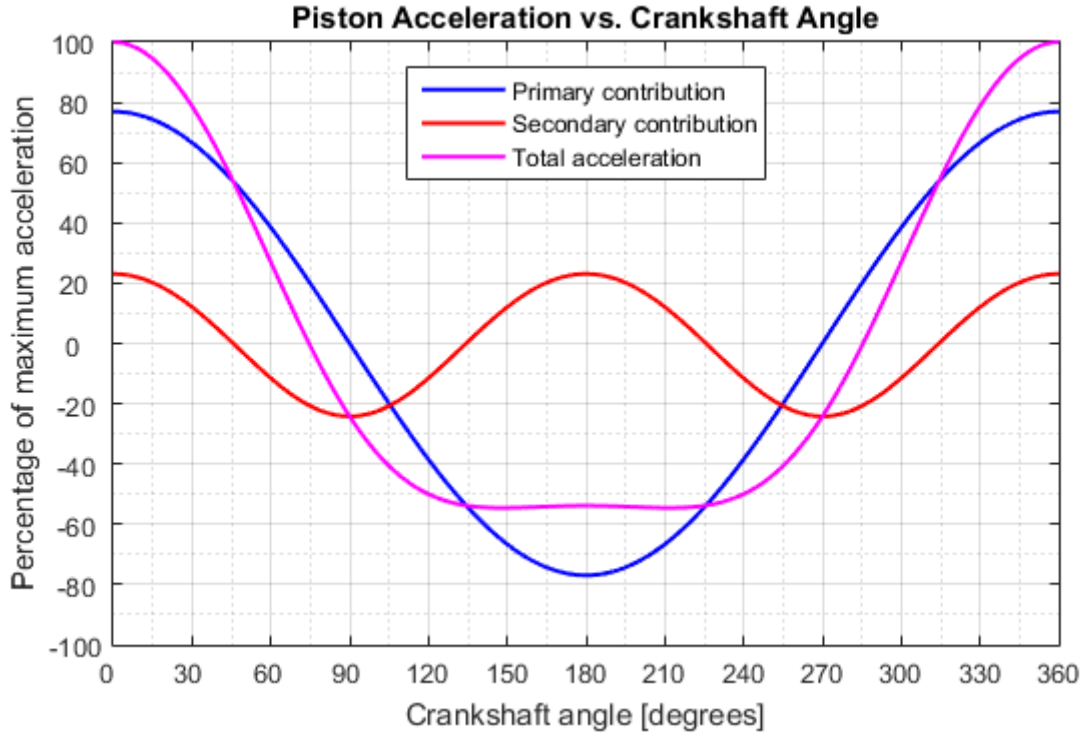
Figure 7: Piston acceleration

Modeling the friction loss caused by the connecting rod system is done by defining a rotational friction with the total friction model from equation 2, and a viscous damper (equation 1), on the joint in the connecting rod big end bearing. It is desired to make the virtual test bench model able to reflect change in friction as a result of changes in component mass and moments of inertia. Since the friction model shows dependency on the inertia force (through normal force), as much as possible of the 2nd degree polynomial friction torque is modeled using this approach. The rest is introduced through the viscous damper, by using a scaling function for the viscous coefficient (which is defined as 1). Tuning this scaling function until the combined friction and damping coincides with the 2nd degree polynomial friction torque, produces the total connecting rod system friction. No friction is modeled in the small end of the connecting rod, as the friction loss from the small end bearing is negligible compared to the big end and the crankshaft bearings [12]. The same approach as the one just described for the connecting rod, is used to model the crankshaft system friction loss. The main difference is that there are two bearing joints in the crankshaft system.

The situation for the piston assembly is a bit more complex, because the coefficient of friction changes with the lubrication regime, as seen in the Stribeck diagram (figure 1). It is also affected by the compression of the air on the underside of the piston. A translational friction with the total friction model is applied to the free joint representing the piston/cylinder interaction. The friction model in FEDEM does not support a variable coefficient of friction, which would have been the appropriate way of modeling changes in lubrication regime. Analogous to the approach for the connecting rod, as much friction as possible is introduced through the translational friction. The rest is compensated for by adding a viscous damper with a coefficient of 1, and using a scaling function to obtain the desired response. Adding the viscous damper to the reciprocating cylinder free joint, causes the motoring torque to get out of control. The suspected reason is discussed in the "Discussion" section. The viscous damping is instead applied as an addition to the scaling function for the connecting rod damping, and tuned until total friction behavior matches the test data for the whole speed range. While this might not be an completely accurate approach, the error resulting from the translational friction's inability to account for changes in the coefficient of friction (lubrication regime), is suspected to be of greater concern. The compression of crankcase air by the piston is not modeled as a separate phenomenon, but included in the overall piston assembly loss. The parameters used in the rotational and translational frictions are seen in table 5, and the scaling functions for the viscous damping are presented in table 6. A simplified flowchart describing the tuning process can be seen in figure 8.
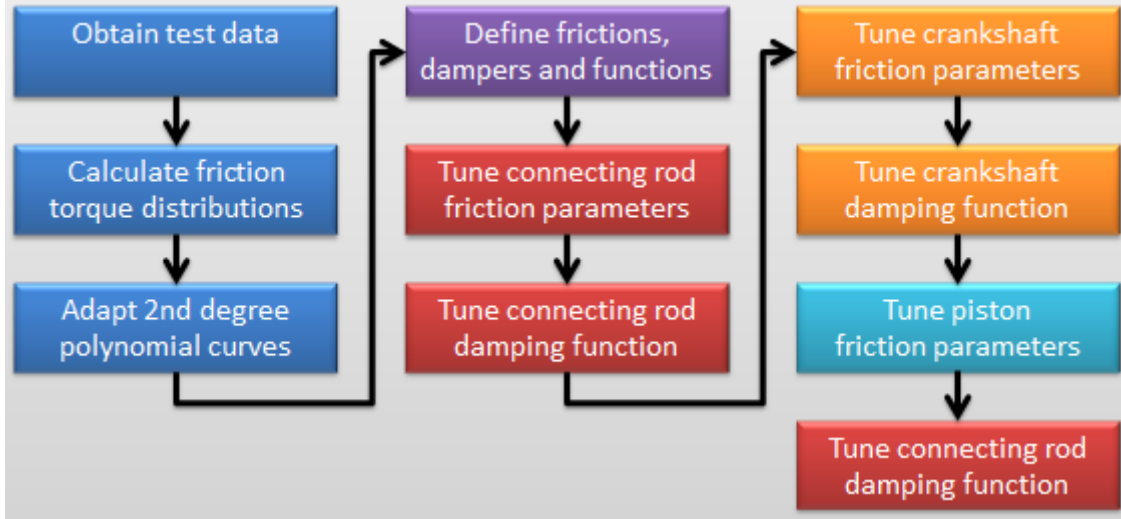
Figure 8: Simplified flowchart for virtual test bench tuning

Parameter	Connecting rod	Crankshaft	Piston
Force caused by pre-stress	X	X	0
Coulomb coefficient	0.0025	0.00245	0.08
Magnitude of Stribeck effect, S	0	0	0
Critical Stribeck speed, V_{slip}	0	0	0
Radius of contact surface, R	0.017	0.02	X
Torque caused by pre-stress	0	0	X

Table 5: Friction parameters

Regarding the operation of both the connecting rod and the crankshaft bearings, no Stribeck (stick-slip) effects are expected. The bearings only turn in one direction and are constantly turning at speeds far greater than what is associated with the Stribeck effect. A parameter study of S and V_{slip} was performed for the translational piston friction (since the piston reaches zero velocity at TDC and BDC), but in the case of the piston friction, the effect was negligible. This is thought to be because the acceleration experienced by the piston near the dead centers causes piston velocity to increase past the critical Stribeck speed over a very short distance. This means that the Stribeck effect is only active in a relatively small part of total piston travel, resulting in a minuscule impact on the total average friction.

Function X-value (argument is engine speed)	Function Y-value (crankshaft)	Function Y-value (connecting rod)	Function Y-value (connecting rod + piston)
314.159 rad/s	0.091	0.180	0.655
418.879 rad/s	0.085	0.160	1.157
523.599 rad/s	0.073	0.140	0.972
628.319 rad/s	0.060	0.115	0.582
733.038 rad/s	0.040	0.085	0.303
837.758 rad/s	0.020	0.045	0.110
942.478 rad/s	0	0	0.032

Table 6: Viscous damping poly line scaling functions

Results

After assembling the test rig for the first time, a function test was performed. The test data was recorded and can be seen in figure 9. Extracted representative results are shown in table 7. Since this was an early function test, the complete test procedure was not fully developed and followed, and the engine was not yet broken-in. Despite this, the results are still usable for comparison purposes.
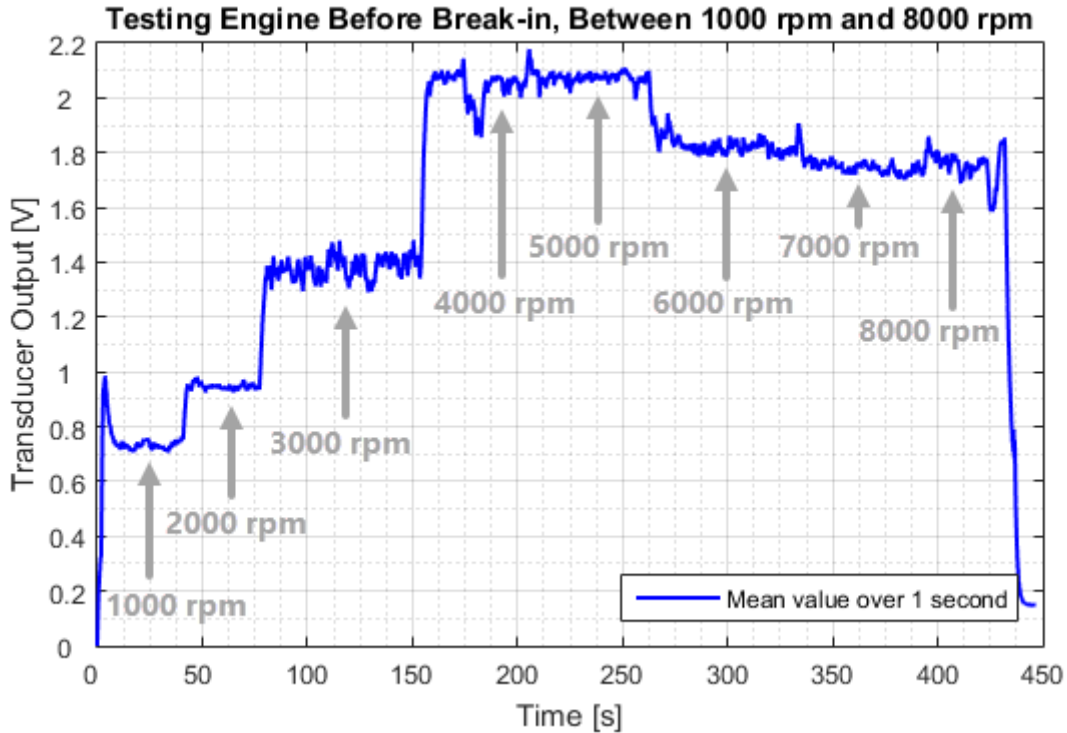

Figure 9: Function test results

Approximate test cycle time	Engine speed	Transducer output	Oil temperature	Oil heating setting
0 - 40 s	1000 rpm	0.73 V	78 °C	3
50 - 75 s	2000 rpm	0.94 V	77 °C	3
85 - 150 s	3000 rpm	1.37 V	75 °C	3
185 - 210 s	4000 rpm	2.04 V	74 °C	3
220 - 250 s	5000 rpm	2.07 V	77 °C	3
290 - 325 s	6000 rpm	1.82 V	80 °C	3
350 - 390 s	7000 rpm	1.75 V	82 °C	3
400 - 420 s	8000 rpm	1.76 V	86 °C	3

Table 7: Function test representative results

The engine was broken-in with the Simmerstat heat cartridge regulator set to level 3. The engine speed was stepped up from zero, and reached 4000 rpm 200 seconds into the test. It was held at 4000 rpm for approximately 22 minutes. After reaching an oil temperature of 85 °C, the oil heating was turned off. It was observed that the engine produced enough heat on its own at 4000 rpm to keep the oil temperature at 87 °C for the remainder of the test. The transducer output (equivalent to friction torque) showed a steady decrease from approximately 2 V to 1.6 V over the course of 17 minutes, before stabilizing (see figure 10). With no substantial change in measured value for the last 5 minutes, the break-in was considered complete.
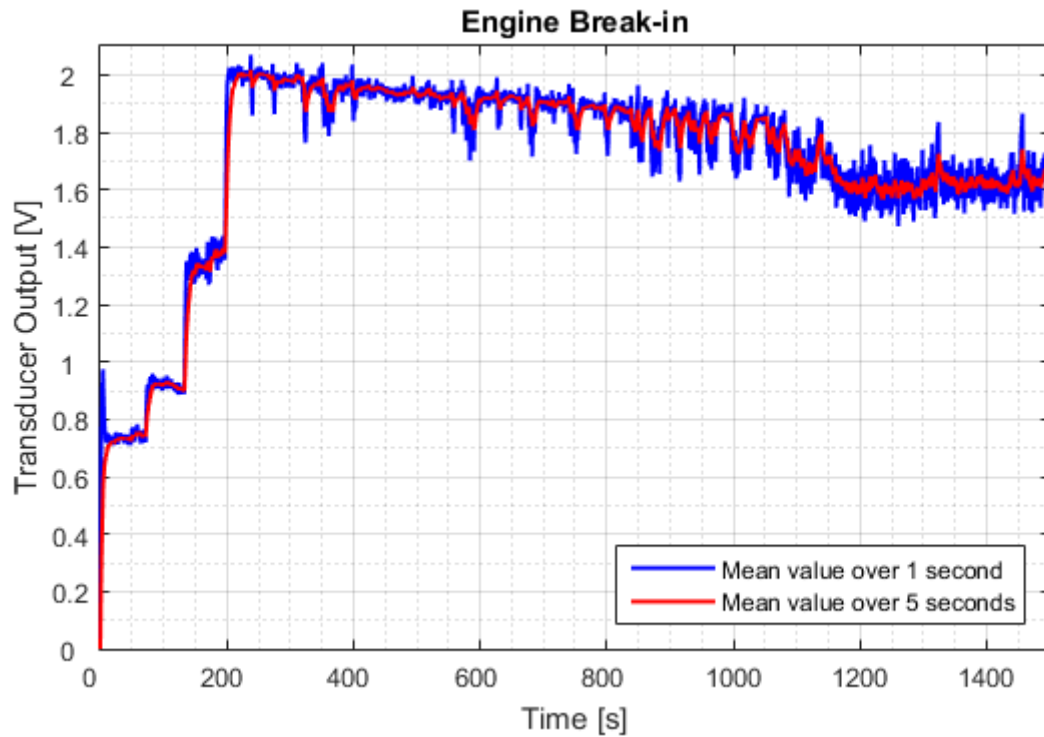
Figure 10: Engine break-in

Before any further testing was performed, the engine oil used during the initial test and engine break-in was replaced. A full test cycle was performed, and the results can be seen in figure 11. Extracted representative results (using the five second mean values) are shown in table 8. It looks like the first 6000 rpm plateau (between 235 and 275 seconds) was held a bit to short, since the values did not stabilize completely before continuing with the test. The dip in output between 275 and 300 seconds appears because the test speed was reduced for a short period of time, to approach and inspect the test rig before continuing.
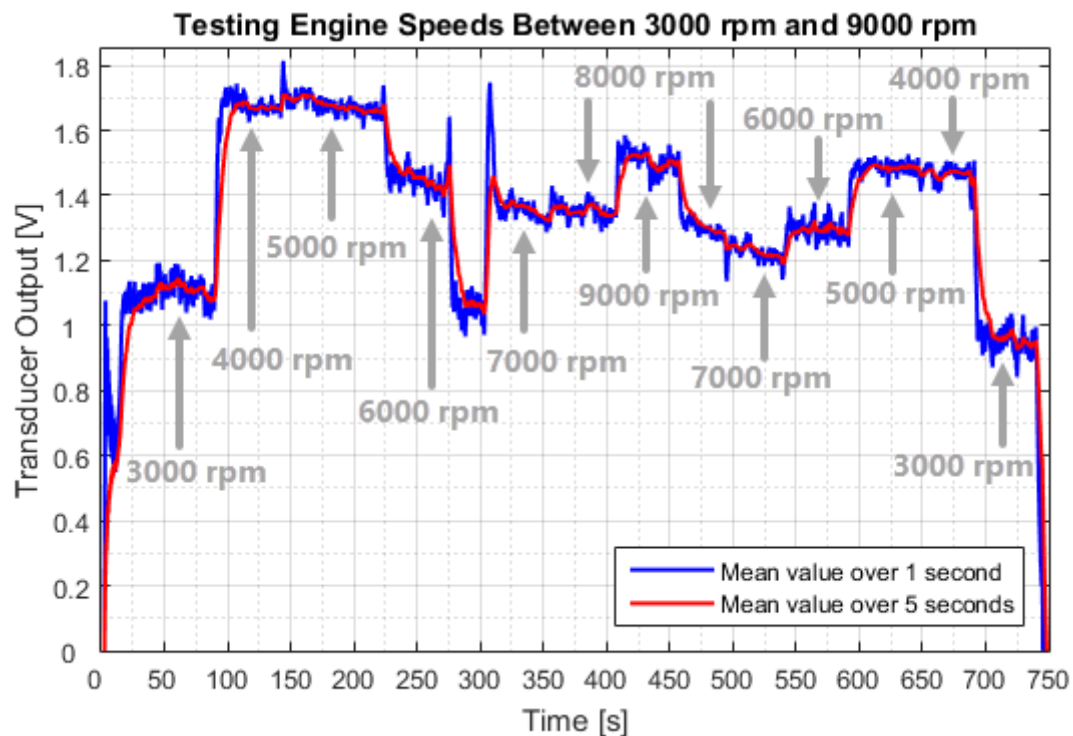

Figure 11: Full test results

15

Approximate test cycle time	Engine speed	Transducer output	Oil temperature	Oil heating setting
15 - 90 s	3000 rpm	1.08 V	75 °C	3
100 - 140 s	4000 rpm	1.67 V	75 °C	3
150 - 225 s	5000 rpm	1.66 V	77 °C	3
235 - 275 s	6000 rpm	1.41 V	80 °C	3
310 - 350 s	7000 rpm	1.32 V	79 °C	0
360 - 400 s	8000 rpm	1.34 V	80 °C	0
410 - 450 s	9000 rpm	1.50 V	82 °C	0
460 - 490 s	8000 rpm	1.28 V	82 °C	0
500 - 540 s	7000 rpm	1.21 V	83 °C	0
550 - 590 s	6000 rpm	1.29 V	84 °C	0
600 - 640 s	5000 rpm	1.49 V	85 °C	0
650 - 690 s	4000 rpm	1.47 V	85 °C	0
700 - 740 s	3000 rpm	0.94 V	84 °C	0

Table 8: Full test representative results

Early in the second full test (4000 rpm), it was discovered that the output did not behave as expected. The measured values did not appear to stabilize, and the problem became more pronounced at 5000 rpm. The measured output continued to increase until transducer failure occurred. The results can be seen in figure 12. Extracted representative results (using the five second mean values) are shown in table 9.
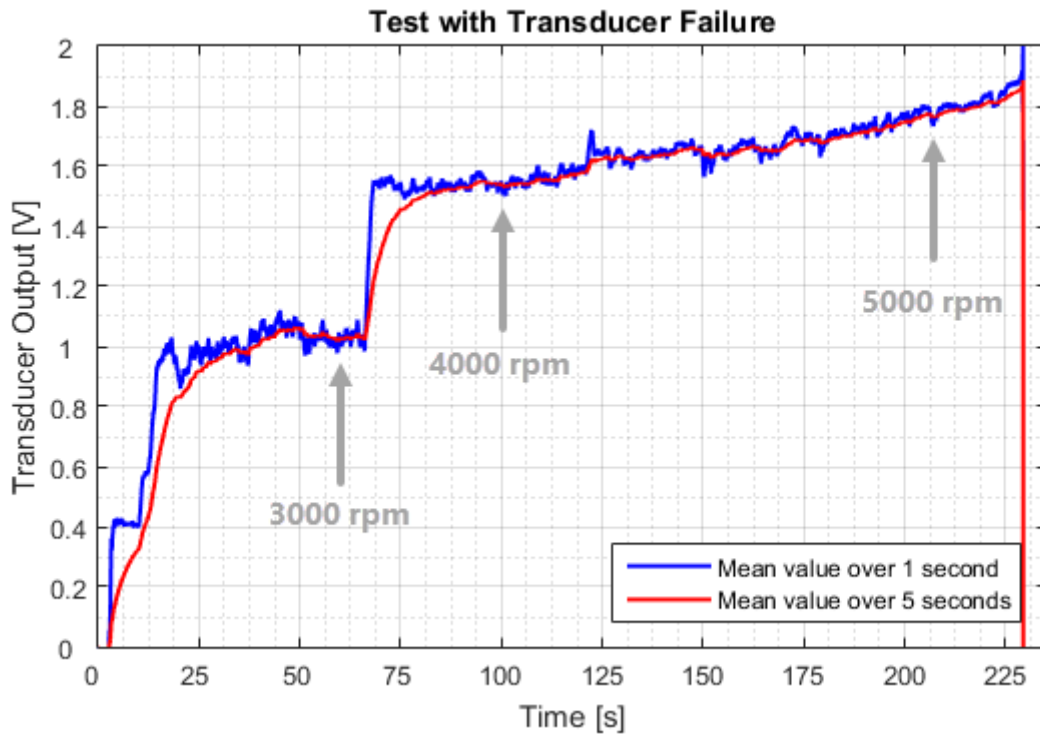

Figure 12: Transducer failure test results

Approximate test cycle time	Engine speed	Transducer output	Oil temperature	Oil heating setting
50 - 65 s	3000 rpm	1.03 V	82 °C	2
75 - 120 s	4000 rpm	1.57 V	83 °C	2
130 - 225 s	5000 rpm	1.86 V	83 °C	0

Table 9: Transducer failure test representative results

16

A summary of the test results is presented in figures 13 and 14. The average values of the tests with rising and falling rpm steps were used as representative values in tuning of the virtual test bench. These values are found in table 10.
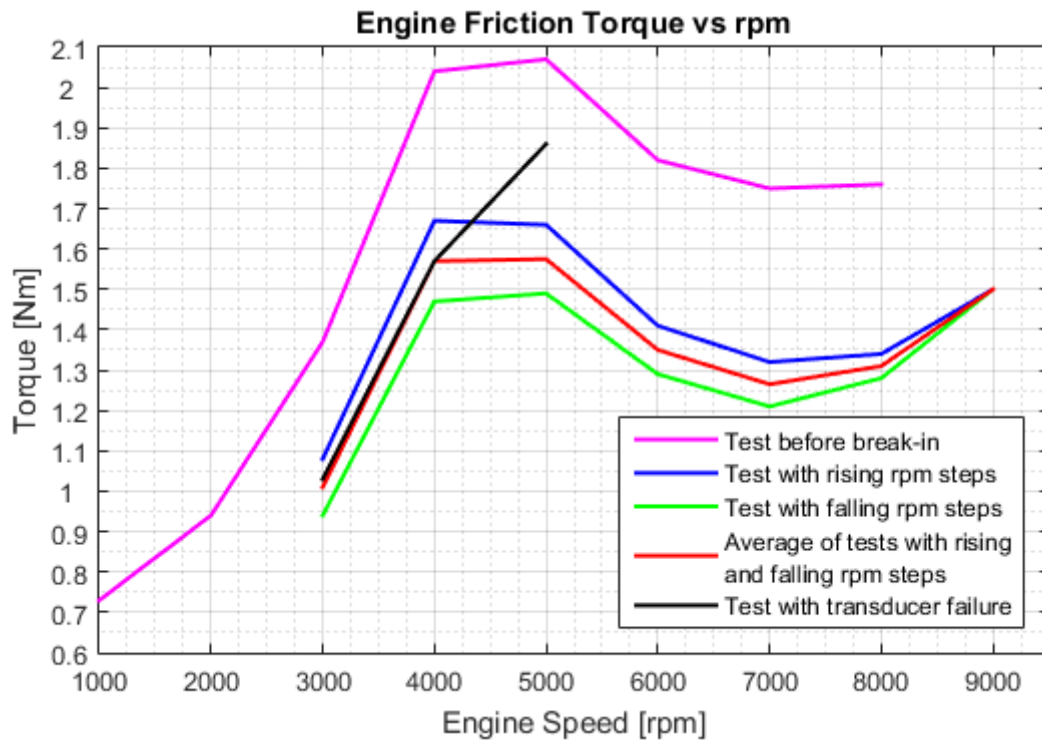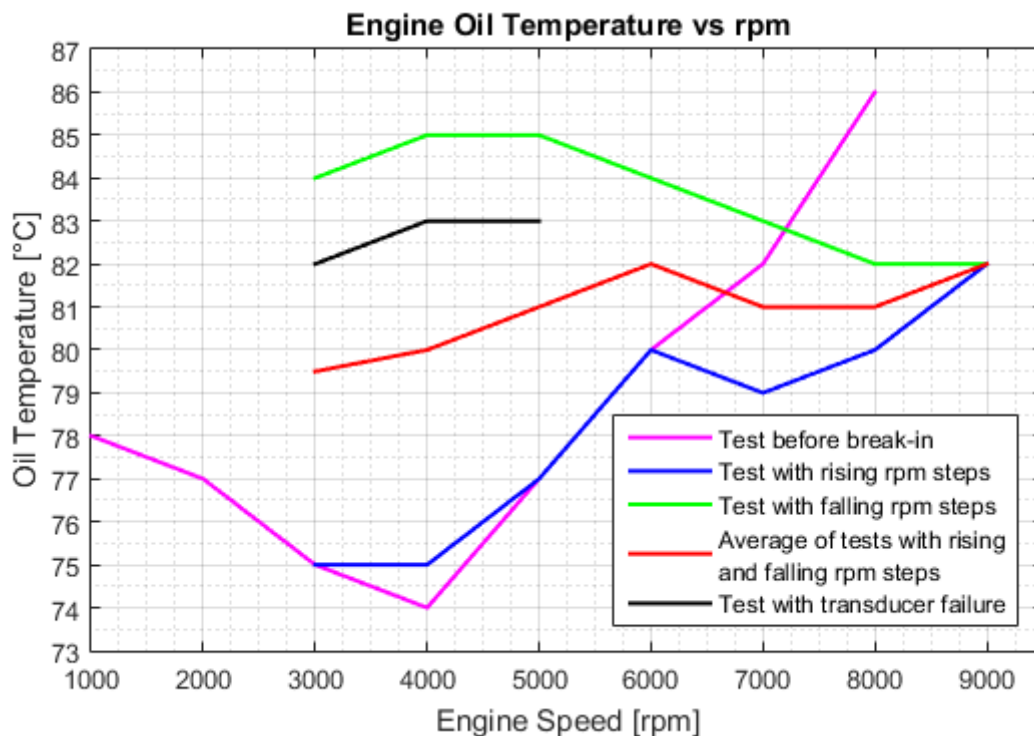

Figure 13: Friction torque vs. engine speed

Figure 14: Oil temperature vs. engine speed

Engine speed	Friction torque	Oil temperature
3000 rpm	1.01 Nm	80 °C
4000 rpm	1.57 Nm	80 °C
5000 rpm	1.58 Nm	81 °C
6000 rpm	1.35 Nm	82 °C
7000 rpm	1.27 Nm	81 °C
8000 rpm	1.31 Nm	81 °C
9000 rpm	1.50 Nm	82 °C

Table 10: Averaged results summary

The final result from the virtual test bench tuning is presented in figure 15 and table 11. The values were extracted from the filtered motoring torque using the mean value from the curve statistics in FEDEM. The mean was taken over 0.1 seconds at the end of each engine speed plateau. The result from the engine testing was plotted in the same graph for easy comparison. A simulation run in the virtual test bench is completed in approximately 20 minutes.

As a result of introducing resistance in the test bench model, the parameters for the PI controller established in the reference test bench model caused the simulation engine speed to be too low. To remedy this, the PI controller integral term was reduced to 3. As seen from both figure 16 and the results in table 11, the engine speed from the simulation still deviated slightly from the set points from the reference speed curve, but on average the new PI controller setting performed acceptably well. To investigate the virtual test bench's response to weight changes in a part, a simulation was set up where the connecting rod's mass was scaled down to 60%. FEDEM provides options for scaling mass and stiffness of individual parts, without changing the FE model. The result can be seen in table 11.
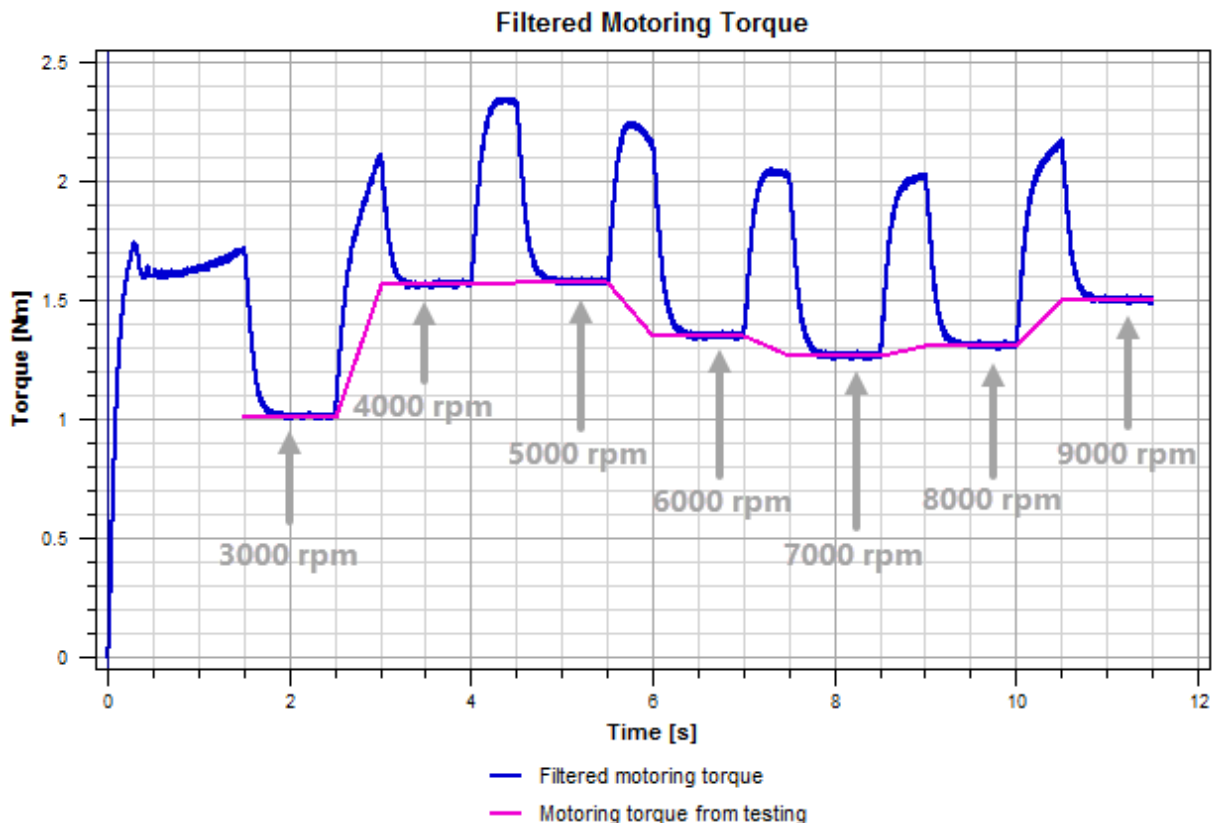

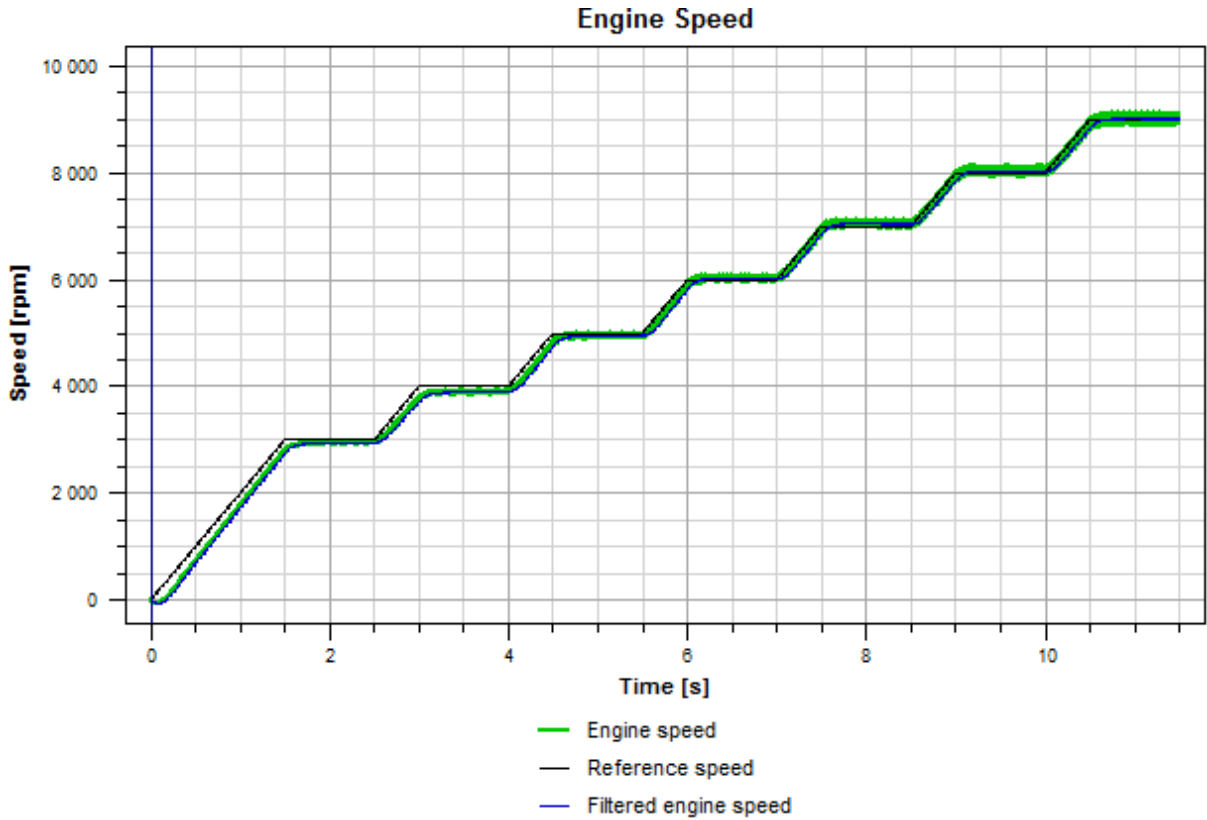Figure 15: Graphic representation of final result

18

Figure 16: Engine speed from final result

Engine speed		Simulation speed	Simulation torque	Simulation speed, reduced connecting rod mass	Simulation torque, reduced connecting rod mass
3000 rpm	314.159 rad/s	308.786 rad/s	1.01 Nm	308.775 rad/s	1.01 Nm
4000 rpm	418.879 rad/s	409.308 rad/s	1.57 Nm	409.298 rad/s	1.57 Nm
5000 rpm	523.599 rad/s	519.495 rad/s	1.58 Nm	519.486 rad/s	1.57 Nm
6000 rpm	628.319 rad/s	630.735 rad/s	1.35 Nm	630.747 rad/s	1.34 Nm
7000 rpm	733.038 rad/s	737.388 rad/s	1.27 Nm	737.416 rad/s	1.25 Nm
8000 rpm	837.758 rad/s	841.448 rad/s	1.31 Nm	841.498 rad/s	1.29 Nm
9000 rpm	942.478 rad/s	943.699 rad/s	1.50 Nm	943.774 rad/s	1.48 Nm

Table 11: Results from the virtual test bench

Discussion

During testing it was observed that some engine oil seemed to squeeze past the piston rings, and ended up on the upper side of the piston. It is suspected that this issue occurred as a consequence of motored testing without the cylinder head. As the engine rotates, oil is splashed onto the cylinder wall by the crankshaft. Each time the piston moves down, some oil is scraped off and accumulated near the bottom of the piston rings, and pressure is built up under the piston due to compression of the crankcase air. Since no combustion pressure was present during testing, there was no back-pressure helping the piston rings seal during the power stroke. Any oil managing to squeeze past the oil control ring during the intake stroke under fired operation would most likely be squeezed back before passing the compression ring, by the pressure during the compression stroke and the blow-by of combustion gases during the power stroke. Resolving this test issue while maintaining atmospheric pressure in the cylinder would mean introducing a pumping loss through venting of the crankcase. Instead, it was decided to perform the tests with some

oil squeezing past the piston rings, being aware that this might change the lubrication conditions for the piston compared to during fired operation. A soft-box made from an oil-absorbing mat was placed on top of the four cylinder head bolts (not completely around the engine top), catching the oil flinging off the piston without restricting the air flow into the cylinder.

Originally, the connection between the transducer and the Ø20 mm axle was done using a 0.02 mm shrink-fit aluminum sleeve, but it showed signs of slipping after the initial function test. A new shrink-fit sleeve made from steel was fabricated, but it turned out to be difficult to align properly. In the process of improving the alignment, the torque transducer was damaged by excessive heat and/or mechanical force, which resulted in a bent transducer axle. Due to the high cost and delivery time associated with obtaining a new transducer, it was decided to repair the damaged transducer. The torque transducer was disassembled and the axle straightened. After reassembly, the torque transducer seemed to function properly, but the output at zero torque had shifted. Not an unexpected result, as plastic deformation of the axle would naturally affect the transducer's strain gauges. To investigate if the transducer could still be used, it was connected to the data acquisition system and calibrated in such a way that a zero reading in Catman coincided with zero transducer torque. Then, one side of the transducer was held stationary while a precision torque wrench was used on the socket-side to apply torque in 0.5 Nm increments from 1 Nm to 5 Nm. The transducer's response revealed a predictable and relatively linear response. It was decided to use the repaired transducer with a steel sleeve with set screws to connect the axle to the transducer, to avoid damaging the transducer further. Additional damage accumulated through high frequency torsion cycling (varying torque over each crankshaft revolution), and possibly also bending (misalignment), caused fatigue failure of the axle inside the transducer early in the second full test.

It would have been an advantage to get data from more tests, particularly to avoid variations due to measurement values not stabilizing entirely before moving on to the next engine speed. One might speculate in the validity and accuracy of the test data obtained with the repaired transducer, but the results in figure 13 show that the same trend is present in all of the test runs. Even in the test where the transducer ultimately failed, the first measurements closely match the average from the test with rising and falling rpm steps. This gives credibility to the test results. The curves from the test with rising and falling rpm steps both show the same behavior, but different values. This can be explained by looking at the corresponding oil temperatures in figure 14. Since oil viscosity is sensitive to temperature, the friction losses are too. This applies to both the bearings and the piston assembly. The work by Daniels and Braun [5] confirms this relation between temperature and losses. As the oil temperature increases, the viscosity is reduced, resulting in lower friction for the hydrodynamic part of the stroke. It is interesting to note that the test performed before engine break-in shows the same trend as the others, but at higher friction values. This highlights the importance of engine break-in on the friction properties, in agreement with the findings of Fadel et al. [7].

Assuming that bearing friction is strictly increasing with engine speed, means that the piston assembly friction is responsible for the shape of the curves in figure 13. An interesting observation is that the overall shape of the curves resemble the Stribeck diagram (figure 1). The Stribeck diagram shows the friction coefficient as a function of the duty parameter $\left(\frac{viscosity \times speed}{load}\right)$. This explains the test data's curves to some extent, seeing as the mean piston velocity increases with engine speed. (This assumes that the oil viscosity and normal load from inertia forces behave in such a manner that the duty parameter is strictly increasing with engine speed). When the engine speed is below 4000 rpm, the dominating piston assembly lubrication regime appears to be boundary. Between 4000 rpm and 5000 rpm, the dominating lubrication regime seems to shift to mixed, and gradually transition towards hydrodynamic at 7000 rpm. From there and up, hydrodynamic lubrication appears to be the dominating regime. It is important to note that even if a specific regime is seen to "dominate" the friction behavior, this does not mean that it is the only one in effect. Different regimes still occur during a piston stroke, but which one contributes the most, changes.

Even with the oil heating system turned off, oil temperature continued to rise as the tests proceeded. Since no heat was supplied from combustion, this must mean that bearing and piston friction, together with oil shearing, were responsible for the temperature rise. This is further exemplified by the results from the engine break-in, where it was observed that the engine produced enough heat on its own at 4000 rpm to keep the oil temperature at 87 °C, despite the whole engine acting as a heat sink. The engine is normally

liquid cooled, but the testing was performed without the cooling system. Including it in the test rig would most likely keep the oil temperature more stable.

The results from the virtual test bench shows that it was successfully able to recreate the measurements from the engine testing. The results from the simulation run with a lighter connecting rod were however not as expected. Even with the connecting rod weighing in at 60% of the OEM rod, the reduction in required motoring torque was barely noticeable (0.02 Nm at the most). The reason is suspected to be that the modeling approach does not replicate the actual friction behavior in the piston assembly. It has already been mentioned that the FEDEM friction model for translational friction is not comprehensive enough to capture the changes in lubrication regime. It does not support a variable coefficient of friction, but requires the Coulomb coefficient to have a constant value. Working around this limitation meant modeling the lubrication regime changes by viscous damping with a variable viscous coefficient. This causes the friction behavior to be less dependent on the weight of the engine components (through inertia forces).

An additional challenge was adding the viscous damping to translation of the piston assembly. In order to get the desired effect, the magnitude of the viscous coefficient would have to be fairly large, and this caused the motoring torque to get out of control. The reason is suspected to be the varying piston velocity, and the fact that viscous damping depends on this. As the piston reaches maximum velocity (and viscous damping force) mid-stroke, the PI controller ramps up the torque to keep the engine speed constant. As the piston starts to slow towards dead center, the viscous damping force decreases, causing the engine speed to increase while the PI controller tries to slow it down. The PI controller is not able to react fast enough, and therefore causes motoring torque overshoot. This problem could possibly be solved by implementing a different control strategy for the engine speed, but this would mean starting from scratch with both modeling of the reference test bench and the tuning. Since this issue was discovered rather close to the deadline, it was decided to work around this problem to see if viable results could be produced with the existing model. The workaround by adding the viscous damping to the scaling function for the connecting rod damping seemed to work, but is not an accurate representation of real engine friction behavior.

When introducing friction in the virtual test bench, it was noted that the existing parameters for the PI controller caused the simulation engine speed to be too low. Reducing the PI controller integral term was seen to acceptably remedy the issue, but the simulation engine speeds still deviated slightly from the reference speed curve. To implement this change of a control system parameter perfectly, the modeling of the reference test bench (with time steps) and the tuning should have been performed from scratch. This would have been too time consuming considering the deadline, but is something that should be considered in future work.

The modeling performed in the virtual test bench only considers one piston assembly loss. This approach does not consider the separate effects of piston rings and piston skirt, and secondary motion is not accounted for. The piston friction is applied to the free joint, representing the piston/cylinder interaction in the virtual test bench. A more detailed approach would be to employ contact formulations for the piston rings and skirt, and apply the friction through these. This approach would necessarily increase the model complexity and computational cost, but whether it is necessary in terms of result accuracy is difficult to answer without more detailed testing and simulation. A possible solution to improve the friction and damping modeling could be utilizing an external .dll file for this task. By using this approach, better control over the parameters (such as variable Coulomb coefficients) and friction behavior is possible, at the expense of a more complex modeling procedure. Exploring this option would be a natural step in improving the accuracy of the virtual test bench.

The general approach used during modeling was to add as much as possible of the piston, crankshaft, and connecting rod contributions as frictions. The remaining parts were added as viscous damping. This choice was based on possibilities and limitations in FEDEM. The unfortunate impact on the modeling of piston assembly friction has already been discussed. For the crankshaft and connecting rod systems, it is difficult to tell if this was an appropriate way to distribute the contributions from fiction and viscous drag. Some test data on the matter would be beneficial to improve the model. The final choice of Coulomb coefficients for the rotational (bearing) frictions was typically 0.0025, and the coefficient for the translational (piston) friction

was 0.08. Both values are very low, but a higher friction for lubricated translational friction than bearing friction makes good sense. The choice of coefficients was limited by the desired friction contribution at certain engine speeds, and this means that their values might not be exact compared to real life measurements.

To further investigate the accuracy of the virtual test bench simulations, more test data is needed. By performing physical testing with different engine parts (piston, connecting rod, crankshaft), and comparing the results to the virtual test bench simulations with the same parts, information on the accuracy and impact on friction behavior can be obtained. Strip/teardown tests would be beneficial in determining the exact friction contribution of the crankshaft.

Summary and Conclusion

A customized engine test rig was designed, and motored testing was performed to measure the friction torque of a partial assembly of a Honda CRF 250 R motocross engine in the speed range from 3000 rpm to 9000 rpm. The end result of the work performed in this paper is a virtual test bench modeled in FEDEM, capable of recreating the results from physical engine testing.

Concerns were raised regarding the accuracy of the test data obtained with a damaged and repaired torque transducer. A function check revealed that the transducer showed a predictable and relatively linear response, with sufficient accuracy. Despite this, the transducer failed relatively early in the testing phase, resulting in only one complete test run (with both increasing and decreasing rpm steps) after engine break-in. The results showed that the same trend was present and repeatable in all of the test runs, both complete and partial, adding credibility to the test results.

It was noted that motored testing without a cylinder head can be problematic in terms of piston ring sealing and oil film behavior. The test results showed that the dominating piston assembly lubrication regime changes from boundary, via mixed, to hydrodynamic with increasing engine speed. This caused the measured friction torque to go from 1 Nm (3000 rpm), via a peak of 1.6 Nm (5000 rpm), to 1.5 Nm (9000 rpm). The engine friction's sensitivity to oil temperature was noted, as a higher oil temperature leads to reduced viscosity, affecting the friction losses. Engine friction and oil shearing produced enough heat to keep the oil temperature at 87 °C at 4000 rpm, exemplifying the need for liquid cooling to control engine temperature accurately. Comparing test results from before and after engine break-in clearly shows the break-in's impact on the engine's friction losses.

The virtual test bench was successfully able to recreate the measurements from the engine testing, with both fairly accurate engine speeds, and a matching motoring torque for each investigated engine speed. A simulation run with reduced connecting rod mass did not produce the expected friction reduction, and it was suspected that a weakness in the modeling approach was responsible.

The friction modeling formulation in FEDEM did not have the capability to capture the changes in lubrication regime for the piston assembly. It does not support a variable coefficient of friction, but requires the Coulomb coefficient to have a constant value. This meant working around the problem by adding additional viscous damping with a variable viscous coefficient, resulting in a less realistic model behavior. High levels of translational viscous damping was also seen to cause problems with the PI controller responsible for keeping the desired motoring speeds. Using an external .dll file for friction and damping modeling was mentioned as a possible solution to the friction modeling problem.

It is concluded that more test data and improved friction modeling in FEDEM is required to obtain a virtual test bench accurate enough to predict real engine behavior, when inertia and mass properties of critical engine components are changed. Additional physical testing and simulation with different engine parts would provide information on the simulation accuracy and the impact of different parts on the engine's total friction behavior.

Bibliography

[1] Abu-Nada, Al-Hinti, Al-Sarkhi, and Akash. Effect of piston friction on the performance of si engine: A new thermodynamic approach. *ASME Journal of Engineering for Gas Turbines and Power*, 130(2), 2008.

[2] Ozgen Akalin and Golam M. Newaz. Piston ring-cylinder bore friction modeling in mixed lubrication regime: Part i-analytical results. *Journal of Tribology*, 123(1):211–218, 1999.

[3] Ozgen Akalin and Golam M. Newaz. Piston ring-cylinder bore friction modeling in mixed lubrication regime: Part ii-correlation with bench test data. *Journal of Tribology*, 123(1):219–223, 1999.

[4] H. Allmaier, C. Priestner, D.E. Sander, and F.M. Reich. *Tribology in Engineering*, chapter 9 Friction in Automotive Engines, pages 149–184. InTech, 2013.

[5] C. C. Daniels and M. J. Braun. The friction behavior of individual components of a spark-ignition engine during warm-up. *Tribology Transactions*, 49(2):166–173, 2006.

[6] P S Dellis. Effect of friction force between piston rings and liner: A parametric study of speed, load, temperature, piston-ring curvature, and high-temperature, high-shear viscosity. *Proceedings of the Institution of Mechanical Engineers, Part J: Journal of Engineering Tribology*, 224(5):411–426, 2010.

[7] C. Fadel, N. G. Chalhoub, G. A. Kfoury, and N. A. Henein. Direct measurement of the piston-assembly friction force in a single cylinder engine under motoring conditions. In *ASME 2008 Dynamic Systems and Control Conference*, number DSCC2008-2173, pages 505–512, 2008.

[8] Fedem Technology AS. *Fedem Release 7.1 Theory Guide*, October 2014.

[9] Michael Gore, Michael Theaker, Sebastian Howell-Smith, Homer Rahnejat, and Paul D King. Direct measurement of piston friction of internal-combustion engines using the floating-liner principle. *Proceedings of the Institution of Mechanical Engineers, Part D: Journal of Automobile Engineering*, 228(3):344–354, 2014.

[10] Kenneth Holmberg, Peter Andersson, and Ali Erdemir. Global energy consumption due to friction in passenger cars. *Tribology International*, 47:221–234, 2012.

[11] M. Hoshi. Reducing friction losses in automobile engines. *Tribology International*, 17(4):185–189, 1984.

[12] Riaz Ahmad Mufti. *Total and Component Friction in a Motored and Firing Engine*. PhD thesis, The University of Leeds School of Mechanical Engineering, 2004.

[13] Terje Rølvåg and Matteo Bella. Dynamic test bench for motocross engines. Unpublished, submitted to the International Journal of Automotive and Mechanical Engineering on 2. June, 2015.